

**Vanadium-Schiff Base Complexes as Catalysts for the
Four-Electron Reduction of Dioxygen**

Thesis by
Zenghe Liu

In Partial Fulfillment of the Requirements
For the Degree of
Doctor of Philosophy

California Institute of Technology

Pasadena, California

2002

(Defended February 7, 2002)

ACKNOWLEDGEMENTS

I would like to express my deep gratitude to my advisor, Professor Fred C. Anson, for his advice, patience and encouragement during the years of my study at Caltech. As his last student, I feel extremely lucky to have caught the train and finally become a proud Anson-ite.

I thank Professors Bercaw, Marcus and Peters for serving on my thesis committee. I learned a lot from those questions asked by them during my prop exam and candidacy exam. Special thanks are due to Dr. Chunnian Shi and other former members of the Anson Group for their support and friendship. I am also grateful to Drs. Angelo Di Bilio and Sean J. Elliott for their help in EPR experiments.

I thank the Electrochemical Society for awarding me a 2000 summer research fellowship. I also want to thank the Physical Electrochemistry Division of the Society for awarding me travel grants to cover part of my expenses in attending two national conferences of the Society. I really enjoy meeting fellow electrochemists at these conferences.

I could never thank enough my wife and my family members in China, especially my parents. Their constant and love, support, understanding and confidence during my endless years of schooling have been an immense source of inspiration to me.

ABSTRACT

The coordination chemistry and electrochemistry of complexes of vanadium(III, IV, V) with salen ($H_2\text{salen} = N,N'$ -ethylenebis-(salicylideneamine)) were first examined. The origin of the puzzling results reported in previous reports in the literature was identified using microelectrode voltammetry and the modifications required are specified. $VO(\text{salen})$ was found to disproportionate in acidified acetonitrile. The equilibrium constant for this disproportionation reaction was measured. The stoichiometry and kinetics of the reaction between O_2 and the V(III)-salen complex were examined and a possible mechanism for this four-electron reduction of O_2 is suggested.

The study was then expanded to vanadium complexes with fifteen Schiff base (SB) ligands analogous to salen. Electrochemical and spectral characteristics of the complexes were evaluated and compared. With several of the ligands the V(III) complexes are much more stable in the presence of acid than is the complex with salen. Equilibrium constants for the disproportionation of the oxovanadium (IV) complexes were evaluated. The vanadium(III) complexes reduce dioxygen to form two oxo ligands. In the presence of acid some of the complexes investigated participate in a catalytic electroreduction of dioxygen.

The otherwise slow reaction between O_2 and decamethylferrocene or $V^{III}(\text{SB})^+$ is significantly accelerated if these three reactants are present. In the absence of acid the reduction of O_2 proceeds stoichiometrically to

yield the two oxo groups in (SB)V^{IV}O. In the presence of acid the reaction becomes catalytic and the O₂ is reduced to H₂O. Preliminary results on the kinetics of the O₂ reduction was presented.

Electrochemical study on vanadium-naphophen (naphophen = N, N'-1, 2-phenylenebis-(2-hydroxy-1-naphthylideneimine)) complexes in acetonitrile containing excess acetic anhydride was also conducted. V^{IV}O(naphophen) was found to undergo deoxygenation by two equivalents of acid to give V^{IV}(naphophen)²⁺, which had not persisted in previous study. Several reactions proposed previously to describe the chemistry of vanadium-Schiff base complexes in acetonitrile were directly demonstrated with this species.

The oxovanadium-naphophen complexes were found to spontaneously adsorb on EPG electrodes. They also exhibited remarkable stability towards acid after adsorption. Their surface electrochemical behavior was studied and characterized using cyclic voltammetry.

TABLE OF CONTENTS

ACKNOWLEDGEMENTS	ii
ABSTRACT	iii
TABLE OF CONTENTS	v
LIST OF FIGURES	viii
LIST OF TABLES	xii
CHAPTER I. Introduction.....	I-1
CHAPTER II. Electrochemical Properties of Vanadium(III, IV, V)- Salen Complexes and Four-Electron Reduction of O ₂ by V(III)- Salen in Acetonitrile	II-1
ABSTRACT	II-2
INTRODUCTION.....	II-3
EXPERIMENTAL.....	II-4
RESULTS	II-7
DISSCUSSION	II-25
CONCLUSIONS	II-38
APPENDIX II-A. Determiration of the pK _a for HBF ₄ in Acetonitrile.....	II-40
APPENDIX II-B. Digital Simulation of the Reduction of V ^V O(salen) ⁺ in Acetonitrile in the Presence of Acid	II-45
REFERENCES.....	II-50
CHAPTER III. Schiff Base Complexes of Vanadium(III, IV, V) as Catalysts for the Electroreduction of O ₂ to H ₂ O in Acetonitrile	III-1
ABSTRACT	III-2
INTRODUCTION.....	III-3

EXPERIMENTAL.....	III-4
RESULTS	III-7
DISSCUSSION	III-23
CONCLUSIONS	III-29
APPENDIX III-A. Cyclic Voltammetry of V ^{IV} O(SB) in CH ₂ Cl ₂	III-30
REFERENCES.....	III-36
CHAPTER IV. Rate Enhancements in the Four-electron Reduction of O ₂ by Mixtures of Vanadium(III)-Schiff Base Comp- lexes and Decamethylferrocene in Acetonitrile	IV-1
ABSTRACT	IV-2
INTRODUCTION.....	IV-3
EXPERIMENTAL.....	IV-4
RESULTS	IV-7
DISSCUSSION	IV-20
CONCLUSIONS	IV-25
APPENDIX IV-A. Kinetics of Reaction 4 When DMFc Is the Limiting Reactant.....	IV-27
REFERENCES.....	IV-29
CHAPTER V. Electrochemistry of Vanadium-N, N'-1, 2- phenylene- bis-(2-hydroxy-1-naphthylideneimine) Complexes in Acetonitrile Containing Excess Acetic Anhydride	V-1
ABSTRACT	V-2
INTRODUCTION.....	V-3
EXPERIMENTAL.....	V-5
RESULTS	V-7
DISSCUSSION	V-17
CONCLUSIONS	V-20
REFERENCES AND NOTES.....	V-21

CHAPTER VI. Electrochemistry of Oxovanadium-N, N'-1, 2-phenylenebis(2-hydroxy-1-naphthylideneimine) Complexes Irreversibly Adsorbed on Edge Plane Graphite Electrodes.....	VI-1
ABSTRACT	VI-2
INTRODUCTION.....	VI-3
EXPERIMENTAL.....	VI-4
RESULTS AND DISCUSSION.....	VI-5
CONCLUSIONS	VI-20
REFERENCES.....	VI-21

LIST OF FIGURES

CHAPTER I

- Figure 1.1** Diffusion layer profiles and representing cyclic voltammo-grams for microelectrodes and macroelectrodes I-7

CHAPTER II

- Figure 2.1** Steady-state voltammetry of a 1.0 mM solution of $V^{IV}O(salen)$ in CH_3CN recorded with a carbon microelectrode scanned at 10 mV s^{-1} II-8
- Figure 2.2** ^{51}V NMR and EPR spectra of: (1) a 2 mM $V^{IV}O(salen)$ solution in CH_3CN ; (2) after addition of 2 millimoles per liter of CF_3SO_3H to (1). II-11
- Figure 2.3** Steady-state voltammograms showing the titration of a 1.0 mM solution of $V^{IV}O(salen)$ with CF_3SO_3H II-12
- Figure 2.4** Steady-state voltammetry of a 1.0 mM solution of $V^VO(salen)^+$ in the presence of acid II-15
- Figure 2.5** Cyclic voltammetry of a 1.0 mM solution of $V^VO(salen)^+$ in the presence or absence of acid II-17
- Figure 2.6** Steady-state voltammetry and infrared spectra of $V^{IV}O(salen)$ and $V^{III}(salen)^+$ II-19
- Figure 2.7** (A). UV-vis spectra of $V^VO(salen)^+$ and $V^{III}(salen)^+$. (B) Pseudo-first-order kinetic plots for the reaction between $V^{III}(salen)^+$ O_2 II-24

- Figure 2.8** UV-Vis. spectra of neutral red II-42
- Figure 2.9** UV-Vis. spectra of neutral red in the presence of $\text{CF}_3\text{SO}_3\text{H}$ and different amount of TBABF_4 II-43
- Figure 2.10** Determination of pK_a for HBF_4 in acetonitrile. II-44

CHAPTER III

- Figure 3.1** Steady-state current-potential curves in a 1 mM solution of $\text{V}^{\text{IV}}\text{O}(\text{SB})$ (for SB No. 1 in Table 3.1)..... III-13
- Figure 3.2** Steady-state voltammograms showing the titration of a suspension of $\text{V}^{\text{IV}}\text{O}(\text{SB})$ (for SB No.14 in Table 3.1) with $\text{CF}_3\text{SO}_3\text{H}$ III-16
- Figure 3.3** (A) Current-time transients recorded during the reaction of $\text{V}^{\text{III}}(\text{SB})^+$ (for SB No. 1 in Table 3.1) with O_2 in pure CH_3CN . (B) Pseudo-first-order kinetic plots. III-22
- Figure 3.4** Cathodic charge flow during the electroreduction of O_2 catalyzed by V-Schiff base complexes III-27
- Figure 3.5** Cyclic voltammograms of 1 mM $\text{VO}(\text{SB})$ (SB No. 2 in Table 3.1) in CH_2Cl_2 III-33
- Figure 3.6** Cyclic voltammograms of 1 mM $\text{VO}(\text{SB})$ for SB Nos. 1 (top) and 2 (bottom) in Table 3.1 in CH_2Cl_2 III-34
- Figure 3.6** Cyclic voltammograms of 0.3 (top) and 3 (bottom) mM $\text{VO}(\text{SB})$ (SB No. 2 in Table 3.1) in CH_2Cl_2 III-35

CHAPTER IV

- Figure 4.1** Steady-state voltammetry of a mixture of $\text{V}^{\text{III}}(\text{SB})^+$ (SB = ligand 2 in Table 4.1) and DMFc in CH_3CN IV-9

Figure 4.2	Kinetics of the oxidation of $V^{III}(\text{salen})^+$ and DMFc by O_2	IV-11
Figure 4.3	Steady-state voltammograms showing the stoichiometry of the oxidation of $V^{III}(\text{salen})^+$ and DMFc by O_2	IV-14
Figure 4.4	Steady-state voltammograms showing the catalysis of O_2 reduction by DMFc.....	IV-16
Figure 4.5	Kinetics of the oxidation of $V^{III}(\text{salen})^+$ and DMFc by O_2 in the presence of acid.....	IV-19
Figure 4.6	Current-time transients showing the oxidation of $V^{III}(\text{salen})^+$ and DMFc by O_2	IV-28

CHAPTER V

Figure 5.1	Steady-state voltammograms and EPR spectra of $V^{IV}O(\text{naphophen})$ and $V^{IV}(\text{naphophen})^{2+}$	V-8
Figure 5.2	Steady-state voltammograms showing the two directions of reaction 4.....	V-11
Figure 5.3	Cyclic voltammograms of $V^{III}(\text{naphophen})^+$ and $V^{IV}(\text{naphophen})^{2+}$	V-14
Figure 5.4	Steady-state voltammograms recorded during the electrolysis of $V^{IV}(\text{naphophen})^{2+}$	V-16

CHAPTER VI

Figure 6.1	Cyclic voltammograms of a 0.1 mM $V^VO(\text{naphophen})^+$ solution in CH_3CN at glassy carbon and EPG electrodes.	VI-7
Figure 6.2	Cyclic voltammogram of a 7.5 μM $V^VO(\text{naphophen})CF_3SO_3$ solution in CH_3CN at an EPG electrode.....	VI-8

- Figure 6.3** Cyclic voltammogram of a 7.5 μM $\text{V}^{\text{VO}}(\text{naphophen})\text{CF}_3\text{SO}_3$ solution at different scan rates VI-10
- Figure 6.4** Surface concentration Γ of $\text{V}^{\text{VO}}(\text{naphophen})^+$ on an 6 mm EPG electrode vs. its solution concentration VI-13
- Figure 6.5** Cyclic voltammogram of adsorbed $\text{V}^{\text{VO}}(\text{naphophen})^+$ on a 6 mm EPG electrode in 50 mM HClO_4 VI-15
- Figure 6.6** Cyclic voltammograms showing the desorption of adsorbed $\text{V}^{\text{VO}}(\text{naphophen})^+$ on EPG VI-17
- Figure 6.7** Cyclic voltammogram of $\text{V}^{\text{III}}(\text{naphophen})^+$ and $\text{V}^{\text{VO}}(\text{naphophen})^+$ at EPG electrodes VI-18

LIST OF TABLES

CHAPTER II

Table 2.1	Evaluation of the Equilibrium Constant for Reaction 2	II-13
Table 2.2	Diffusion Coefficients for Complexes Examined in This Study.....	II-29
Table 2.3	Formal Potentials for Redox Couples Examined in This Study.....	II-33

CHAPTER III

Table 3.1	Schiff Base Ligands Utilized in This Study	III-8
Table 3.2	Colors, Solubilities and Elemental Analyses for the Oxovanadium(IV) Complexes of the Schiff Base Ligands in Table 3.1	III-9
Table 3.3	IR and EPR Spectral Data for V ^{IV} O(SB) Complexes of the Ligands in Table 3.1	III-10
Table 3.4	Equilibrium Constants for the Acid-induced Disproportionation of V ^{IV} O(SB)	III-15
Table 3.5	Titration Data Used to Evaluate the Equilibrium Constant of Reaction 1 for Schiff Base No. 14	III-17
Table 3.6	Formal Potentials of Redox Couples for Schiff Base Complexes of V(III, IV, V)	III-19

CHAPTER IV

Table 4.1	Schiff Base Ligands Utilized in This Study	IV-5
------------------	--	------

CHAPTER VI

Table 6.1	Parameters Obtained From Figure 6.3A and Electron-Transfer Rate Constants Calculated From Equation 1	VI-11
------------------	--	-------

CHAPTER I

Introduction

Electrocatalysis for O₂ Reduction

The oxygen reduction reaction can proceed by two overall pathways¹ in aqueous electrolytes, as shown below:

(1) Direct four-electron pathway

a) in an alkaline electrolyte

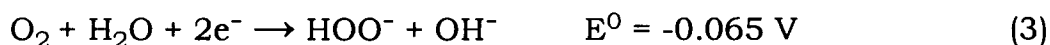


b) in an acidic electrolyte



(2) Peroxide pathway

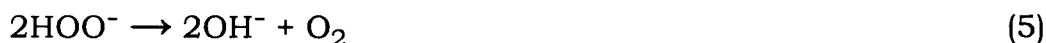
a) in an alkaline electrolyte



followed by either peroxide reduction



or peroxide decomposition



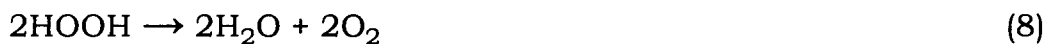
b) in an acid electrolyte



followed by either



or



The standard potentials for all the half-reactions are quoted with respect to the normal hydrogen electrode (NHE) at 25 °C.

For the cathodic reaction of fuel cells² that utilize dioxygen as the reducible reactant, the direct four-electron pathway is preferable since it does not involve peroxide species in solution and the charge efficiency (Faradaic efficiency) of the reaction is greater. This pathway, which involves the rupture of the O-O bond and the formation of four O-H bonds, however, requires the use of catalysts (often called electrocatalysts, which include molecules, functional groups, or metallic deposits that accelerate the rates of electrode reactions when they are confined to the surfaces of electrodes) to obtain useful rates at cathode potentials of interest in practical applications. The highest cathode potentials achievable with currently available catalysts are ca. 0.79 V (vs. NHE). Realizing four-electron reduction of dioxygen to water at potentials close to the thermodynamically permitted value, i.e., 1.23 V (vs. NHE), remains a daunting challenge for the development of superior fuel cells.

Finely divided platinum supported on high area carbon is the electrocatalyst employed most frequently to achieve the electroreduction of O₂ to H₂O in presently available fuel cells. However, this type of electrocatalyst suffers from the disadvantages of high cost and gradual loss in catalytic activity as the surface area of the active platinum particles decreases because of sintering, dissolution, physical dislodgment, and/or adsorption of impurities. Over the past two decades, searches for alternative electrocatalysts for the reduction of O₂

have been very active and have often focused on transition metal porphyrins. It was discovered in recent years that a variety of molecular catalysts consisting of dimeric cofacial cobalt porphyrins adsorbed on the surface of graphite electrodes are able to catalyze the direct four-electron electroreduction of O_2 without passing through H_2O_2 as an intermediate.³⁻¹⁵ Both dimeric and monomeric iridium porphyrins have also been found to accomplish the electroreduction of O_2 to H_2O at unusually positive potentials.¹⁶⁻¹⁸ Recently, novel multinuclear catalysts based on cobalt porphyrin molecules with ligand sites attached to the periphery of the porphyrin ring have been developed in this group.¹⁹ Four-electron reduction of O_2 at 0.47 ~ 0.59 V (vs. NHE) with these catalysts were achieved. In addition to these metal-porphyrin catalysts, transition metal complexes with other macrocyclic ligands has been studied.

Thesis Outline

Explored in this project are the chemistry and electrochemistry of a series of both known and newly synthesized vanadium complexes of multidentate Schiff base ligands. Their catalytic activity towards four-electron reduction of O_2 is also investigated. With these two themes running through, this thesis is organized into six chapters. The current chapter introduces some background information about oxygen reduction as well as microelectrode voltammetry. Chapter II describes the coordination chemistry and electrochemistry of vanadium-salen

(H₂salen = N, N'-ethylenebis(salicylideneamine)) complexes. The chemistry of the acid-induced disproportionation of VO(salen) established in this chapter forms the basis for following chapters. A new method is devised based on the disproportionation to prepare the V(III)-salen complex, which can reduce O₂ by four electrons. The kinetics of the reduction is also studied and a possible mechanism is suggested. The reduction could not be made catalytic because of the instability of the catalyst and the slow reaction rate. Chapter III describes an expanded study of 15 analogous Schiff base ligands modified to enhance the stability and catalytic activity of their complexes with V(III). Catalytic four-electron electroreduction of O₂ is successfully achieved with several of the new complexes. The results may provide a useful foundation on which to base the design of complexes with even better catalytic activity. The topic of Chapter IV concerns the exploration of the redox chemistry of a three-component system consisting of V(III)-Schiff base complexes, decamethylferrocene and O₂. This system can be employed to perform the four-electron chemical reduction of O₂ catalytically. Chapter V presents results concerning the electrochemical studies of vanadium-naphophen (naphophen = N, N'-1, 2-phenylenebis-(2-hydroxy-1-naphthylideneimine)) complexes in the presence of excess anhydride. The remarkable stability of the V(III)-naphophen complexes towards acid makes it possible to directly demonstrate the chemistries regarding the

interconversions among the vanadium-Schiff base complexes as proposed in Chapters II and III. Surface electrochemical properties of oxovanadium-naphophen complexes are described in Chapter VI. The results also provide further supporting evidence for the solution chemistries described in previous chapters.

Introduction to Microelectrodes

Since steady-state microelectrode voltammetry is used as a major electrochemical technique in this project, the features of microelectrodes are briefly introduced here. Detailed theory and applications about microelectrodes are given in references 20 and 21.

Microelectrodes, also known as ultramicroelectrodes, are electrodes whose critical dimension is in the micrometer range. These small voltammetric probes have several typical attributes including small currents, steady-state responses, and short response times. The small currents observed at microelectrodes typically lie in the pA to nA range, which is several orders of magnitude smaller than those observed at conventional macroelectrodes, whose radii are usually several millimeters. The reduced currents are a key element in the successful applications of microelectrodes. Electrochemical measurements with conventional electrodes are restricted to highly conducting media, such as aqueous solutions. This restriction arises from the solution resistance which causes "ohmic drop." The small currents of microelectrodes often

completely eliminate this effect and allow one to perform amperometric experiments in highly resistive media such as non-polar solvents, supercritical fluids, and even solids.

The small size of microelectrodes makes diffusional mass transfer extremely efficient. In fact, mass transport rates to a microelectrode are comparable to those of a conventional macroelectrode rotating at several thousand r.p.m. At relatively long experimental timescales, the dimensions of the diffusional layer exceed the radius of the microelectrode, resulting in a spherical diffusion field. This efficient mass transfer allows one to observe steady-state responses when the applied potential is slowly scanned in cyclic voltammogram. A comparison of the diffusion profiles at conventional electrodes and at microelectrodes, and typical cyclic voltammograms of the two types of electrodes are shown in Figure 1.1.

Another distinctive feature of microelectrodes is their ability to respond rapidly to changes in the applied potential because of their low electrode capacitance. Microelectrodes can accurately monitor electrochemical processes on a low microsecond or even a nanosecond timescale, compared with tens or even hundreds of milliseconds timescale of conventional electrodes.

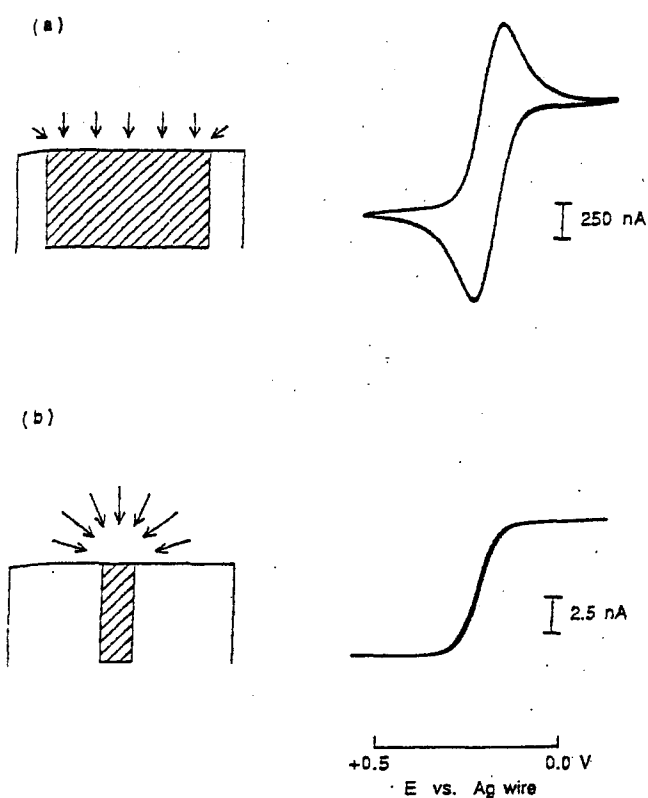


Figure 1.1. Diffusion layer profiles and representative cyclic voltammograms for (a) a 2 mm conventional macroelectrode; (b) a 10 μm microelectrode. Solution: 1 mM ferrocene in $\text{CH}_3\text{CN}/\text{TBAPF}_6$. Scan rate: 50 mV s^{-1} . The figure is copied from reference 22.

REFERENCES

- (1) Yeager, E. *Electrochim. Acta* **1984**, *29*, 1527-1537.
- (2) For a recent review, see Carrette, L.; Friedrich, K. A.; Stimming, U. *CHEMPHYSICHEM* **2000**, *1*, 162-193.
- (3) Collman, J. P.; Marrocco, M.; Denisevich, P.; Koval, C.; Anson, F. C. *J. Electroanal. Chem.*, **1979**, *101*, 117-122.
- (4) Chang, C. K. *Adv. Chem. Ser.* **1979**, *173*, 162-177.
- (5) Collman, J. P.; Denisevich, P.; Konai, Y.; Marrocco, M.; Koval, C.; Anson, F. C. *J. Am. Chem. Soc.* **1980**, *102*, 6027-6036.
- (6) Collman, J. P.; Anson, F. C.; Bencosme, S.; Chong, A.; Collins, T.; Denisevich, P.; Evitt, E.; Geiger, T.; Ibers, J. A.; Jameson, G.; Konai, Y.; Koval, C.; Meier, K.; Okaley, P.; Pettman, R.; Schmittou, E.; Sessler, J. In *Organic Synthesis Today and Tomorrow*; Trost, B. M., Hutchinson, C. R., Eds.; Pergamon Press: Oxford, U.K., 1981; pp 29-45.
- (7) Liu, H.-Y.; Weaver, M. J.; Wang, C.-B.; Chang, C. K. *J. Electroanal. Chem.* **1983**, *145*, 439-447.
- (8) Durand, R. R., Jr.; Bencosme, C. S.; Collman, J. P.; Anson, F. C. *J. Am. Chem. Soc.* **1983**, *105*, 2710-2718.
- (9) Chang, C. K.; Liu, H. Y.; Abdalmuhdi, I. *J. Am. Chem. Soc.* **1984**, *106*, 2725-2726.
- (10) Liu, H. Y.; Abdalmuhdi, I.; Chang, C. K.; Anson, F. C. *J. Phys. Chem.* **1985**, *89*, 665-670.

- (11) Collman, J. P.; Hendricks, N. H.; Leidner, C. R.; Ngameni, E.; L'Her, M. *Inorg. Chem.* **1988**, *27*, 387-393.
- (12) Guillard, R.; Brandes, S.; Tardieux, C.; Tabard, A.; L'Her, M.; Miry, C.; Gouerec, P.; Knop, Y.; Collman, J. P. *J. Am. Chem. Soc.* **1995**, *117*, 11721-11729.
- (13) Karaman, R.; Jeon, S.; Almarsson, O. ; Bruice, T. C. *J. Am. Chem. Soc.* **1992**, *114*, 4899-4905.
- (14) Jeon, S.; Almarsson, O.; Karaman, R.; Blasko, A.; Bruice, T. C. *Inorg. Chem.* **1993**, *32*, 2562-2569.
- (15) Chang, C. J.; Deng, Y. Q.; Shi, C. N.; Chang, C. K.; Anson, F. C.; Nocera, D. G. *Chem. Commun.* **2000**, *15*, 1355-1356.
- (16) Collman, J. P.; Kim, K. *J. Am. Chem. Soc.* **1986**, *108*, 7847-7849.
- (17) Collman, J. P.; Chng, L. L.; Tyvoll, D. A. *Inorg. Chem.* **1995**, *34*, 1311-1324.
- (18) Shi, C.; Mak, K. W.; Chan, K.-S.; Anson, F. C. *J. Electroanal. Chem.* **1995**, *397*, 321-324.
- (19) Anson, F. C.; Shi, C.; Steiger, B. *Accounts Chem. Soc.* **1991**, *113*, 9564-9570; and references therein.
- (20) Querios, M. A.; Montenegro, I.; Daschbach, J. L., Eds. *Microelectrodes: Theory and Applications*; Kluwers, Dordrecht, 1991.
- (21) Forster, R. J. *Chem. Soc. Rev.* **1994**, 289-297.
- (22) Ching, S.; Dudek, R.; Tabet, E. *J. Chem. Edu.* **1994**, *71*, 602-605.

CHAPTER II

Electrochemical Properties of Vanadium(III, IV, V)-Salen Complexes and Four-Electron Reduction of O₂ by V(III)-Salen in Acetonitrile*

*Major part of the work described in this chapter has been published in:

Liu, Z.; Anson, F. C. *Inorg. Chem.* **2000**, 39, 274-280.

ABSTRACT

The coordination chemistry and electrochemistry of complexes of vanadium(III, IV, V) with salen (H_2 salen = N,N'-ethylenebis(salicylideneamine)) were re-examined in an attempt to uncover the origin of puzzling results reported in a previous study (*Inorg. Chem.* **1994**, 33, 1056). Microelectrodes were utilized to allow measurements in the absence of supporting electrolyte. The source of the puzzling results was identified and the modifications required in the previous interpretations are specified. Corrected values of formal potentials and diffusion coefficients are also given. The acid-induced disproportionation of $V^{IV}O(\text{salen})$, as originally proposed by Bonadies et al. (*Inorg. Chem.* **1987**, 26, 1218.), was largely supported by the present results. The equilibrium constant for this disproportionation reaction was measured. The stoichiometry and kinetics of the reaction between O_2 and the V(III)-salen complex were examined and a possible mechanism for this four-electron reduction of O_2 is suggested.

INTRODUCTION

The redox and electrochemical behavior of oxovanadium complexes with the ligand salen ($H_2\text{salen} = N, N'$ -ethylenebis(salicylideneamine)) in acetonitrile solution were first studied by Bonadies and co-workers.¹ Abundant structural studies of these complexes have also been reported.^{2, 3} Recently, additional electrochemical studies of the complexes in both acetonitrile⁴ and dichloromethane⁵ have been described. With acetonitrile as solvent, the results were interpreted by invoking an acid-induced conversion of $V^{IV}O(\text{salen})$ to, first, an oxo-bridged dimeric complex, and, with a sufficient excess of acid, to the oxo-free complex, $V^{IV}(\text{salen})^{2+}$. The results also included the surprising observation that the formal potentials of the $VO(\text{salen})^{+/0}$ and $V(\text{salen})^{2+/+}$ couples were almost the same.⁴ The interpretation of the electrochemical results in reference 4 differed from that of Bonadies et al.¹ who had proposed an acid-induced disproportionation reaction of $V^{IV}O(\text{salen})$ without the intervention of an oxo-bridged dimeric complex. Because of the different interpretations offered for essentially the same experimental observations and the puzzling coincidence of the formal potentials given in reference 4, we decided to re-examine the electrochemistry of the vanadium-salen system in the presence of little or no supporting electrolyte to determine if ionic interactions in the non-aqueous environment might have been responsible for some of the unexplained

anomalies in the previous report.⁴ Our interest was also stimulated by the indications that vanadium-salen complexes are capable of acting as catalysts for the electrochemical reduction of O₂ by four electrons in non-aqueous solvents.^{5b, 5c}

The new results, summarized in this chapter, provide what we believe to be a more satisfying account of the effect of strong acids on the chemistry and electrochemistry of the vanadium-salen system in acetonitrile. The participation of a disproportionation reaction, as originally proposed by Bonadies et al.,¹ is strongly supported by the present results. The equilibrium constant for the disproportionation was estimated. The origin of the puzzling behavior that led Tsuchida et al.⁴ to propose an alternative interpretation is identified. In addition, we devised a method to prepare V^{III}(salen)⁺ based on the disproportionation chemistry. The stoichiometry and kinetics of the reaction between O₂ and this V(III) complex are studied and a possible mechanism is proposed for the catalysis by the complex of the electroreduction of O₂ by four electrons in acidified acetonitrile.

EXPERIMENTAL

Materials

N,N'-Ethylenebis(salicylideneamine) (H₂salen) and tris(acetyl-acetonato)vanadium(III) were obtained from Pfaltz & Bauer and Aldrich

respectively. $V^{IV}O(\text{salen})$ was prepared according to a published procedure⁶ and purified by recrystallization from dichloromethane-methanol. Supporting electrolytes from Fluka were of electrochemical grade. They were dried overnight at 75 °C in a vacuum oven. Distilled acetonitrile containing 0.001% water was supplied by EM Science and stored over 3Å molecular sieves. Trifluoromethanesulfonic (triflic) acid from Sigma was received under argon and was maintained O_2 -free by saturation with Ar.

$[V^{III}(\text{salen})]CF_3SO_3 \cdot 2CH_3CN$

$V^{IV}O(\text{salen})$ (0.600 mmol, 0.2 g) was dissolved in acetonitrile (75 mL). In the solution was placed a platinum gauze that had been cleaned with HNO_3 and washed thoroughly with water, acetone and acetonitrile. The solution was purged with argon for 20 minutes and an equimolar quantity of CF_3SO_3H (56 μL) was slowly added to the solution under an argon atmosphere. Hydrogen was then passed through the solution until the reaction was complete (as determined by the disappearance of the wave for the reduction of $V^{V}O(\text{salen})^+$, formed by disproportionation of $V^{IV}O(\text{salen})$, in microelectrode voltammograms). The solvent was removed under argon and the brownish yellow powder obtained was placed under vacuum to complete the solvent removal. Elemental analysis: Calculated for $[V^{III}(\text{salen})]CF_3SO_3 \cdot 2CH_3CN$: C, 45.99; H, 3.68;

N, 10.22; Found: C, 45.59; H, 3.60; N, 10.32.

Apparatus and Procedures

Electrochemical measurements were carried out in conventional one- or two-compartment cells using a Bioanalytical Systems Model 100B/W electrochemical analyzer. Solutions were kept under an atmosphere of argon which was purified by passing through a gas scrubber (Oxiclear; Aldrich) and two columns filled with molecular sieves. A 10 μm diameter carbon microelectrode or a 5 mm diameter glassy-carbon disk were used as the working electrodes in voltammetric experiments. The electrodes were polished with 0.3 μm and 0.05 μm alumina pastes before use. A porous glassy-carbon working electrode was used for bulk electrolyses. The auxiliary electrode was a platinum wire or foil. The reference electrode was Ag/AgCl in CH_3CN saturated with NaCl. All potentials are quoted with respect to this electrode. The half-wave potentials of the ferrocinium/ferrocene couple measured from microelectrode voltammograms recorded in pure acetonitrile and in a 0.1 M tetrabutylammonium hexafluorophosphate (TBAPF_6) solution in acetonitrile were 0.47 V and 0.44 V, respectively, vs. this Ag/AgCl reference electrode.

The rate of the reaction between $\text{V}^{\text{III}}(\text{salen})^+$ and O_2 in acetonitrile solution at 24 ± 0.5 °C was measured by following the formation of the

product, $V^V O(\text{salen})^+$, with a Hewlett-Packard 8452A Diode-Array spectrophotometer. IR spectra were obtained with a Perkin Elmer 1600 FT-IR spectrophotometer and a cell with CaF_2 windows separated by 1 mm. Background spectra were measured with pure acetonitrile. ^{51}V NMR spectra were obtained on a Varian Inova 500 spectrometer operating at 131.47 MHz with neat VOCl_3 as an external reference. EPR spectra were recorded on a Varian E-line spectrometer operating at X-band. A cylindrical quartz cell with a diameter of 2 mm was used as the sample tube. Digital simulation was conducted with the software DigiSim[®] 3.05 (Bioanalytical Systems, Inc.).

RESULTS

Acid-induced Disproportionation of $V^{IV} O(\text{salen})$.

The reaction of $V^{IV} O(\text{salen})$ with triflic acid ($\text{CF}_3\text{SO}_3\text{H}$) in anhydrous acetonitrile containing no other electrolyte is readily monitored by means of steady-state voltammetry using a carbon microelectrode.⁷ Curve 1 in Figure 2.1 is the response obtained from $V^{IV} O(\text{salen})$ before the addition of acid. The single oxidation wave, corresponding to half-reaction 1, matches that reported in previous studies in the presence of supporting electrolyte.^{1, 4}



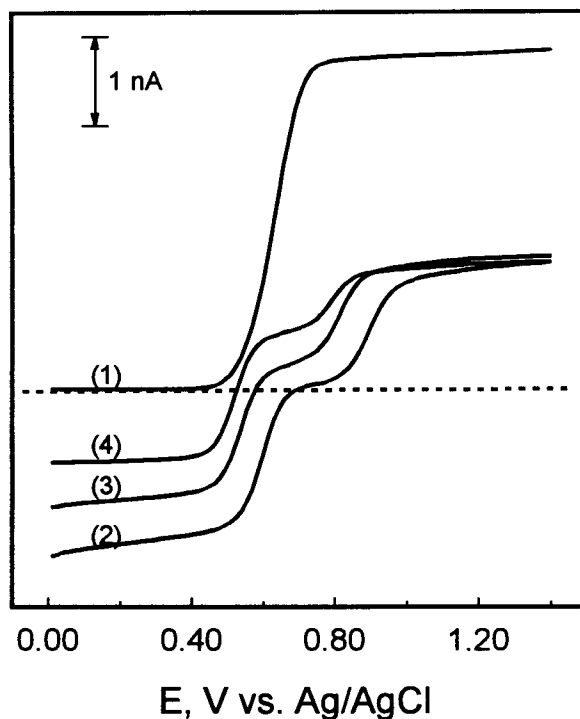
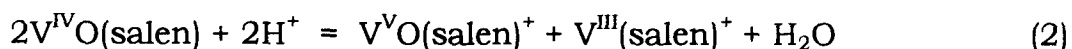


Figure 2.1. Steady-state voltammetry of a 1.0 mM solution of V^{IV}O(salen) in CH₃CN recorded with a carbon microelectrode scanned at 10 mV s⁻¹. For this and the subsequent Figures, the position of zero current is shown by the dotted line. Supporting electrolyte: (1) none; (2) 1 mM CF₃SO₃H; (3) 1 mM CF₃SO₃H + 20 mM TBABF₄; (4) 1 mM CF₃SO₃H + 60 mM TBABF₄.

Addition of one mole of $\text{CF}_3\text{SO}_3\text{H}$ per mole of $\text{V}^{\text{IV}}\text{O}(\text{salen})$ produced the separated oxidation and reduction waves shown in curve 2. This behavior differs significantly from that reported in reference 4 where tetrabutylammoniumtetrafluoroborate (TBABF_4) was employed as a supporting electrolyte. In that study, the addition of an equimolar quantity of acid produced a composite anodic/cathodic wave followed by an anodic wave at more positive potentials. Curve 3 in Figure 2.1 shows the voltammetric response obtained in the presence of TBABF_4 . As the concentration of TBABF_4 is increased, the cathodic plateau currents corresponding to the reduction of $\text{V}^{\text{VO}}(\text{salen})^+$ become much smaller and the magnitude of the second anodic plateau current is also diminished (curve 4 in Figure 2.1). The anomalous behavior provoked by the presence of TBABF_4 originates in the BF_4^- anion. With supporting electrolytes consisting of 0.1 M TBAPF_6 , TBAClO_4 or $\text{TBACF}_3\text{SO}_3$, voltammetric responses similar to curve 2 in Figure 1 are obtained.

The separated anodic and cathodic waves in curve 2 of Figure 2.1 are consistent with an acid-induced disproportionation of $\text{V}^{\text{VO}}(\text{salen})$ according to reaction 2



with the cathodic wave at 0.65 V and the anodic wave at 0.9 V assigned to half-reactions 3 and 4, respectively.



The presence of vanadium(V) in acidified solutions of $\text{V}^{\text{IV}}\text{O}(\text{salen})$ was confirmed by recording a ^{51}V NMR spectrum which contained a peak at -598 ppm assignable to the diamagnetic $\text{V}^{\text{V}}\text{O}(\text{salen})^+$ complex,⁸ as shown in Figure 2.2A. In addition, the eight-line ESR spectrum exhibited by pure solutions of $\text{V}^{\text{IV}}\text{O}(\text{salen})$ disappeared in the presence of an equimolar quantity of acid (Figure 2.2B), as expected if reaction 2 proceeded essentially to completion.

Equilibrium Constant for the Disproportionation Reaction.

If less than equivalent quantities of $\text{CF}_3\text{SO}_3\text{H}$ are added to solutions of $\text{V}^{\text{IV}}\text{O}(\text{salen})$ in anhydrous acetonitrile, reaction 2 still proceeds too extensively to allow its equilibrium constant to be measured. However, in the presence of excess H_2O , the reaction comes to equilibrium with substantial quantities of the acid remaining which permits the equilibrium constant to be estimated. Shown in Figure 2.3 is a set of current-potential curves recorded after increasing quantities of $\text{CF}_3\text{SO}_3\text{H}$ were added to a solution of $\text{V}^{\text{IV}}\text{O}(\text{salen})$ in CH_3CN containing $0.1 \text{ M H}_2\text{O}$. The composite cathodic/anodic wave and the separate anodic wave near 0.8 V reflect the simultaneous presence in the solution of all three of the

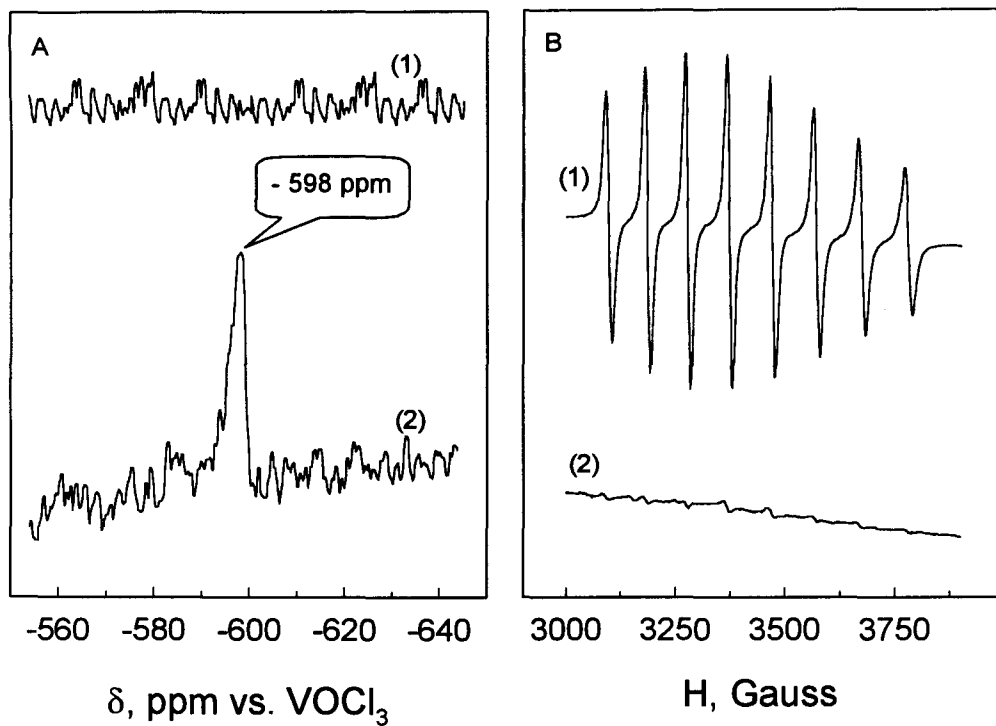


Figure 2.2. ^{51}V NMR (A) and EPR (B) spectra of: (1) a 2 mM $\text{V}^{\text{IV}}\text{O}(\text{salen})$ solution in CH_3CN ; (2) after addition of 2 millimoles per liter of $\text{CF}_3\text{SO}_3\text{H}$ to (1).

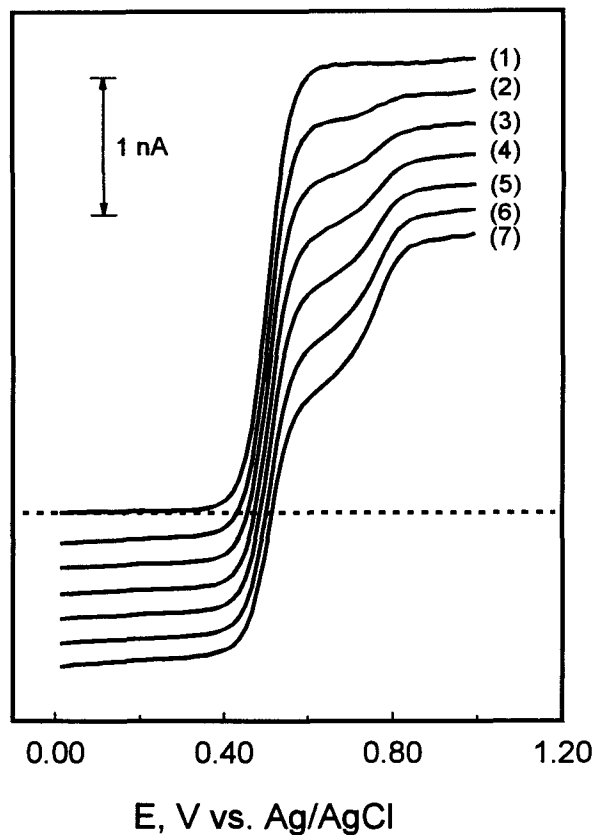


Figure 2.3. Steady-state voltammograms recorded with a carbon microelectrode in an initially 1.0 mM solution of $V^{IV}O(\text{salen})$ in CH_3CN also containing 0.1 M TBAClO_4 + 0.1 M H_2O . Aliquots $\text{CF}_3\text{SO}_3\text{H}$ were added to the solution in quantities corresponding to (1) 0, (2) 0.15, (3) 0.30, (4) 0.45, (5) 0.60, (6) 0.75, (7) 0.90 moles of $\text{CF}_3\text{SO}_3\text{H}$ per mole of $V^{IV}O(\text{salen})$. Other conditions as in Figure 1.

complexes involved in reaction 2. The well-formed cathodic plateau current measured the concentration of $V^V O(\text{salen})^+$ in each solution which was used to calculate the corresponding equilibrium concentrations of the other reactants in the equilibrium of reaction 2. The various concentrations were combined to obtain values for the equilibrium constant as summarized in Table 2.1. The reasonably constant value obtained for K_2 supports the proposition that reaction 2 reliably describes the acid-induced disproportionation of $V^V O(\text{salen})$.

Table 2.1. Evaluation of the Equilibrium Constant for Reaction 2 from the Plateau Currents of the Curves in Figure 3.

Equivalents of CF_3SO_3H added	$[V^{IV}O(\text{salen})]^a$ mM	$[V^V O(\text{salen})^+]^b$ mM	$[V^{III}(\text{salen})^+]^c$ mM	$[H^+]^d$ mM	$10^{-6} K_2^e$ M^{-1}
0	1.0	0	0	0	
0.15	0.87	0.065	0.065	0.02	1.4
0.30	0.74	0.13	0.13	0.04	1.9
0.45	0.63	0.18	0.18	0.08	1.3
0.60	0.52	0.24	0.24	0.12	1.5
0.75	0.41	0.29	0.29	0.17	1.7
0.90	0.33	0.34	0.34	0.22	2.1
					Avg. (1.6 ± 0.3)

^a Calculated as $1.0 - 2 [V^V O(\text{salen})^+]$.

^b Evaluated from the cathodic plateau currents of the curves in Figure 3.

^c Taken as equal to $[V^V O(\text{salen})^+]$.

^d Calculated from the difference between the amount of CF_3SO_3H added (assumed to be totally dissociated¹²) and $[V^V O(\text{salen})^+]$ using the stoichiometry of reaction 2.

^e $K_2 = [V^V O(\text{salen})^+] [V^{III}(\text{salen})^+] [H_2O] / [V^{IV}O(\text{salen})]^2 [H^+]^2$.

Electrochemical Behavior of $V^VO(\text{salen})^+$

The disproportionation of $V^{IV}O(\text{salen})$ in acidic acetonitrile would be expected to enhance the cathodic plateau current for the reduction of $V^VO(\text{salen})^+$ in the presence of acid. Shown in Figure 2.4 is a set of steady-state voltammograms that demonstrate the expected effect. In the absence of acid (curve 1 in Figure 2.4) a one-electron reduction according to half-reaction 3 proceeds. However, in the presence of acid, larger cathodic plateau currents result (curves 2-5). The reason is that half-reaction 3 is followed by reaction 2 which produces additional $V^VO(\text{salen})^+$ that again undergoes half-reaction 3, etc.

As expected, the rate of reaction 2 increases with the concentration of acid so the plateau current increases until it reaches a value close to the diffusion-controlled, two-electron reduction of $V^VO(\text{salen})^+$ according to the stoichiometry given in half-reaction 5.



The positive shift in the half-wave potentials of the curves in Figure 2.4 as the concentration of acid is increased is also a reflection of the increase in the rate of reaction 2 which diminishes the concentration of $V^{IV}O(\text{salen})$ at the electrode surface.

Electrolysis at 0.4 V of solutions of $V^VO(\text{salen})^+$ like the one used to record curve 2 in Figure 2.4 consumed two electrons per molecule of

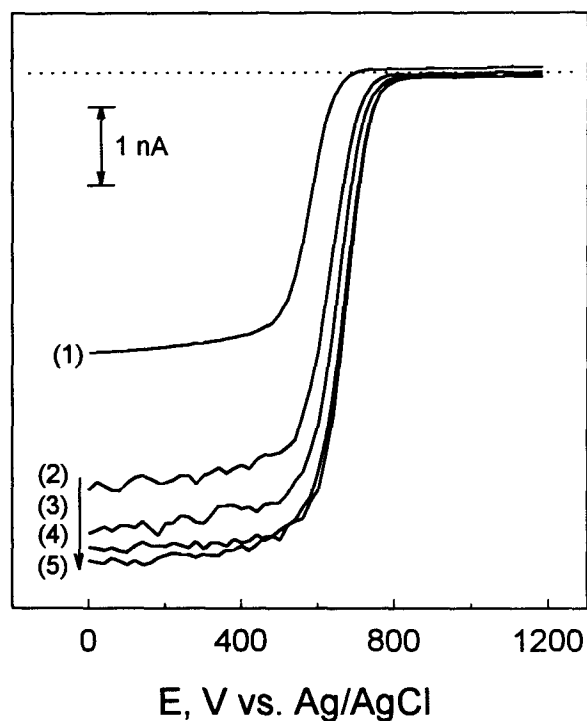


Figure 2.4. Steady-state voltammetry of a 1.0 mM solution of $V^V O(salen)^+$ prepared by saturating a mixture of 1 mM $V^{IV} O(salen)$ and 1 mM CF_3SO_3H with O_2 for 30 min. followed by removal of the O_2 with Ar. Supporting electrolyte: (1) 0; (2) 1; (3) 2; (4) 4; (5) 8 mM CF_3SO_3H . Other conditions as in Figure 2.1.

$V^V O(\text{salen})^+$ even though the plateau current of curve 2 corresponds to fewer than two electrons. The reason is that the rate of reaction 2 was ample for the quantitative disproportionation of all $V^{IV} O(\text{salen})$ produced during the 30-40 minutes required for the electrolysis.

Additional evidence of the occurrence of reaction 2 is provided by the cyclic voltammograms shown in Figure 2.5. In the absence of acid (Figure 2.5A), only a single reversible response, corresponding to the $VO(\text{salen})^{+/0}$ couple, is observed. However, in the presence of acid (Figure 2.5B) the occurrence of reaction 2 produces a second reversible response near 0.8 V that corresponds to the $V(\text{salen})^{2+/+}$ couple. This response can be detected at scan rates as high as $\sim 2.5 \text{ V s}^{-1}$ so that, under the experimental conditions employed, the disproportionation of $V^{IV} O(\text{salen})$ according to reaction 2 occurs within a few tenths of a second.

Quantitative Conversion of $V^{IV} O(\text{salen})$ to $V^{III}(\text{salen})^+$

In the absence of acid, $V^{IV} O(\text{salen})$ exhibits no reductive electrochemistry at potentials as negative as -1.6 V so that its direct reduction to the V(III) oxidation state is very slow. However, the reduction of $V^V O(\text{salen})^+$ (generated via reaction 2) to $V^{IV} O(\text{salen})$ followed by the recurrence of reaction 2 provides a pathway for the quantitative electrolytic conversion of $V^{IV} O(\text{salen})$ to $V^{III}(\text{salen})^+$. To avoid the presence

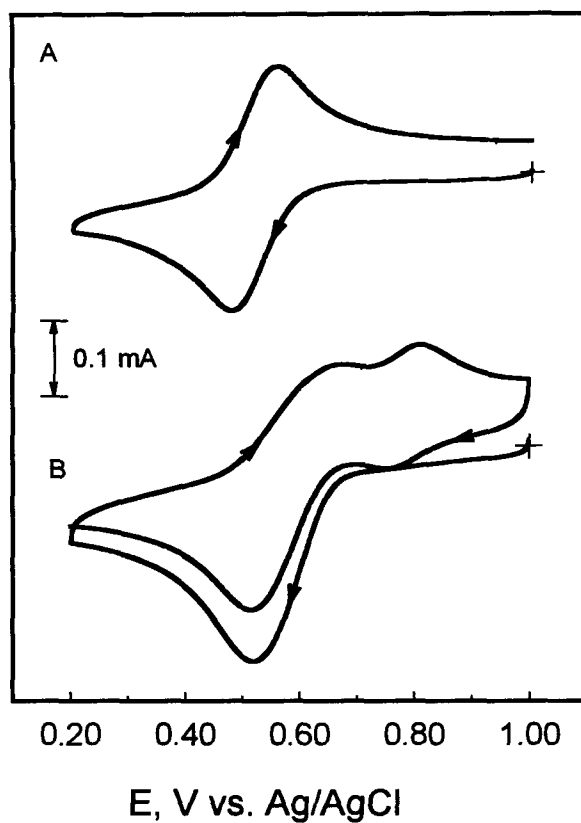
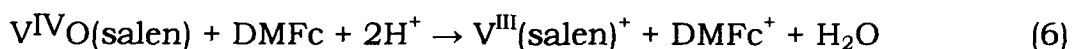


Figure 2.5. Cyclic voltammetry of a 1.0 mM of a solution of $\text{V}^{\text{V}}\text{O}(\text{salen})^+$ (prepared by electro-oxidation of $\text{V}^{\text{IV}}\text{O}(\text{salen})$). (A) before and (B) after the solution was made 2 mM in $\text{CF}_3\text{SO}_3\text{H}$. Supporting electrolyte: 0.1 M TBAPF_6 ; scan rate: 250 mV s^{-1} ; electrode: 5 mm diameter glassy carbon.

of supporting electrolytes required in electrolytic reductions, chemical reductants were examined. Decamethylferrocene (DMFc) proved to be suitable. Shown in Figure 2.6A, curve 1, is the steady-state voltammogram obtained with a solution that contained 1 mM $V^{IV}O(\text{salen})$ and 1 mM DMFc. The anodic wave near 0 V corresponds to the oxidation of DMFc to $DMFc^+$ and that at 0.65 V to the oxidation of $V^{IV}O(\text{salen})$. (The larger plateau current for the first wave reflects the larger diffusion coefficient of DMFc.) The addition of 2 millimoles per liter of CF_3SO_3H to the solution used to record curve 1 caused the steady-state voltammogram to change into the one shown in curve 2. The wave for the oxidation of $V^{IV}O(\text{salen})$ has been replaced by the wave near 0.9 V corresponding to the oxidation of $V^{III}(\text{salen})^+$ and the DMFc has been oxidized to $DMFc^+$, which is responsible for the cathodic wave near 0 V. Thus, the addition of two equivalents of acid caused reaction 6 to proceed quantitatively.



The loss of the vanadium-oxo bond as a result of reaction 6 was confirmed by comparison of the IR spectra of two solutions similar to those in Figure 2.6A. As shown in Figure 2.5B, a band at 985 cm^{-1} , present in the original solution of $V^{IV}O(\text{salen})$ and originating in the $V=O$

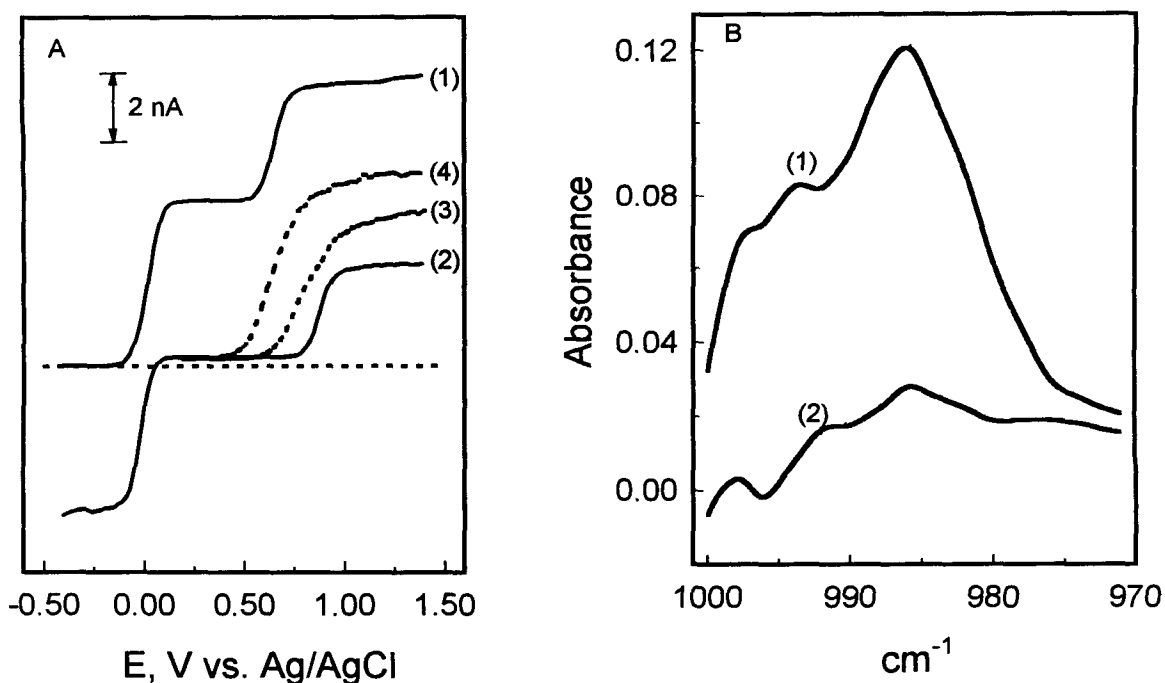


Figure 2.6. (A) Steady-state voltammetry in a solution containing 1.0 mM $V^{IV}O(\text{salen})$ and 1 mM DMFc before (1) and after (2) the solution was made 2 mM in CF_3SO_3H . The dotted curves are the responses obtained when the solution was subsequently made 0.1 M (curve 3) or 1.0 M (curve 4) in H_2O . Other conditions as in Figure 2.1. (B) Infrared spectra of (1) 2 mM $V^{IV}O(\text{salen})$ in CH_3CN ; (2) a mixture of 2 mM $V^{IV}O(\text{salen})$, 2 mM DMFc and 4 mM CF_3SO_3H .

stretching mode,⁹ is absent after the addition of acid caused reaction 6 to occur.

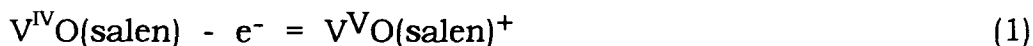
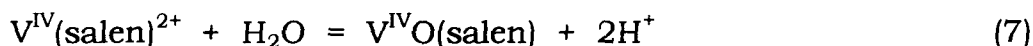
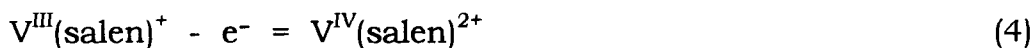
A solid sample of $V(\text{salen})[\text{CF}_3\text{SO}_3]\cdot(\text{CH}_3\text{CN})_2$, prepared by reduction of $\text{VO}(\text{salen})$ with H_2 in the presence of acid (see Experimental Section), also lacked the IR peak at 985 cm^{-1} that was present in solid samples of $\text{V}^{\text{IV}}\text{O}(\text{salen})$. Thus, the reduction of $\text{V}^{\text{IV}}\text{O}(\text{salen})$ in acidified acetonitrile produces an oxo-free complex that probably contains CH_3CN molecules as axial ligands.

Electrochemical Behavior of $\text{V}^{\text{III}}(\text{salen})^+$

The anodic wave near 0.9 V in curves 2 of Figures 2.1 and 2.6A was attributed to the oxidation of $\text{V}^{\text{III}}(\text{salen})^+$. In accord with this assignment, solutions prepared from isolated samples of $V(\text{salen})[\text{CF}_3\text{SO}_3]\cdot(\text{CH}_3\text{CN})_2$ exhibited a single anodic wave identical to those in curve 2 of Figures 2.1 and 2.6A. The magnitude of the anodic plateau current in curve 2 of Figure 2.6A is comparable to that for the one-electron oxidation of $\text{V}^{\text{IV}}\text{O}(\text{salen})$ in curve 1 which suggests that a one-electron oxidation of $\text{V}^{\text{III}}(\text{salen})^+$ to $\text{V}^{\text{IV}}(\text{salen})^{2+}$ is occurring. However, when a solution like the one used to record curve 2 in Figure 2.6A was subjected to controlled potential oxidation at 1.2 V using a large area glassy carbon electrode (after 0.1 M TBAPF_6 was added as a supporting electrolyte), two electrons were removed from each $\text{V}^{\text{III}}(\text{salen})^+$ molecule and the solution turned

deep blue, the color characteristic of $V^VO(salen)^+$. The electrolyzed solution also contained acid (presumably generated during the electrolysis) because a small quantity of $V^{IV}O(salen)$ added to the electrolyzed solution disproportionated into $V^{III}(salen)^+$ and $V^VO(salen)^+$ instead of remaining as $V^{IV}O(salen)$ with its characteristic oxidation potential. The behavior observed can be understood on the basis of the set of reactions in Scheme I.

Scheme I



The oxidation of $V^{III}(salen)^+$ begins with a one-electron oxidation (half-reaction 4). The resulting oxophilic $V^{IV}(salen)^{2+}$ would be expected to undergo reaction with the residual H_2O that was released during the preparation of the $V^{III}(salen)^+$ solution and the resulting $V^{IV}O(salen)$ would be electro-oxidized to $V^VO(salen)^+$ (half-reaction 1) at the positive potential (1.2 V) where the electrolysis was carried out. Thus, an overall two-electron oxidation of $V^{III}(salen)^+$ is obtained. The anodic plateau current in curve 2 of Figure 2.6A corresponds to only a one-electron oxidation because reaction 7 proceeds too slowly to affect the plateau

current in the microelectrode voltammograms that were recorded in *ca.* one minute, but during the 30-40 minutes required for controlled potential electrolysis experiments, reaction 7 has time to occur and two-electrons are removed from each $V^{III}(\text{salen})^+$ complex.

Additional support for Scheme I was obtained when increasing quantities of water were added to solutions of $V^{III}(\text{salen})^+$. The dotted curves in Figure 2.6A show the increases in anodic current produced by the addition of H_2O . The interpretation is that the added water caused the rate of reaction 7 (Scheme I) to increase so that half-reaction 1 could contribute to the anodic plateau current. With 1 M H_2O the magnitude of the current had almost doubled as expected on the basis of Scheme I.

Reaction Between $V^{III}(\text{salen})^+$ and O_2

$V^{III}(\text{salen})^+$ in acetonitrile reacts with O_2 to produce $V^VO(\text{salen})^+$ according to reaction 8:

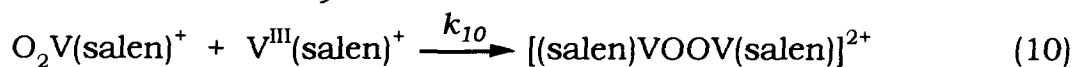
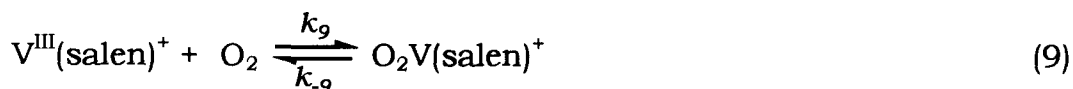


The stoichiometry of reaction 8 was examined by adding measured aliquots of a standard solution of $V^{III}(\text{salen})^+$ in CH_3CN to a solution containing excess O_2 in CH_3CN and measuring (either electrochemically or spectrophotometrically) the quantity of $V^VO(\text{salen})^+$ produced. The conversion of $V^{III}(\text{salen})^+$ to $V^VO(\text{salen})^+$ was quantitative. The ^{51}V NMR

spectrum of the reaction solution also confirmed the production of $V^V O(\text{salen})^+$. The possibility that H_2O_2 might have been among the products of reaction 8 was ruled out by the observation that H_2O_2 oxidizes $V^{III}(\text{salen})^+$ rapidly and quantitatively to $V^V O(\text{salen})^+$.

The kinetics of reaction 8 were examined spectrophotometrically by monitoring the increase in the concentration of $V^V O(\text{salen})^+$. Shown in Figure 2.7A are the absorption spectra of $V^{III}(\text{salen})^+$ and $V^V O(\text{salen})^+$ in acetonitrile. The absorbance at 570 nm is dominated by the oxidized complex so that the reaction was conveniently followed at this wavelength. Typical pseudo-first order kinetic plots (with O_2 in excess) are shown in Figure 2.7B. The linearity of the plots and the ratio of their slopes demonstrated that the reaction rate was first order with respect to $V^{III}(\text{salen})^+$ and O_2 , respectively. A likely mechanism consistent with this behavior is given in Scheme II.

Scheme II



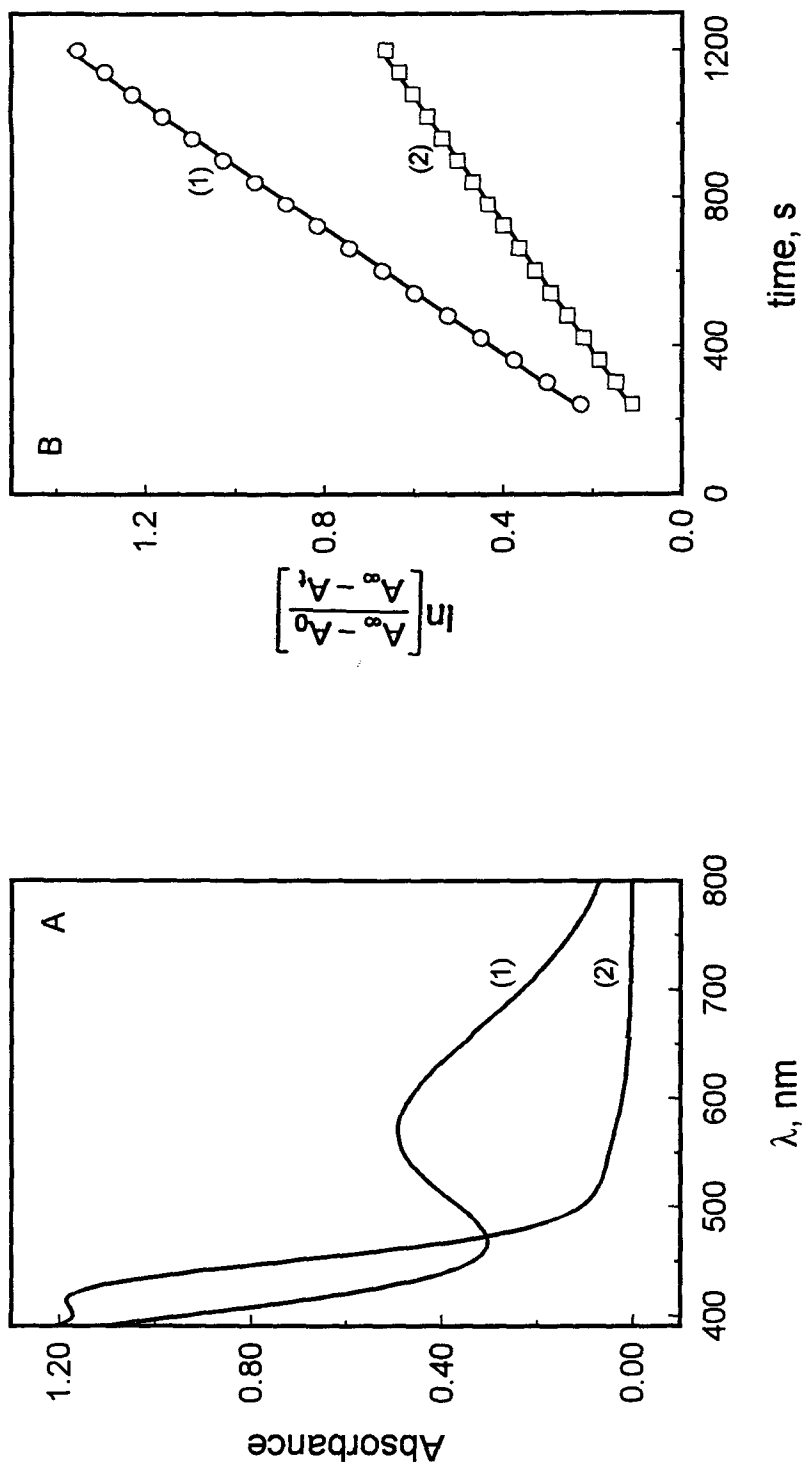


Figure 2.7. (A). UV-vis spectra of (1) $V^VO(salen)^+$ and (2) $V^III(salen)^+$ in CH_3CN . Concentration of complexes: 0.4 mM; Optical path length: 1 cm. (B) Pseudo-first-order kinetic plots for the reaction between (1) 0.4 mM $V^III(salen)^+$ and 8.1 mM O_2 ; (2) 0.2 mM $V^III(salen)^+$ and 4.0 mM O_2 as monitored spectrophotometrically at 570 nm. A_0 = initial absorbance; A_t = absorbance at time t ; A_∞ = absorbance after the completion of the reaction.

Applying the steady-state approximation to $[\text{O}_2\text{V}(\text{salen})]^+$ and $[(\text{salen})\text{VOOV}(\text{salen})]^{2+}$ leads to the rate law in equation 12

$$\frac{-d[\text{V}^{\text{III}}(\text{salen})^+]}{dt} = \frac{2k_9k_{10}[\text{V}^{\text{III}}(\text{salen})^+]^2[\text{O}_2]}{k_{-9} + k_{10}[\text{V}^{\text{III}}(\text{salen})^+]} \quad (12)$$

The observed first order dependence of the rate on $[\text{V}^{\text{III}}(\text{salen})^+]$ implies that $k_{-9} \ll k_{10} [\text{V}^{\text{III}}(\text{salen})^+]$ so that the rate law becomes

$$\frac{-d[\text{V}^{\text{III}}(\text{salen})^+]}{dt} = 2k_9[\text{V}^{\text{III}}(\text{salen})^+][\text{O}_2] \quad (13)$$

Kinetic plots of the integrated rate law (Figure 2.7B) correspond to a value of $0.07 \text{ M}^{-1} \text{ s}^{-1}$ for k_9 . The kinetics of reaction 8 are more complicated when larger concentrations of $\text{V}^{\text{III}}(\text{salen})^+$ are employed: Behavior consistent with Scheme II is observed initially but deviations occur at later times. The origin of this behavior is still under investigation.

DISCUSSION

Comparison with Previous Studies

Examination of the behavior of $\text{V}^{\text{IV}}\text{O}(\text{salen})$ in acetonitrile in the presence of $\text{CF}_3\text{SO}_3\text{H}$, but no other supporting electrolyte, established that disproportionation induced by the added acid controls the electrochemical behavior. The interpretations proposed in the present

study have elements in common with those offered in two previous reports,^{1, 4} but there are also some significant differences.

The puzzling and unexpected coincidence of the formal potentials for the $\text{VO}(\text{salen})^{+/0}$ and $\text{V}(\text{salen})^{2+/+}$ couples reported by Tsuchida et al.⁴ was based on the development of a composite anodic/cathodic wave when acid was added to solutions of $\text{V}^{\text{IV}}\text{O}(\text{salen})$ containing TBABF_4 as supporting electrolyte (as in curves 3 and 4 of Figure 2.1). However, with anhydrous acetonitrile, no composite wave develops in the absence of supporting electrolyte (curve 2 of Figure 2.1) or in the presence of supporting electrolytes that do not contain BF_4^- anions. The behavioral pattern suggests that BF_4^- may exhibit significant basicity in CH_3CN . This basicity of BF_4^- was confirmed qualitatively by experiments with "neutral red," an acid-base indicator: Addition of 50 mM TBABF_4 to a solution containing 10^{-5} M neutral red and 2 mM $\text{CF}_3\text{SO}_3\text{H}$ in acetonitrile changed the color of the solution from red, the color of the acid form of the indicator, to blue, the color of the base form of the indicator. Such a color change could not occur when same amount of TBAPF_6 , TBAClO_4 , or $\text{TBACF}_3\text{SO}_3$ was used. Following the procedures of Kolthoff et al.^{10, 11} the same indicator was employed to measure the pK_a for HBF_4 in CH_3CN (see Appendix II-A for details). The value obtained, $\text{pK}_a = 5.0$, is comparable to the value for HBr ($\text{pK}_a = 5.5^{10}$) but much higher than that for HClO_4

($pK_a = 1.6^{12}$) or CF_3SO_3H ($pK_a = 2.6^{12}$). Thus, BF_4^- is a considerably stronger base in CH_3CN than are ClO_4^- and $CF_3SO_3^-$. The basic character of BF_4^- anions in CH_3CN could cause reaction 2 to proceed only part way in the presence of stoichiometric quantities of strong acids (CF_3SO_3H or $HClO_4$) in supporting electrolytes containing BF_4^- anions. Such behavior would account for the composite cathodic/anodic wave observed by Tsuchida et al.⁴ because both $V^{IV}O(salen)$ and $V^VO(salen)^+$ (as well as $V^{III}(salen)^+$) would have been present in their solutions. In acidified supporting electrolytes containing less basic ClO_4^- , $CF_3SO_3^-$ or PF_6^- anions, we observe only well-separated cathodic and anodic waves. It now seems clear that Tsuchida et al.⁴ were misled by the appearance of the composite cathodic/anodic wave in their experiments.

Bonadies et al.¹ reported results similar to those shown in curve 2 of Figure 2.1 when $HClO_4$ (presumably a concentrated aqueous solution) was added to solutions of $V^{IV}O(salen)$ in acetonitrile containing 0.1 M $TBAPF_6$ as supporting electrolyte. An acid-induced disproportionation of the $V^{IV}O(salen)$ was proposed but the stoichiometry of the reaction appeared to require two equivalents of acid for each $V^{IV}O(salen)$ complex rather than the single equivalent of acid we found to be sufficient to cause reaction 2 to proceed quantitatively (curve 2 in Figure 2.1). We believe the difference can be attributed to the presence of water in

solutions of HClO_4 . (The commercially available 70% solution of HClO_4 contains 27.2 M H_2O .) The acidity of HClO_4 in (wet) acetonitrile is weaker than that of anhydrous $\text{CF}_3\text{SO}_3\text{H}$ so that additional HClO_4 is required to force reaction 2 to completion. When water was added to the anhydrous $\text{CF}_3\text{SO}_3\text{H}$ (or to anhydrous acetonitrile, see Figure 2.2), or if the commercially available acetonitrile solvent was not subjected to a desiccating treatment before it was used, more than one equivalent of the acid was required to cause reaction 2 to proceed quantitatively.

The results of the present re-examination of the system indicate that the acid-induced “deoxygenation” reaction proposed by Tsuchida et al.⁴ and the acid-induced disproportionation reaction proposed by Bonadies et al.¹ can be assigned to the same process, reaction 2, which goes to completion in the absence of BF_4^- or excess H_2O but reaches an intermediate equilibrium state in their presence unless significant excesses of acid are added. Thus, except for its stoichiometry, the disproportionation step originally proposed by Bonadies et al. (1) is fully supported by the present results.

Tsuchida et al.⁴ also proposed an important role for an oxo-bridged dimer, $(\text{salen})\text{VOV}(\text{salen})^{2+}$, in the electrochemical responses of acidified solutions of $\text{V}^{\text{IV}}\text{O}(\text{salen})$ in $\text{CH}_3\text{CN}/0.1 \text{ M TBABF}_4$. Similar oxo-bridged oligomers have been reported in crystalline samples by Leigh and co-workers² but their persistence in dilute CH_3CN solutions is doubtful. For

example, acidified solutions of $V^{IV}O(\text{salen})$ in CH_3CN containing BF_4^- which exhibit a composite wave like curve 4 in Figure 2.1, give ESR spectra indicating the presence of only $V^{IV}O(\text{salen})$, not the $V^{IV}(\text{salen})^{2+}$ complex, which was proposed in reference 4 to result from the dissociation of the oxo-bridged dimeric complex. The electrochemical results obtained in the present study were satisfactorily accounted for without the need to invoke the presence of stable dimeric species. The formal potentials and diffusion coefficients reported for the dimeric complexes in reference 4 should be disregarded.

In addition, the diffusion coefficients that were reported in reference 4 require correction in the light of the present results. Revised values are listed in Table 2.2.

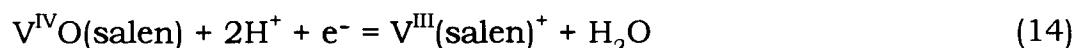
Table 2.2. Diffusion Coefficients for Complexes
Examined in This Study^a

Complex	$10^5 D, \text{cm}^2 \text{s}^{-1}$
$V^VO(\text{salen})^+$	1.0
$V^{IV}O(\text{salen})$	1.2
$V^{III}(\text{salen})^+$	1.0

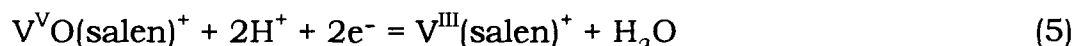
^a Calculated from plateau currents at rotating glassy carbon disk electrodes in CH_3CN containing 0.1 M TBAPF_6 .

Thermodynamic Properties of the System

The equilibrium constant obtained for the disproportionation reaction, $K_2 = 1.6 \times 10^6 \text{ M}^{-1}$, can be combined with the formal potential of the $\text{VO}(\text{salen})^{+/0}$ couple, 0.51 V, to calculate the formal potential for half-reaction 14, $E^f = 0.88 \text{ V}$



and half reaction 5, $E^f = 0.70 \text{ V}$



Comparing the formal potential of half-reaction 14 with that of the $\text{VO}(\text{salen})^{+/0}$ indicates that in the presence of (1 M) acid, $\text{V}^{\text{IV}}\text{O}(\text{salen})$ is a considerably stronger one-electron oxidant than is $\text{V}^{\text{VO}}(\text{salen})^+$, an observation that accounts for the acid-induced disproportionation of $\text{V}^{\text{IV}}\text{O}(\text{salen})$.

A likely mechanism for the disproportionation reaction might begin with the removal of the oxo group from $\text{V}^{\text{IV}}\text{O}(\text{salen})$ by the added acid according to reaction 15:



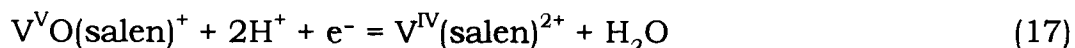
followed by a simple, outer-sphere oxidation of a second $\text{V}^{\text{IV}}\text{O}(\text{salen})$ molecule by $\text{V}^{\text{IV}}(\text{salen})^{2+}$ according to reaction 16 for which an

equilibrium constant of 3.8×10^4 can be calculated:

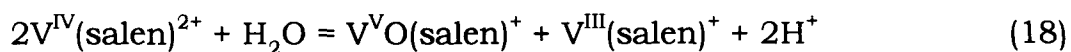


The equilibrium constant for reaction 15 can be calculated from those of reactions 2 (the disproportionation reaction) and 16: $K_{15} = 42 \text{ M}^{-1}$. The combination of reactions 15 and 16 accounts for the observed stoichiometry of the disproportionation reaction.

Combining the equilibrium constant of reaction 15 with the formal potential of the $\text{VO}(\text{salen})^{+/0}$ couple gives the formal potential for another reaction, half-reaction 17, $E^{\text{f}} = 0.61 \text{ V}$.



Comparing this value with the formal potential for the $\text{V}(\text{salen})^{2+/+}$ couple, 0.78 V, indicates that in the presence of water (as long as its concentration is comparable to that of H^+), $\text{V}^{\text{IV}}(\text{salen})^{2+}$ is a stronger one-electron reducing agent than is $\text{V}^{\text{III}}(\text{salen})^+$, an observation which predicts that $\text{V}^{\text{IV}}(\text{salen})^{2+}$ would disproportionate under this condition according to reaction 18.



A likely mechanism for this water-induced disproportionation

reaction might begin with the addition of the oxo group from water to the oxophilic $V^{IV}(\text{salen})^{2+}$, i.e., the reverse of reaction 15, followed by reaction 16. The equilibrium constant for reaction 18 can also be calculated from those of reactions 15 and 16, $K_{18} = K_{16}/K_{15} = 9.0 \times 10^2$ M. This value indicates that $V^{IV}(\text{salen})^{2+}$ would disproportionate considerably in the presence of water, especially when the acid concentration is low. Thus, it is not surprising that the $V^{IV}(\text{salen})^{2+}$, generated by electro-oxidizing $V^{III}(\text{salen})^+$, does not persist because of the water produced during the preparation of $V^{III}(\text{salen})^+$, and the residual water in the acetonitrile solvent, which (initially) also contains no acid. The resulting product can only be $V^VO(\text{salen})^+$.

A possible strategy to obtain $V^{IV}(\text{salen})^{2+}$ is to add excess acid to the solvent to eliminate the disproportionation of $V^{IV}(\text{salen})^{2+}$, but the acid results in the decomposition of the complex (see below). This problem can be solved by using another analogous complex which is more stable towards acid. The details will be described in Chapter V.

The formal potentials calculated in this section are collected in Table 2.3. These values should supercede those given in reference 4.

Table 2.3. Formal Potentials for Redox Couples Examined in This Study^a

Redox Couple	E ^f , V vs Ag/AgCl ^b
VO(salen) ^{+ / 0}	0.51
V(salen) ^{2+ / +}	0.78
V ^{IV} O(salen) + 2H ⁺ + e ⁻ = V ^{III} (salen) ⁺ + H ₂ O	0.88 ^c
V ^V O(salen) ⁺ + 2H ⁺ + 2e ⁻ = V ^{III} (salen) ⁺ + H ₂ O	0.70 ^c
V ^V O(salen) ⁺ + 2H ⁺ + e ⁻ = V ^{IV} (salen) ²⁺ + H ₂ O	0.61 ^d

^a The potentials apply to anhydrous CH₃CN in the presence of 0.1 M supporting electrolyte (TBAClO₄ or TBAPF₆). The values supercede those given in reference 4.

^b The potential of the ferrocenium/ferrocene couple was 0.44 V vs. this reference electrode.

^c Calculated from the equilibrium constant for reaction 2 and E^f for VO(salen)^{+ / 0}.

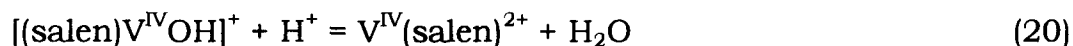
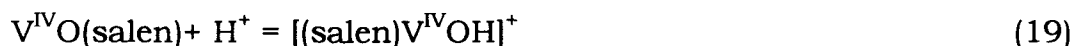
^d Calculated from the equilibrium constant for reaction 15 and E^f for VO(salen)^{+ / 0}.

Digital Simulation of the System

The disproportionation of $V^{IV}O(\text{salen})$, i.e., reaction 2, was found to proceed quite rapidly. From the cyclic voltammograms of $V^VO(\text{salen})^+$ in the presence of acid (Figure 2.5), a qualitative rate for the disproportionation was obtained. (The half-life is less than a few tenths of a second, see Page II-16.) Now that the thermodynamic properties about the system are known, kinetic information about the disproportionation can be estimated in a more quantitative manner through the digital simulation of the reduction of $V^VO(\text{salen})^+$ in the presence of acid. The details of the simulation will be described in Appendix II-B. Following is a summary of the simulation results.

The plateau currents of a rotating disk electrode (RDE), rather than the peak currents of from cyclic voltammograms (such as Figure 2.5), were simulated because of the simplicity of the steady-state behavior of the RDE. The mechanism used for the simulation is shown in Scheme III.

Scheme III



In this scheme, the sum of reactions 19 and 20 corresponds to reaction

15, the equilibrium constant of which was already obtained earlier. At potentials on the plateau of the reduction of $V^V O(\text{salen})^+$, the current is limited by the diffusion of $V^V O(\text{salen})^+$. Assuming the rate of reaction 16 is also limited by diffusion, the observed current would be limited by the rate of reactions 19 and 20. Through the simulation of the reduction of $V^V O(\text{salen})^+$ at different concentrations and in the presence of different amounts of acids, it was obtained that the second-order rate constants of reactions 19 and 20 have the magnitude of $10^8 \text{ M}^{-1} \text{ s}^{-1}$, close to the diffusion-limited value.¹⁴ It can thus be concluded that the acid-induced disproportionation of $V^V O(\text{salen})$ proceeds at such a rate.

Instability of V-salen Complexes towards Acid

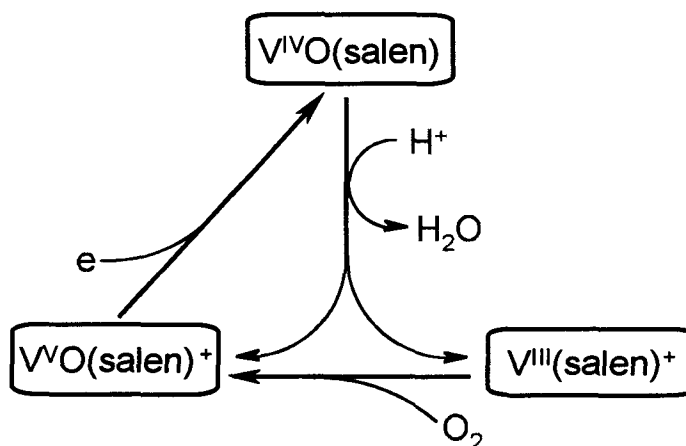
The voltammetric responses obtained with pure solutions of $V^{III}(\text{salen})^+$ or $V^V O(\text{salen})^+$ are quite stable in the absence of acid. $V^V O(\text{salen})^+$ is equally stable in the presence of acid but $V^{III}(\text{salen})^+$ is slowly decomposed by millimolar acid. When a mixture of $V^{III}(\text{salen})^+$ and $V^V O(\text{salen})^+$ is exposed to acid, the voltammetric response changes slowly: The plateau currents for the oxidation of $V^{III}(\text{salen})^+$ and the reduction of $V^V O(\text{salen})^+$ gradually diminish as a second anodic wave develops that corresponds to the oxidation of $V^{IV} O(\text{salen})$. This behavior reflects more than a slow approach to equilibrium of reaction 2 because the overall magnitude of the plateau currents falls below the values

expected for an equilibrated mixture of the three complexes. The ESR spectrum of aged mixtures of $V^{III}(\text{salen})^+$ and $V^VO(\text{salen})^+$ indicates the presence of both $V^{IV}O(\text{salen})$ and a second V(IV) complex generated as the mixture decomposes. This behavior can be understood if the $V^{III}(\text{salen})^+$ complex is presumed to decompose in the presence of acid to yield a complex of V(III) that is a stronger reducing agent so that it can reduce $V^VO(\text{salen})^+$ to produce $V^{IV}O(\text{salen})$ and a decomposed complex of V(IV) that is not electroactive in the potential range of interest. This explanation is in accord with the observation that addition of H_2O to mixtures of $V^{III}(\text{salen})^+$ and $V^VO(\text{salen})^+$ accelerates their decomposition as comproportionation (the reverse of reaction 2) generates acid that causes the $V^{III}(\text{salen})^+$ complex to decompose. The smaller plateau currents in curves 3 and 4 of Figure 2.1 can also be understood on the same basis.

Reactions with O_2

The reactions in Scheme II account for the kinetics observed during the stoichiometric oxidation of $V^{III}(\text{salen})^+$ by O_2 . The proposed formation of a $O_2V(\text{salen})^+$ complex in reaction 9 has precedent in the results of Swinehart who examined the reaction of $V^{III}(\text{salen})^+$ with O_2 in pyridine.¹³ However, in this solvent, the oxidation proceeds only to $V^{IV}O(\text{salen})$. The reactions in Scheme II occur both in the absence and in the presence of

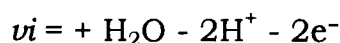
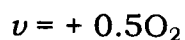
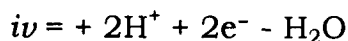
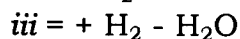
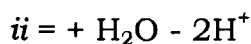
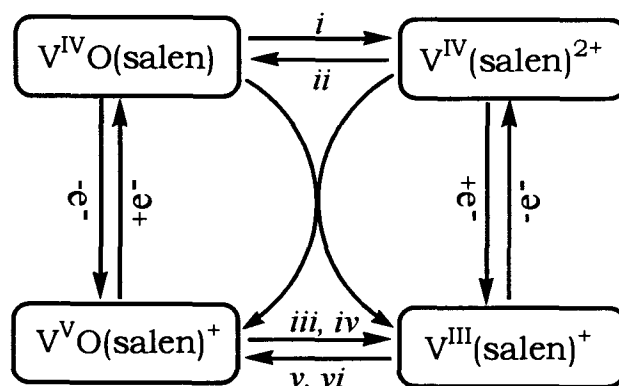
acid but the reduction of O_2 ceases once all of the $V^{III}(\text{salen})^+$ is oxidized to $V^VO(\text{salen})^+$. However, in the presence of excess acid, the combination of Scheme II and the electrochemical regeneration of $V^{III}(\text{salen})^+$ (via half-reaction 3 followed by reaction 2) provides a catalytic route for the four-electron electroreduction of O_2 as shown in Scheme IV. For the current system, two problems must be overcome in order to achieve efficient catalytic reduction of O_2 via this route. First, the rate of this catalytic cycle is too slow and is limited by the reaction between $V^{III}(\text{salen})^+$ and O_2 . The kinetics is probably retarded by the CH_3CN molecules coordinated to the axial sites in $V^{III}(\text{salen})^+$. Second, the acid-induced decomposition of the complex is an undesirable side-reaction. These problems will be attacked by exploring the properties of analogous vanadium-Schiff base complexes in the next chapter.

Scheme IV

CONCLUSIONS

In an attempt to uncover the origin of puzzling results reported in previous studies,^{1, 4} the coordination chemistry and electrochemistry of V(III, IV, V)-salen complexes in acetonitrile containing no supporting electrolytes were examined using steady-state microelectrode voltammetry and other spectroscopic techniques. The interconversions among the several V-salen complexes that were demonstrated in this study are summarized in Scheme V. The chemistry shown in this

Scheme V



scheme is largely supportive of the acid-induced disproportionation of $\text{V}^{\text{IV}}\text{O}(\text{salen})$ as originally proposed by Bonadies et al.,¹ except for the

stoichiometry of the disproportionation reaction. The source of the puzzling results reported by Tsuchida et al.⁴ was identified to be the BF_4^- anion of the supporting electrolyte employed by the authors, which was found to exhibit considerable basicity in acetonitrile. Modifications required in the previous interpretations are specified and corrected values of formal potentials and diffusion coefficients are also given. The equilibrium constant of the acid-induced disproportionation of $\text{V}^{\text{IV}}\text{O}(\text{salen})$ was measured.

In addition, the complex that plays the key role in the four-electron reduction of O_2 was shown to be $\text{V}^{\text{III}}(\text{salen})^+$. A simple yet efficient method to prepare this complex was devised by using H_2 as a clean reducing agent to reduce $\text{V}^{\text{V}}\text{O}(\text{salen})^+$ (or $\text{V}^{\text{IV}}\text{O}(\text{salen})$ in the presence of acid). The stoichiometry and kinetics of the reaction between $\text{V}^{\text{III}}(\text{salen})^+$ and O_2 were studied and a possible mechanism is proposed for the catalysis by the V-salen complexes of the electroreduction of O_2 by four electrons in acidified acetonitrile. The current system is limited by the slow kinetics of the catalytic cycle and the undesirable acid-induced decomposition of the catalyst. Future efforts are directed to develop more catalytically interesting systems by improving the stability of catalysts towards acid and enhancing the rate of the reaction between V(III) complexes and O_2 .

APPENDIX II-A**Determination of the pK_a for HBF₄ in Acetonitrile**

Following the procedures of Kolthoff et al.^{10, 11} the acid-base indicator “neutral red” was employed to measure the pK_a for HBF₄ in CH₃CN. The indicator has a pK_a of 6.0 in CH₃CN. Its acid and base forms are red and blue and exhibit absorption maxima at 608 nm and 530 nm, respectively. From the UV-Vis. spectra of the two forms as shown in Figure 2.8, it can be seen that the base form has no absorption at 608 nm.

The determination of the pK_a for HBF₄ was started with a solution containing 1.0×10^{-5} M neutral red and 2.0 mM CF₃SO₃H. The indicator in this solution existed as its acid form, HIn, as seen from its absorption spectrum (curve 1 in Figure 2.9). Addition of TBABF₄ to this solution resulted in the conversion of the indicator from its acid form to its base form, In, because of the basicity of the BF₄⁻ anion. By monitoring the spectrum change (Figure 2.9), the pH of the solution can be calculated using the Henderson-Hasselbalch equation:

$$\begin{aligned} \text{pH} &= \text{pK}_a (\text{HIn}) - \log([\text{HIn}]/[\text{In}]) \\ &= 6.0 - \log[A/(A_0 - A)] \end{aligned} \quad (21)$$

where A₀ and A are the absorbance of the indicator at 608 nm (at which the base form has no absorption) before and after the addition of TBABF₄. For HBF₄, the same equation applies, i.e.,

$$\text{pH} = \text{pK}_a (\text{HBF}_4) - \log\left(\frac{[\text{HBF}_4]}{[\text{BF}_4^-]}\right) \quad (22)$$

The concentration of HBF_4 can be approximated as 2 mM, assuming complete dissociation of $\text{CF}_3\text{SO}_3\text{H}$. The concentration of BF_4^- can then be simply obtained by subtracting 2 mM from the total analytical concentration of TBABF_4 . A plot of pH vs. the log term would give a straight line and its intercept would be the desired pK_a . Figure 2.10 shows such a plot based on the data from Figure 2.9. A pK_a of 5.0 for HBF_4 is thus obtained.

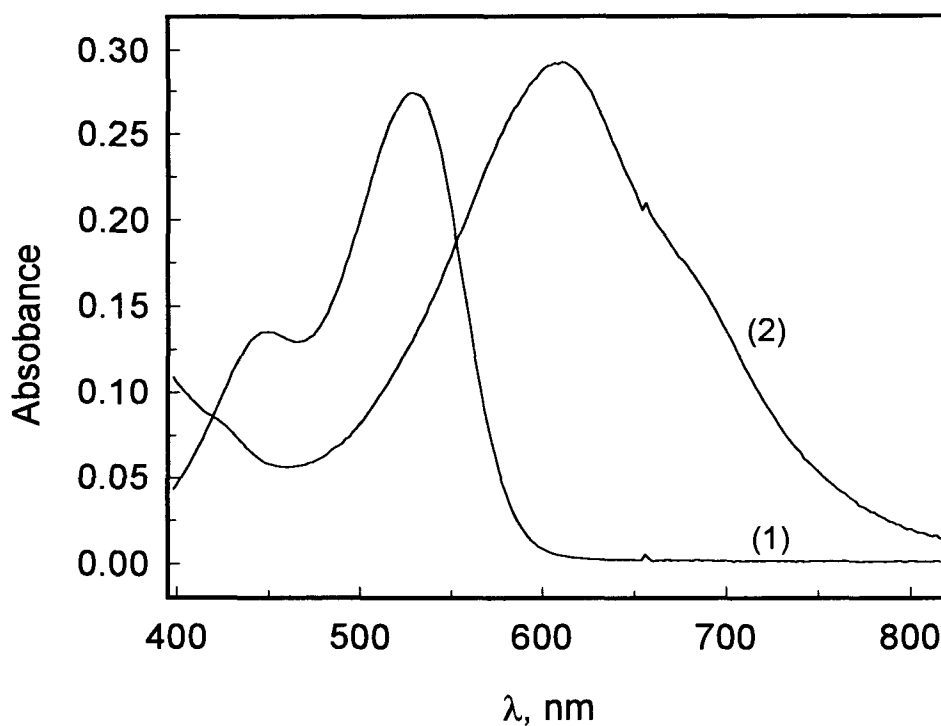


Figure 2.8. UV-Vis. spectra of (1) 1.0×10^{-5} M neutral red in its base form in acetonitrile. (2) after the solution used to record curve 1 was made 2 mM in $\text{CF}_3\text{SO}_3\text{H}$ so that the indicator was converted into its acid form. The spectra were recorded with a 10 cm quartz cell and pure acetonitrile was used as the background.

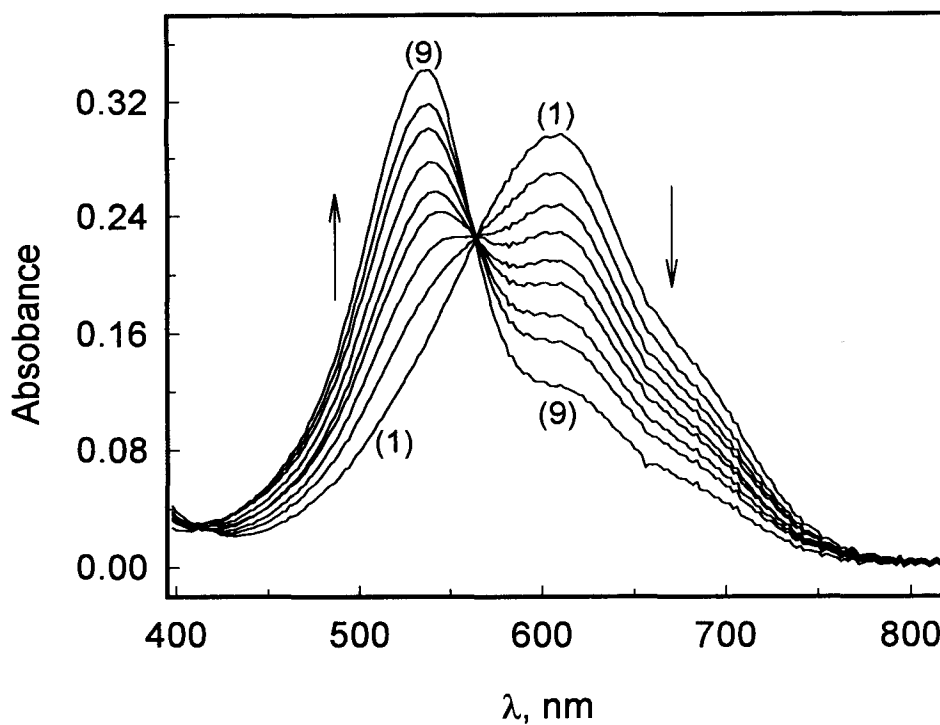


Figure 2.9. UV-Vis. spectra of an acetonitrile solution containing 1.0×10^{-5} M neutral red and 2 mM $\text{CF}_3\text{SO}_3\text{H}$ after this solution was made (1) 0; (2) 4; (3) 6; (4) 8; (5) 10; (6) 12; (7) 16; (8) 20; (9) 30 mM in TBABF_4 . Other conditions as in Figure 2.8.

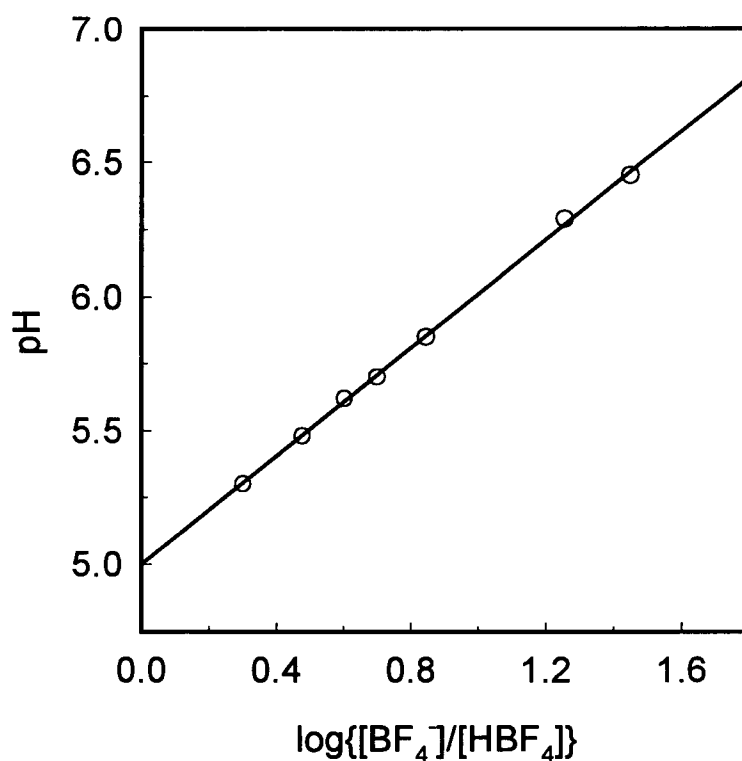


Figure 2.10. Determination of pK_a for HBF_4 in acetonitrile. The pH values were calculated based on the spectra in Figure 2.9 using equation 21. The intercept of the straight line on the pH axis gives $pK_a = 5.0$ for HBF_4 .

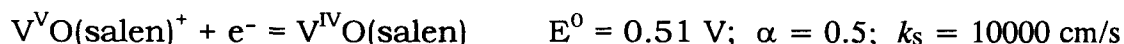
APPENDIX II-B**Digital Simulation of the Reduction of $V^V O(\text{salen})^+$
in Acetonitrile in the Presence of Acid**

Quantitative kinetic information about the acid-induced disproportionation of $V^{IV}O(\text{salen})$ can be obtained by digital simulation of the electrochemistry of $V^V O(\text{salen})^+$ in the presence of acid. The steady-state plateau currents of the reduction of $V^V O(\text{salen})^+$ at a rotating disk electrode were simulated with DigiSim[®] 3.05, a commercial software from Bioanalytical Systems. The parameters and mechanisms used in the simulation are listed in Scheme VI. In this scheme, the sum of reactions 19 and 20 corresponds to reaction 15, the equilibrium constant of which was already obtained earlier (42 M^{-1} , see Page II-31). At potentials on the plateau of the reduction of $V^V O(\text{salen})^+$, the current is limited by the diffusion of $V^V O(\text{salen})^+$. A high heterogeneous electron transfer rate constant was assigned to this reduction. Assuming the rate of reaction 16, a simple outsphere redox reaction between $V^{IV}(\text{salen})^{2+}$ and $V^{IV}O(\text{salen})$, is also limited by diffusion, the observed current would be limited by the rate of reactions 19 and 20. Using these thermodynamic data and other parameters in Scheme VI, the plateau currents of the reduction of $V^V O(\text{salen})^+$ at different concentrations and in the presence of different amounts of acids were simulated. The results are shown in Figures 2.11 and 2.12. It can be seen from these figures that the

simulated currents are in good agreement with the experimental data over a wide range of concentrations. The second-order rate constants of reactions 19 and 20 used in the simulation have the magnitude of $10^8 \text{ M}^{-1} \text{ s}^{-1}$. It can thus be concluded that the acid-induced disproportionation of $\text{V}^{\text{IV}}\text{O}(\text{salen})$ proceeds at a rate close to the diffusion-limited value.¹⁴

Scheme VI. Mechanism and parameters used for the digital simulation of the reduction of $V^VO(\text{salen})^+$ in the presence of acid

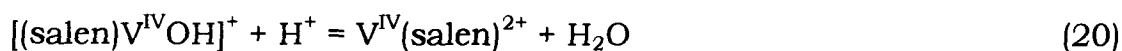
Charge transfer reaction:



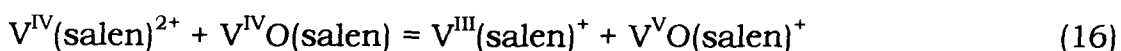
Homogeneous chemical reactions:



$$K = 10 \text{ M}^{-1}; k_f = 1 \times 10^8 \text{ M}^{-1} \text{ s}^{-1}$$



$$K = 4.2; k_f = 2 \times 10^8 \text{ M}^{-1} \text{ s}^{-1}$$



$$K = 3.8 \times 10^4; k_f = 1 \times 10^9 \text{ M}^{-1} \text{ s}^{-1}$$

Experimental parameters:

$E_{\text{start}} = 1 \text{ V}$; $E_{\text{switch}} = 0 \text{ V}$; $E_{\text{end}} = 0 \text{ V}$; Scan rate = 0.01 V/s ; $T = 298 \text{ K}$;
 $R_u = 0 \text{ } \Omega$; $C_{dl} = 0 \text{ F}$; cycles = 1; Electrode geometry = planar; Electrode
radius = 0.2999 cm ; Diffusion mode = hydrodynamic;
Kinematic viscosity = $0.0044 \text{ cm}^2/\text{s}$

Diffusion coefficients:

The available values from Table 2.2 were used for $V^VO(\text{salen})^+$, $V^{IV}O(\text{salen})$ and $V^{III}(\text{salen})^+$. A value of $1 \times 10^{-5} \text{ cm}^2/\text{s}$ were used for all other species.

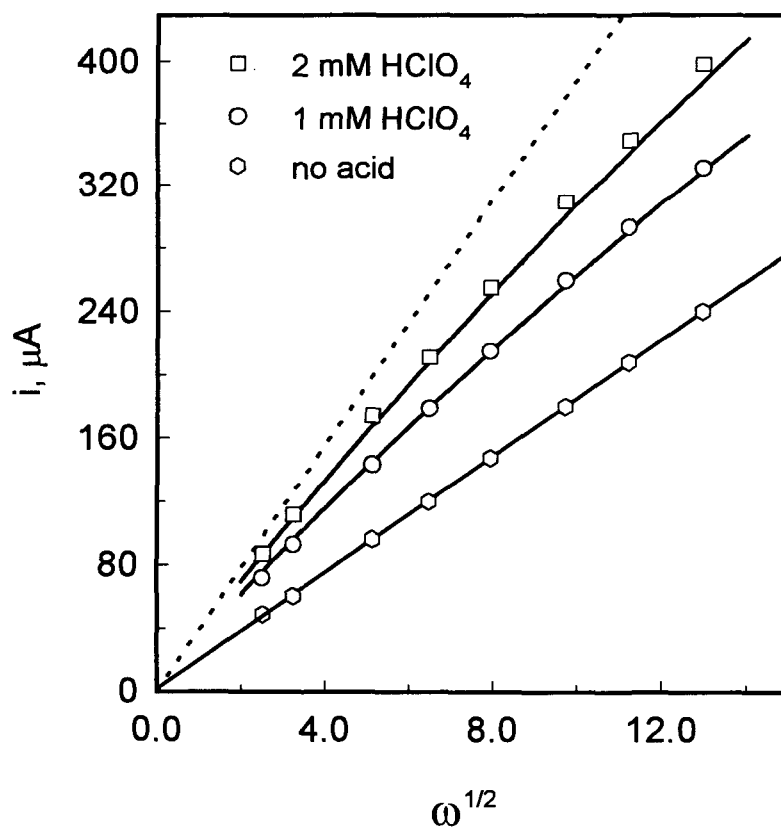


Figure 2.11. Simulated plateau currents (obtained with Scheme VI) for the reduction of 1.0 mM $\text{V}^{\text{V}}\text{O}(\text{salen})^+$ in the presence of different concentrations of HClO_4 in CH_3CN containing 0.1 M TBAClO_4 . A 6 mm glassy carbon rotating disk electrode was used. The symbols on the lines represent experimental values. The dotted line corresponds to the limiting case when $\text{V}^{\text{V}}\text{O}(\text{salen})^+$ is reduced by two electrons to form $\text{V}^{\text{III}}(\text{salen})^+$ (half-reaction 5).

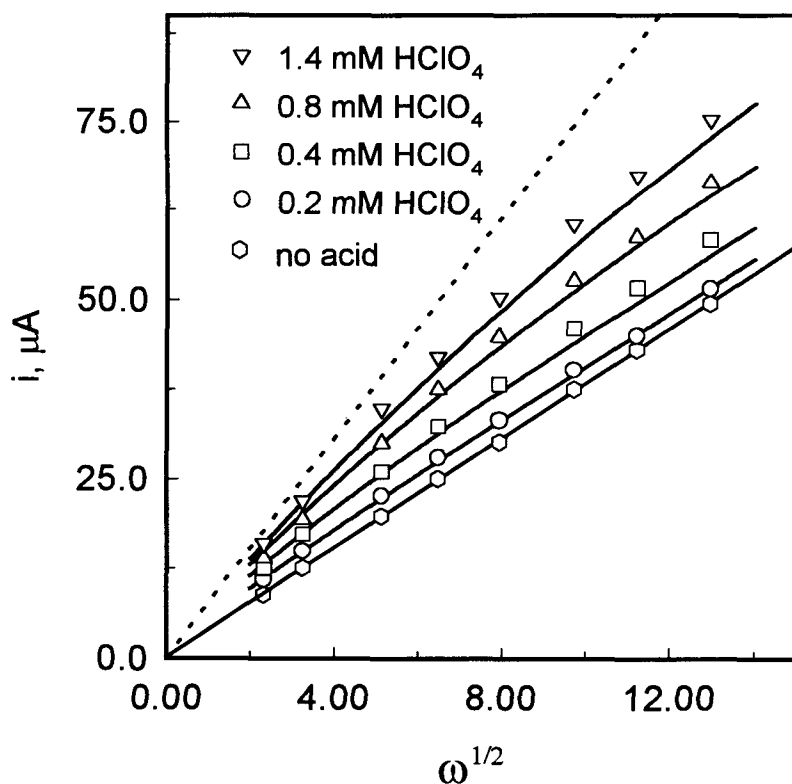


Figure 2.12. Simulated plateau currents for the reduction of 0.2 mM $\text{V}^{\text{VO}}(\text{salen})^+$ in the presence of different concentrations of HClO_4 in CH_3CN . The symbols on the lines represent experimental values. The dotted line corresponds to the limiting case when $\text{V}^{\text{VO}}(\text{salen})^+$ is reduced by two electrons to form $\text{V}^{\text{III}}(\text{salen})^+$ (half-reaction 5). Other conditions as in Figure 2.10.

REFERENCES

- (1) (a) Bonadies, J. A.; Pecoraro, V. L.; Carrano, C. J. *J. Chem. Soc., Chem. Commun.* **1986**, 1218. (b) Bonadies, J. A.; Butler, W. M.; Pecoraro, V. L.; Carrano, C. J. *Inorg. Chem.* **1987**, *26*, 1218.
- (2) (a) Fairhurst, S. A.; Hughes, D. L.; Kleinkes, U.; Leigh, G. J.; Sanders, J. R.; Weisner, J. *J. Chem. Soc., Dalton Trans.* **1995**, 321. (b) Fairhurst, S. A.; Hughes, D. L.; Leigh, G. J.; Sanders, J. R.; Weisner, J. *J. Chem. Soc., Dalton Trans.* **1994**, 2591. (c) Hughes, D. L.; Kleinkes, U.; Leigh, G. J.; Maiwald, M.; Sanders, J. R.; Sudbrake, C. *J. Chem. Soc., Dalton Trans.* **1994**, 2457. (d) Hughes, D. L.; Kleinkes, U.; Leigh, G. J.; Maiwald, M.; Sanders, J. R.; Sudbrake, C.; Weisner, J. *J. Chem. Soc., Dalton Trans.* **1993**, 3093. (e) Hills, A.; Hughes, D. L.; Leigh, G. J.; Sanders, J. R. *J. Chem. Soc., Chem. Commun.* **1991**, 827. (f) Hills, A.; Hughes, D. L.; Leigh, G. J.; Sanders, J. R. *J. Chem. Soc., Dalton Trans.* **1991**, 61. (g) Leigh, G. J.; Sanders, J. R. *Polyhedron* **1989**, *8*, 1782. (h) Choudhary, N.; Hughes, D. L.; Kleinkes, U.; Larkworthy, L. F.; Leigh, G. J.; Maiwald, M.; Marmion, C. J.; Sanders, J. R.; Smith, G. W.; Sudbrake, C. *Polyhedron* **1997**, *16*, 1517. (i) Hills, A.; Hughes, D. L.; Leigh, G. J.; Sanders, J. R. *J. Chem. Soc., Dalton Trans.* **1991**, 325.
- (3) For a recent review see Aly, M. A. *J. Coord. Chem.* **1998**, *45*, 89.
- (4) Tsuchida, E.; Yamamoto, K.; Oyaizu, K.; Iwasaki, N.; Anson, F. C. *Inorg. Chem.* **1994**, *33*, 1056.

- (5) (a) Oyaizu, K.; Yamamoto, K.; Yoneda, K.; Tsuchida, E. *Inorg. Chem.* **1996**, *35*, 6634. (b) Tsuchida, E.; Yamamoto, K.; Oyaizu, K. *J. Am. Chem. Soc.* **1996**, *118*, 12665. (c) Tsuchida, E.; Oyaizu, K.; Dewi, E. L.; Imai, T.; Anson, F. C. *Inorg. Chem.* **1999**, *38*, 3704.
- (6) Bonadies, J. A.; Carrano, C. J. *J. Am. Chem. Soc.* **1986**, *108*, 4088.
- (7) Querios, M. A.; Montenegro, I.; Daschbach, J. L., Eds. *Microelectrodes: Theory and Applications*; Kluwers, Dordrecht, **1991**.
- (8) (a) Howarth, O. W. *Prog. Nucl. Magn. Spectrosc.* **1991**, *22*, 453. (b) Hibbert, R. C.; Logan, N.; Howarth, O. W. *J. Chem. Soc., Dalton Trans.* **1996**, 569. (c) Slebodnic, C.; Pecoraro, V. L. *Inorg. Chim. Acta* **1998**, *283*, 37.
- (9) Zamian, J. R.; Dockal, E. R. *Trans. Met. Chem.* **1996**, *21*, 3170.
- (10) Kolthoff, I. M.; Bruckenstein, S.; Chantooni, M. K., Jr. *J. Am. Chem. Soc.* **1961**, *83*, 3927.
- (11) Kolthoff, I. M.; Chantooni, M. K., Jr.; Bhowmik, S. *Anal. Chem.* **1967**, *39*, 315. (Note that the curves in Figure 1 are mislabeled.)
- (12) Fujinaga, T.; Sakamoto, I. *J. Electroanal. Chem.* **1977**, *85*, 185.
- (13) Swinehart, J. H. *Chem. Commun.* **1991**, 1443.
- (14) Espenson, J. H. *Chemical Kinetics and Reaction Mechanisms*; McGraw-Hill: New York, **1995**.

CHAPTER III

Schiff Base Complexes of Vanadium(III, IV, V) as Catalysts for the Electroreduction of O₂ to H₂O in Acetonitrile *

*Adapted from: Liu, Z.; Anson, F. C. *Inorg. Chem.* **2001**, *40*, 1329-1333.
Part of the work also appeared as a summary report to The Electrochemical Society for the 2000 Department of Energy Summer Research Fellowship in: Liu, Z. *Electrochem. Soc. Interface* **2001**, *10(1)*, 58.

ABSTRACT

Fifteen Schiff base ligands were synthesized and used to form complexes with vanadium in oxidation states III, IV and V. Electrochemical and spectral characteristics of the complexes were evaluated and compared. In acidified solutions in acetonitrile, the vanadium(IV) complexes undergo reversible disproportionation to form V(III) and V(V) complexes. With several of the ligands the V(III) complexes are much more stable in the presence of acid than is the previously studied complex with salen, an unelaborated Schiff base ligand (H_2 salen = N, N'-ethylenebis(salicylideneamine)). Equilibrium constants for the disproportionation were evaluated. The vanadium(III) complexes reduce dioxygen to form two oxo ligands. The reaction is stoichiometric in the absence of acid, and second-order rate constants were evaluated. In the presence of acid, some of the complexes investigated participate in a catalytic electroreduction of dioxygen.

INTRODUCTION

In a recent report¹ (see also Chapter II), we examined the stoichiometric reaction of the vanadium(III) complex of salen, $V^{III}(\text{salen})^+$, ($H_2\text{salen} = N, N'$ -ethylenebis(salicylideneamine)) with O_2 in acetonitrile. The reaction has also been examined in dichloromethane by other authors.² The possibility that the complex could serve as a catalyst for the four-electron reduction of O_2 in acidified acetonitrile was noted but not pursued because of the instability of $V^{III}(\text{salen})^+$ in the presence of acid and the low rate of its reaction with O_2 . The novelty of the chemistry involved in the proposed catalytic mechanism and the likelihood that it could also be applied to the electroreduction of O_2 provided impetus for an expanded study of analogous Schiff base ligands modified to enhance the stability and catalytic activity of their complexes with V(III). In the present study, 15 modified Schiff base ligands and their complexes with vanadium were prepared and examined as potential catalysts for the reduction of O_2 . Much greater resistances to acid decomposition were exhibited by some of the complexes and two reacted with O_2 at rates that exceeded by seven-fold that of $V^{III}(\text{salen})^+$. Spectroscopic and, especially, electrochemical properties of this expanded set of Schiff base complexes of V(III, IV, V) are described in this report. The results may provide a useful foundation on which to base the design of complexes with even greater catalytic reactivities.

EXPERIMENTAL

Materials

Distilled acetonitrile containing 0.001% water (EM Science) was stored over 3 Å molecular sieves. Trifluoromethanesulfonic (triflic) acid (Sigma) was used as received and was maintained O₂-free by saturation with Ar. All supporting electrolytes were electrochemical grade (Fluka). They were placed under vacuum at 75 °C overnight before use. The diamines, aromatic aldehydes and other reagents used in syntheses were obtained from commercial sources and used as received. The Schiff bases and their complexes with vanadium(IV) were prepared according to literature procedures.³ The Schiff base ligands were prepared by condensing aldehydes with diamines in ethanol. The resulting insoluble ligands could be isolated by filtration but were often used without isolation by adding VOSO₄ and refluxing the mixture for ca. 4 hours. The resulting oxovanadium(IV) Schiff base complexes were isolated by filtration with typical yields of 70-90%. Complexes that were soluble in dichloromethane were recrystallized from dichloromethane-ethanol. The preparative procedure for the complex of Schiff base (SB) No. 1 (Table 3.1) is representative: To a solution of 3, 5-di-tertiary-butyl-2-hydroxybenzaldehyde (2.34 g, 10 mmol) in hot ethanol (100 ml), ethylenediamine (0.31 g, 5 mmol) was slowly added. A yellow precipitate formed immediately. The acid released was neutralized by addition of

sodium acetate trihydrate (1.5 g, 11 mmol) and the mixture was stirred for 10 minutes. $\text{VO}_2\text{SO}_4 \cdot 4\text{H}_2\text{O}$ (1.175 g, 5 mmol) dissolved in 20 ml of water was then added dropwise to the suspension and the mixture was refluxed for ca. 4 hours. After cooling to room temperature, a green precipitate was collected by filtration (2.5 g, 4.3 mmol, 86%), washed twice with water and ethanol and dried in vacuo at 70 °C overnight.

Schiff base complexes of V(III) were prepared as previously described¹ by reduction of the corresponding oxovanadium(IV) complexes with H_2 in the presence of a large area Pt gauze and one mole of triflic acid per mole of V(IV).

Apparatus and Procedures

Electrochemical measurements were carried out in conventional one- or two-compartment cells using a BAS Model 100B/W Electrochemical Analyzer. Solutions were kept under an atmosphere of argon which was purified by passage through a gas scrubber (Oxiclear, Aldrich) and two columns filled with molecular sieves. The working electrode in voltammetric experiments was a 10 μm carbon microelectrode which was polished with 0.3 μm and 0.05 μm alumina paste before use. A porous glassy-carbon working electrode was used for bulk electrolyses. Auxiliary electrodes were platinum wires or foils. The reference electrode was Ag/AgCl in CH_3CN saturated with NaCl. All potentials are quoted with respect to this electrode. The half-wave

potentials of the ferrocinium/ferrocene couple measured from microelectrode voltammograms recorded in pure acetonitrile and in a 0.1 M tetrabutylammonium perchlorate solution in acetonitrile were 0.47 V and 0.44 V, respectively, versus this reference electrode.

The rates of the reactions between O_2 and the V(III) complexes of the various Schiff base ligands in acetonitrile solution at 24 ± 0.5 °C were measured by following the decrease of the anodic plateau current for the complexes measured at the microelectrode. The solutions were kept saturated with O_2 or air during the measurements. Solution IR spectra were obtained using a Perkin Elmer 1600 FT-IR spectrophotometer and a cell with CaF_2 windows separated by 1 mm. Baselines were obtained using pure acetonitrile. Solid samples were examined as Nujol mulls. EPR spectra were recorded on a Bruker EMX spectrometer operating at X-band. A cylindrical quartz cell with a diameter of 2 mm was used as the sample tube. Elemental analyses were performed by Desert Analytics.

RESULTS

The Complexes

The structures of the Schiff base ligands that were used to form complexes with V(III, IV, V) in this study are given in Table 3.1. The colors, solubilities and elemental analyses of the complexes are listed in Table 3.2. The observed and calculated elemental analyses were generally satisfactory but in a few instances (complexes of ligands 3, 4, 6, 7 and 9) low solubility prevented recrystallization of the complexes, which thwarted efforts to improve their purity. The low solubility has been attributed to the formation of polymeric structures in which $(V=O \rightarrow V=O)_n$ units link the monomeric complexes.^{4, 5} The factors which favor or disfavor the formation of such polymeric structures remain to be elucidated. Electrochemical experiments were restricted to complexes with satisfactory elemental analyses.

In Table 3.3 are listed the positions of the IR band corresponding to V=O stretching mode for each complex. Band peaks near 985 cm^{-1} are typical for a large variety of oxovanadium(IV) complexes.⁶ The position of this band is similar for both solid and dissolved samples. Band maxima below 900 cm^{-1} , typical for the less soluble complexes (Table 3.2), have been attributed to interactions among V=O groups in the solid state.^{5, 7, 8}

Table 3.1. Schiff Base Ligands Utilized in This Study

No.	R ₁	R ₂	R ₃	R ₄	X
0	H	H	H	H	CH ₂ CH ₂
1	t-Bu	H	t-Bu	H	CH ₂ CH ₂
2	H	H	H	H	1,2-C ₆ H ₄ ^a
3	H	H	H	H	CH ₂ CH ₂ CH ₂
4	H	H	NO ₂	H	CH ₂ CH ₂
5	H	H	H	H	CH ₂ C(CH ₃) ₂ CH ₂
6	H	H	H	H	1,8-C ₁₀ H ₆ ^b
7	t-Bu	H	t-Bu	H	1,8-C ₁₀ H ₆ ^b
8	t-Bu	H	t-Bu	H	1,2-C ₆ H ₄ ^a
9	H	H	NO ₂	H	CH ₂ C(CH ₃) ₂ CH ₂
10	H	H	NO ₂	H	1,2-C ₆ H ₁₀ ^c
11	H	H	MeO	H	CH ₂ CH ₂
12	H	MeO	H	MeO	CH ₂ CH ₂

13	X = CH ₂ CH ₂
14	X = 1,2-C ₆ H ₄ ^a
15	X = 1,8-C ₁₀ H ₆ ^b

a ; **b** ; **c**

Table 3.2. Colors, Solubilities and Elemental Analyses for the Oxovanadium(IV) Complexes of the Schiff Base Ligands in Table 3.1

SB No.	Color	Solubility ^a in		Elemental Analysis C; H; N % (Calc.)
		CH ₃ CN	CH ₂ Cl ₂	
1	green	s	vs	68.9(69.2); 8.3(8.2); 5.0(5.2)
2	green	s	s	63.0(62.8); 3.7(3.5); 7.4(7.4)
3	orange	is	is	58.8(47.2); 4.6(4.5); 8.1(8.3)
4	brown	ss	ss	45.4(32.4); 2.9(2.3); 13.2(9.6)
5	orange	ms	s	60.8(59.0); 5.4(5.4); 7.5(7.3)
6	black	is	is	66.8(70.0); 3.7(3.8); 6.5(7.6)
7	grey	is	is	73.3(73.8); 7.4(7.5); 4.3(7.3)
8	green	s	vs	71.4(72.6); 7.6(7.7); 4.6(5.0)
9	orange	is	is	49.0(44.1); 3.9(4.2); 12.0(11.5)
10	brown	ss	ss	50.3(49.8); 3.8(3.8); 11.7(11.7)
11	green	s	vs	55.0(55.1); 4.6(4.5); 7.1(7.3)
12	light blue	s	vs	53.0(53.1); 4.9(4.8); 6.2(6.3)
13	green	ss	ms	66.5(67.6); 4.2(4.2); 6.5(6.9)
14	olive	ss	ms	69.9(70.0); 3.8(3.9); 5.8(5.9)
15	brown	is	is	72.3(71.6); 3.8(3.6); 5.3(5.7)

^a vs (very soluble): > 5 mM; s (soluble): > 1 mM; ms (moderately soluble): ~ 0.5 mM; ss (slightly soluble): ~ 0.1mM; is (insoluble).

Table 3.3. IR and EPR Spectral Data for $V^{IV}O(SB)$
Complexes of the Ligands in Table 3.1

SB No.	EPR ^a		IR, $\nu_{V=O}$ (cm ⁻¹)	
	g-factor	A (G) ^b	nujol	CH ₃ CN
1	1.986	90	977	980
2	1.988	96	985	990
3	--	--	860	--
4	--	--	875	--
5	1.987	94	985	990
6	--	--	884	--
7	--	--	888	--
8	1.988	96	982	986
9	--	--	881	--
10	--	--	872	--
11	1.986	96	984	984
12	1.987	94	983	993
13	1.986	96	986	982
14	1.987	100	978	984
15	--	--	916	--

^a At room temperature (298 K). The solvent was CH₃CN
except for No. 13 and 14 where CH₂Cl₂ was used.

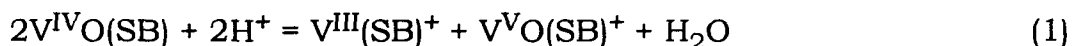
^b Nuclear hyperfine splitting factor.

The EPR spectra recorded with solutions of the eight soluble oxovanadium(IV) complexes were similar. They exhibited the eight-line isotropic spectra expected for coupling of the unpaired electron with the ^{51}V nucleus ($I = 7/2$). The g -factors and nuclear hyperfine splitting factors are listed in Table 3.3.

The low solubilities in acetonitrile of almost half of the oxovanadium(IV) complexes of the ligands in Table 3.1 (SB Nos. 3, 4, 6, 7, 9, 10, 15) prevented investigations of their solution chemistry and electrochemistry. In what follows, we restrict the descriptions to the eight complexes with at least modest solubility in acetonitrile.

Acid-induced Disproportionation of the VO(SB) Complexes

One route to the reduced vanadium(III)-Schiff base complexes, $\text{V}^{\text{III}}(\text{SB})^+$, which react with O_2 , is to induce the disproportionation of the corresponding oxovanadium(IV) complexes, $\text{V}^{\text{IV}}\text{O}(\text{SB})$, by exposing them to acid (reaction 1):¹



To monitor the course of reaction 1, steady state voltammetry with a carbon microelectrode was employed.¹ In the absence of acid, solutions of all of the soluble $\text{V}^{\text{IV}}\text{O}(\text{SB})$ complexes exhibited a single oxidation step corresponding to half-reaction 2:



No reductions of the $V^{IV}O(SB)$ complexes were observed. For example, curve 1 in Figure 3.1 is the voltammogram obtained with a solution of $V^{IV}O(SB)$ for SB No.1 in Table 3.1. (Controlled potential electrolysis at a porous glassy carbon electrode confirmed that the anodic wave involved a one-electron oxidation to $V^{VO}(SB)^+$.) Addition of 1.0 millimole per liter of CF_3SO_3H to the solution used to record curve 1 caused the voltammetric response to change to that shown in curve 2. It consists of an anodic wave with a plateau current half as large as that of curve 1 and a more positive half-wave potential. The addition of acid also produced a cathodic wave with a half-wave potential that matched that of the anodic wave of curve 1 and a plateau current that was half as large. These features are exactly those to be expected if the disproportionation in reaction 1 proceeded essentially quantitatively. The cathodic wave in curve 2 corresponds to the reverse of half-reaction 2 and the new anodic wave corresponds to half-reaction 3.



Curve 2 was obtained with an initially anhydrous acetonitrile solution. When a large stoichiometric excess of water was added to the solution the voltammetric response changed to that shown in curve 3. The diminished cathodic plateau current and the presence of two anodic

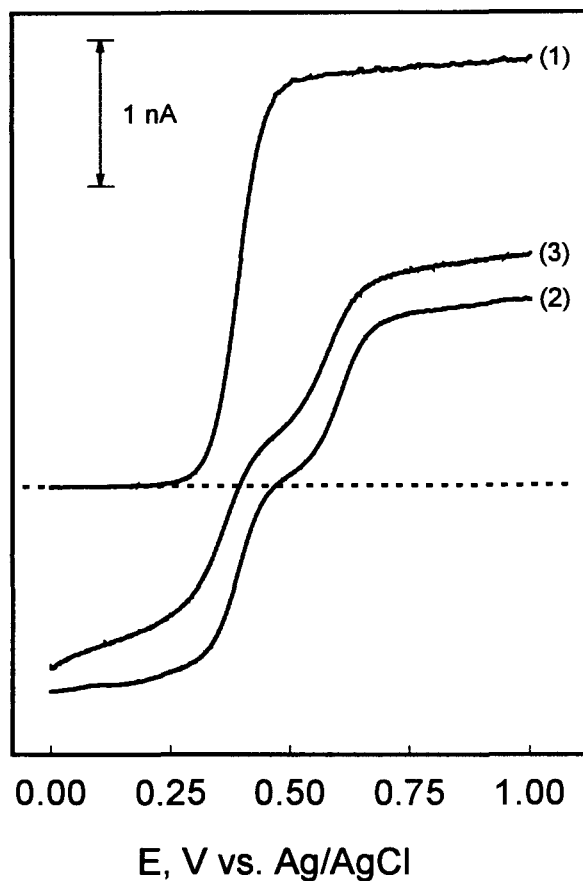


Figure 3.1. (1) Steady-state current-potential curves recorded with a carbon microelectrode in a 1 mM solution of $V^{IV}O(SB)$ (for SB No. 1 in Table 3.1) in anhydrous CH_3CN containing 0.1 M tetrabutylammonium perchlorate. (2) After 1 millimole per liter of CF_3SO_3H was added to the solution. (3) After the solution used to record 2 was made 0.2 M in H_2O . Scan rate = 10 mVs^{-1} . The dotted line marks the position of zero current.

waves is the expected result if the added H₂O caused reaction 1 to come to equilibrium with significant quantities of all three complexes present. This interpretation was supported by the EPR spectra of solutions of V^{IV}O(SB): The initial eight-line spectra disappeared when an equimolar quantity of CF₃SO₃H was added to solutions of the complexes in anhydrous acetonitrile, as expected if reaction 1 proceeded extensively from left to right because neither V^VO(SB)⁺ nor V^{III}(SB)⁺ are EPR-active. Addition of sufficient H₂O to the mixture caused the EPR signal to reappear as the equilibrium of reaction 2 shifted toward the left.

Equilibrium Constants for Reaction 1

The equilibrium constants for the disproportionation of several of the oxovanadium(IV) complexes prepared from ligands in Table 3.1 were evaluated from electrochemical measurements during the titration of a VO(SB) solution with acid in the presence of excess water, using the procedure described on page II-10 in Chapter II. The values obtained are listed in Table 3.4. Uncertainties in the values of K₁ for complexes 1, 11 and 12 were larger because calculation of the low equilibrium concentrations of protons becomes less and less certain as the value of K₁ increases.

The complex formed by Schiff base 14 has limited solubility in acetonitrile (0.15 mM, measured by electrolysis of a solution saturated

Table 3.4. Equilibrium Constants for the Acid-induced Disproportionation of $V^{IV}O(SB)$ According to Reaction 1^a

SB No.	$[H_2O], M$	K_1, M^{-1}
1	0.2	$(6 \pm 4) \times 10^7$
2	0.1	$(3.3 \pm 0.3) \times 10^5$
8	0.1	$(1.0 \pm 0.3) \times 10^6$
11	0.2	$(3 \pm 2) \times 10^7$
12	0.2	$(5 \pm 3) \times 10^7$
14	0.02	$(3.0 \pm 0.5) \times 10^5$
14	0.01	$(3.2 \pm 0.6) \times 10^5$

^aThe initial concentration of $V^{IV}O(SB)$ was 1.0 mM except for SB No. 14 where it was (and remained) 0.15 mM (see Table 3.5). Measurements were conducted at ambient laboratory temperature, 22 ± 2 °C.

with this complex), but the charged products of its disproportionation are much more soluble. In the evaluation of K_1 for this complex a suspension of the solid rather than a solution was employed. As shown in Figure 3.2, the wave (at 0.65 V) resulting from the oxidation of $V^{IV}O(SB)$ remains essentially unchanged throughout the titration (The gradually rising shoulder is probably due to the oxidation of the $V^{III}(SB)^+$ formed during the titration.). Thus, the concentration of $V^{IV}O(SB)$ was assumed to be constant in the calculation of K_1 . Titration data and the equilibrium constant calculated from them for this complex are given in Table 3.5.

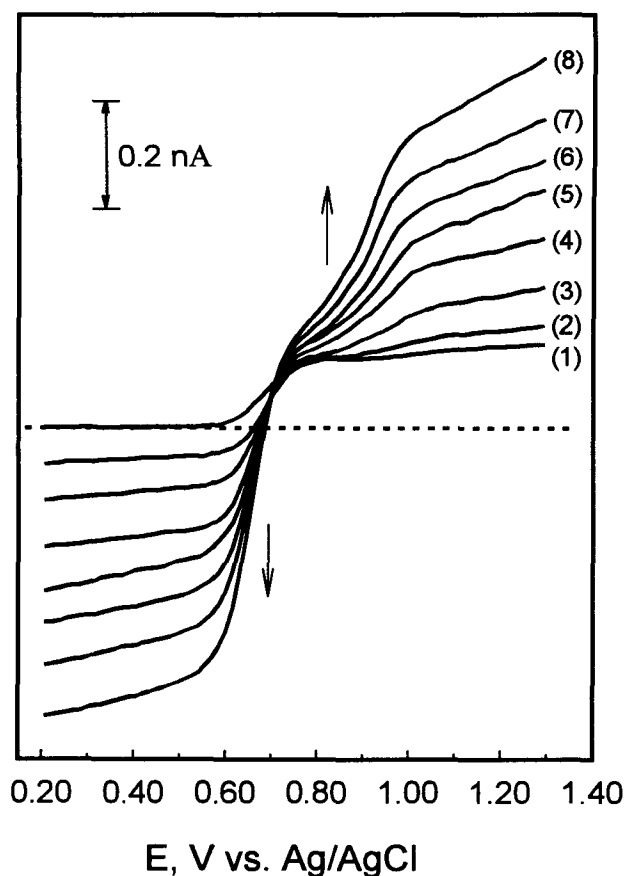


Figure 3.2. Steady-state voltammograms recorded with a carbon microelectrode in a suspension of $V^{IV}O(SB)$ (for SB No.14 in Table 3.1) in CH_3CN containing 20 mM H_2O . Aliquots CF_3SO_3H were added to the suspension in quantities corresponding to (1) 0, (2) 0.15, (3) 0.30, (4) 0.45, (5) 0.60, (6) 0.75, (7) 1.05 millimoles per liter.

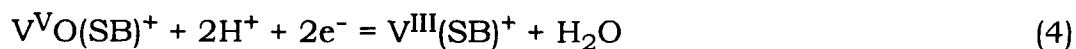
Table 3.5. Titration Data Used to Evaluate the Equilibrium Constant of Reaction 1 for Schiff Base No. 14^a

CF ₃ SO ₃ H added millimoles/L	[V ^V O(SB) ⁺] = [V ^{III} (SB) ⁺] mM	[H ⁺], mM	10 ⁻⁵ K ₁ , M ⁻¹
0.15	0.038	0.074	2.3
0.30	0.074	0.15	2.2
0.45	0.12	0.21	2.9
0.60	0.17	0.27	3.5
0.75	0.20	0.34	3.0
0.90	0.25	0.41	3.3
1.05	0.29	0.46	3.5
			av (3.0 ± 0.5)

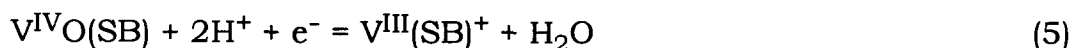
^a The data were obtained with a saturated solution of V^{IV}O(SB) in CH₃CN initially containing 20 mM H₂O. [V^{IV}O(SB)] was assumed to remain constant at 0.15 mM throughout the titration, see text. [V^VO(SB)⁺] was calculated from its reduction currents as shown in Figure 3.2. The concentrations of the other species were calculated from the stoichiometry of reaction 1. The dissociation of CF₃SO₃H was assumed to be complete based on the pK_a of 2.6 reported in dry acetonitrile (Fujinaga, T.; Sakamoto, I., *J. Electroanal. Chem.*, **1977**, 85, 185).

Formal Potentials

Formal potentials for the $V^{VO}(SB)^+/V^{IVO}(SB)$ and $V^{IV}(SB)^{2+}/V^{III}(SB)^+$ couples were estimated from (the half-wave potentials of) current-potential responses like those in Figure 1. (Cyclic voltammetric experiments confirmed that the electrode reactions were reversible.) The values obtained are listed in Table 3.6. Formal potentials for half-reactions



and



are also given in Table 3.6. These two formal potentials cannot be measured directly because of the disproportionation of $V^{IVO}(SB)$ but they can be calculated from E^f for the $V^{VO}(SB)^+/V^{IVO}(SB)$ couple and values of K_1 (Table 3.4).

Table 3.6. Formal Potentials of Redox Couples for Schiff Base Complexes of V(III, IV, V)

SB No.	E^f vs. Ag/AgCl, V ^a			
	VO(SB) ^{+ / 0} ^b	V(SB) ^{2+ / +} ^b	half-reaction 4 ^c	half reaction 5 ^c
1	0.40	0.60	0.63	0.85
2	0.64	0.95	0.81	0.97
8	0.60	0.72	0.78	0.95
11	0.45	0.62	0.67	0.88
12	0.43	0.70	0.66	0.88
14	0.65	0.90	0.81	0.97

^a The estimated uncertainties in the potentials were ± 10 -20 mV.

^b Evaluated from cyclic voltammograms recorded in anhydrous acetonitrile containing 0.1 M tetrabutylammonium perchlorate, 1.0 mM complex (except for SB No. 14; 0.15 mM) and ambient temperatures, 22 ± 2 °C.

^c Calculated from K_1 (Table 3.4) and E^f for VO(SB)^{+ / 0}.

Reaction of V^{III}(SB)⁺ with O₂

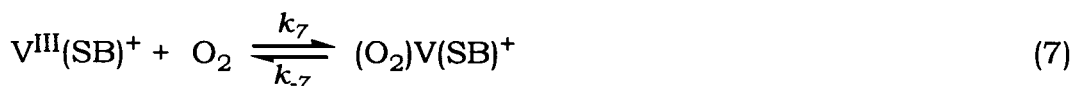
The soluble complexes of V^{IV}O(SB) were converted to V^{III}(SB)⁺ by reduction with H₂ (Experimental Section). The reaction of V^{III}(SB)⁺ with O₂ in anhydrous acetonitrile proceeds according to reaction 6:



The stoichiometry of reaction 6 was established in two ways: (i) An

excess of O_2 was added to a solution of $V^{III}(SB)^+$ which produced a quantitative conversion of the complex to $V^VO(SB)^+$ as determined by steady-state voltammetry. (ii) Aliquots of an acetonitrile solution that was saturated with O_2 were added to a solution of $V^{III}(SB)^+$ in acetonitrile that had been saturated with argon. The mixture was sealed in a Schlenk tube and allowed to react for 24 hours. The resulting solution was analyzed for both $V^{III}(SB)^+$ and $V^VO(SB)^+$ voltammetrically. Two moles of $V^VO(SB)^+$ were produced and two moles of $V^{III}(SB)^+$ were consumed for each mole of O_2 that had been added.

The kinetics of reaction 6 were monitored electrochemically using a carbon microelectrode held at a potential on the plateau of the anodic wave for the oxidation of $V^{III}(SB)^+$ in solutions containing an excess of O_2 . Typical current-time traces are shown in Figure 3.3A and the corresponding pseudo-first-order kinetic plots are shown in Figure 3.3B. Data such as those in Figure 3.3 demonstrated that the rate of reaction 6 is first-order in both $V^{III}(SB)^+$ and O_2 . A possible mechanism for the reaction is given in reactions 7-9.



The corresponding rate law when the steady-state approximation is applied to $[(SB)V(O_2)^+]$ and $k_{-7} \ll k_8[V^{III}(SB)^+]$ is

$$\frac{-d[V^{III}(SB)^+]}{dt} = 2k_7[V^{III}(SB)^+][O_2] \quad (10)$$

Thus, the slopes of the linear plots in Figure 3.3B correspond to $2k_7[O_2]$.

Values of k_7 for the complexes examined are listed in Table 3.7. The

constants span the range from 0.06 to 0.46 $M^{-1} s^{-1}$, but none was large enough to indicate that a catalytically attractive complex was in hand.

The rate of reaction 6 was not affected by the presence of excess acid.

Thus, the rate-limiting formation of the proposed $(O_2)V(SB)^+$ intermediate (reaction 7) is not assisted by the presence of acid.

Table 3.7. Rate Constants for the Oxidation of $V^{III}(SB)^+$ by O_2 ^a

SB No.	$k_7, M^{-1} s^{-1}$
0	0.060 ± 0.003
1	0.44 ± 0.02
2	0.060 ± 0.003
8	0.46 ± 0.02
11	0.13 ± 0.01
12	0.11 ± 0.01
14	0.090 ± 0.005

^a Initial concentration of $V^{III}(SB)^+$ and O_2 were 0.5 mM and 8.1 mM, respectively. Measurements were made at the ambient laboratory temperature, 22 ± 2 °C.

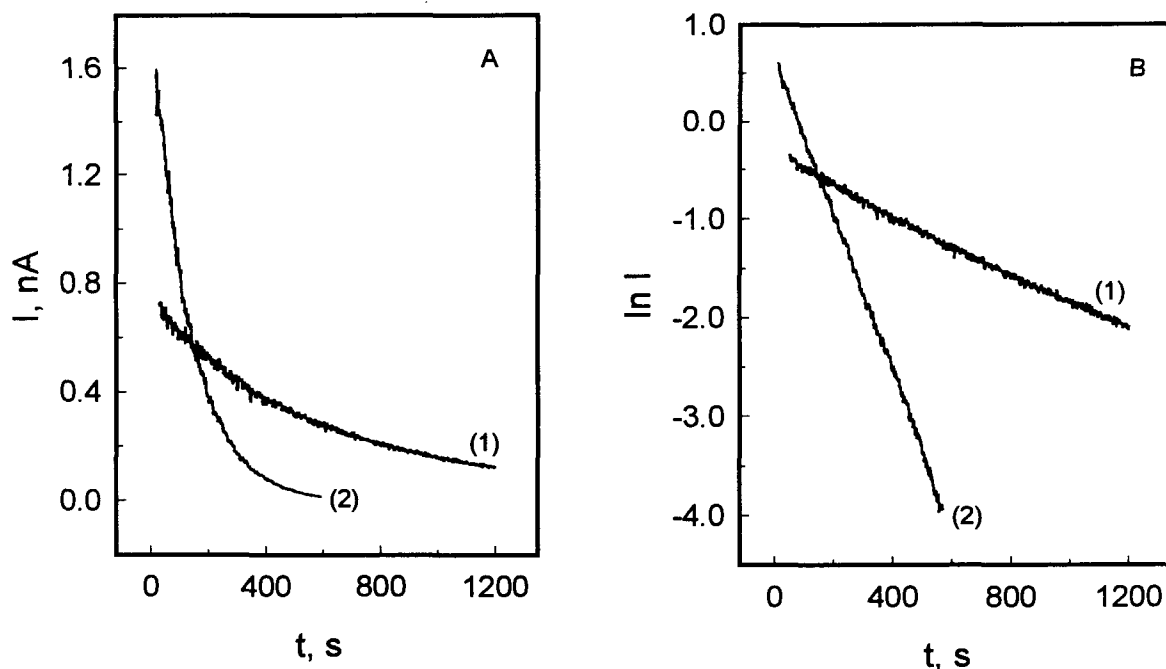


Figure 3.3. (A) Current-time transients recorded during the reaction of $V^{III}(SB)^+$ (for SB No. 1 in Table 3.1) with O_2 in pure CH_3CN . The anodic current was measured with a carbon microelectrode maintained at 0.8 V. The concentrations of O_2 were 1.7 mM (1) and 8.1 mM (2). The initial concentrations of $V^{III}(SB)^+$ were 0.2 mM (1) and 0.5 mM (2). (B) Pseudo-first-order kinetic plots prepared from the transients in (A). The ratio of the slopes of the plots is 4.8.

DISCUSSION

Preparation of $V^{III}(SB)^+$

To generate $V^{III}(SB)^+$ from the readily available $V^{IV}O(SB)$ or $V^VO(SB)^+$ complexes, a reductive deoxygenation is required. Some procedures employed previously for this purpose have used $TiCl_3$ or $(SOCl_2 + Zn \text{ dust})$.⁹ These methods inevitably produced chloro-vanadium(III) Schiff base complexes. The alternative procedure employed in this and our previous study,¹ which utilizes only one equivalent of acid, excess H_2 and a large area platinum gauze (on which H_2 is dissociatively adsorbed), was found to be general and efficient. It has the advantage that the $V^{III}(SB)^+$ is produced without extraneous axial ligands that could interfere in reactivity studies.^{9, 10, 11} The $V^{III}(SB)^+$ prepared this way may also be used as the precursor to prepare V(III) complexes containing other desired axial ligands.

Possible Association of $V^{IV}O(SB)$ and $V^VO(SB)^+$ in Solution

Cyclic voltammograms of $V^{IV}O(SB)$ recorded in acetonitrile are consistent with a simple, uncomplicated reversible conversion to and from $V^VO(SB)$.¹ However, voltammograms that are recorded in dichloromethane exhibit evidence of two closely-spaced waves.⁴ In exploratory experiments (see Appendix III-A) not directly related to the present study, we have confirmed the results reported in reference 4 but

observed that the presence or absence of such double waves depends upon not only the solvent but also the concentration of the complex (e.g., the double wave disappears in CH_2Cl_2 at concentrations of $\text{V}^{\text{IV}}\text{O}(\text{salen})$ below ca. 1 mM), the supporting electrolyte employed and the particular SB ligand employed (e.g., for SB No. 1, which contains four bulky t-butyl groups, no double waves appear in CH_2Cl_2 solutions at concentrations of the complex as great as 10 mM). The behavior observed is consistent with dimerization (or higher oligomerization) of the complexes that exhibit double waves in CH_2Cl_2 . Additional experiments are needed to confirm this speculation.

Stoichiometric Reduction of O_2 by $\text{V}^{\text{III}}(\text{SB})^+$

The purpose of this study was to investigate how variations in the structures of Schiff base ligands used to form complexes of V(III, IV and V) affected the reactivities of the complexes, especially in connection with their participation in the reduction of O_2 by the mechanism shown in reactions 7-9.

All of the soluble $\text{V}^{\text{III}}(\text{SB})^+$ complexes were found to accomplish the stoichiometric reduction of O_2 (to produce two oxo ligands). As can be seen by comparing the rate constants in Table 3.7 and the formal potentials in Table 3.6, the strength of $\text{V}^{\text{III}}(\text{SB})^+$ as a reducing agent (when it is oxidized to $\text{V}^{\text{IV}}\text{O}(\text{SB})^+$ through the reverse of half-reaction 4)

does not correlate with the rate at which it reduces O_2 . However, the formal potential of the $V^VO(SB)^+/V^{III}(SB)^+$ couple would not be expected to correlate with the rate of reaction 7 because the proposed product of the reaction, $(SB)V(O_2)^+$, does not resemble $(SB)V^VO^+$.

$V^{III}(SB)^+$ is not a strong reductant (Table 3.6) and O_2 is not a strong oxidant in acetonitrile (E^f for the O_2/O_2^- couple is ca. -1.0 V versus Ag/AgCl) so the equilibrium constant for reaction 7 would be expected to be very small. The high rate of reaction 8 (and 9) is presumably responsible for the observed, quantitative formation of $V^VO(SB)^+$. The chemical step that controls the overall rate, and to which k_7 applies, is probably the dissociation of a solvent molecule from an axial position on the $V^{III}(SB)^+$ complex to generate a coordination site for the incoming O_2 molecule. For example, addition of 2 mM 1-methylimidazole (a good axial ligand) to a solution of $V^{III}(SB)^+$ changed its color from yellow to green and essentially eliminated the reduction of O_2 by the resulting complex of V(III). In addition, with CH_2Cl_2 instead of CH_3CN as solvent, the reaction of $V^{III}(SB)^+$ complexes with O_2 proceeds significantly more rapidly, probably because CH_2Cl_2 competes with O_2 less effectively than does CH_3CN for the axial coordination sites on the catalyst. The larger rate constants exhibited by complexes 1 and 8 (Table 3.7) may reflect the four tertiary butyl substituents' increasing the lability of ligands coordinated

to axial sites on the $V^{III}(SB)^+$ complexes, perhaps because of steric interactions.

Catalytic Reduction of O_2

The mechanism of reactions 7-9 could be made catalytic if the $V^VO(SB)^+$ produced in reaction 9 were reduced (either by a homogeneous reductant or at an electrode) to $V^{IV}O(SB)$ and acid were present in the solution to induce the disproportionation of the $V^{IV}O(SB)$ (reaction 1). Such a scheme was mentioned in our previous study of the $V^{III}(salen)^+$ complex¹ but the instability of this complex in acetonitrile in the presence of acid prevented the testing of this scheme. Several of the complexes examined in the present study are much more stable in acidic solutions so the possible catalytic electroreduction of O_2 was explored. The $V^{IV}O(SB)$ complex with SB = ligand 8 (Table 3.1) was dissolved in acidified acetonitrile saturated with Ar to obtain an equimolar mixture of $V^{III}(SB)^+$ and $V^VO(SB)^+$. A porous glassy carbon electrode was introduced into the solution to carry out the electroreduction of $V^VO(SB)^+$ to $V^{III}(SB)^+$ (via $V^{IV}O(SB)$ and reaction 1). The cathodic charge consumed in this reduction, shown in curve 1 in the insert in Figure 3.4, corresponds to one electron per vanadium in the starting $V^{IV}O(SB)$ complex. When a similar electrolysis was carried out with O_2 -saturated acetonitrile, the cathodic charge consumed was much greater (curve 2 in

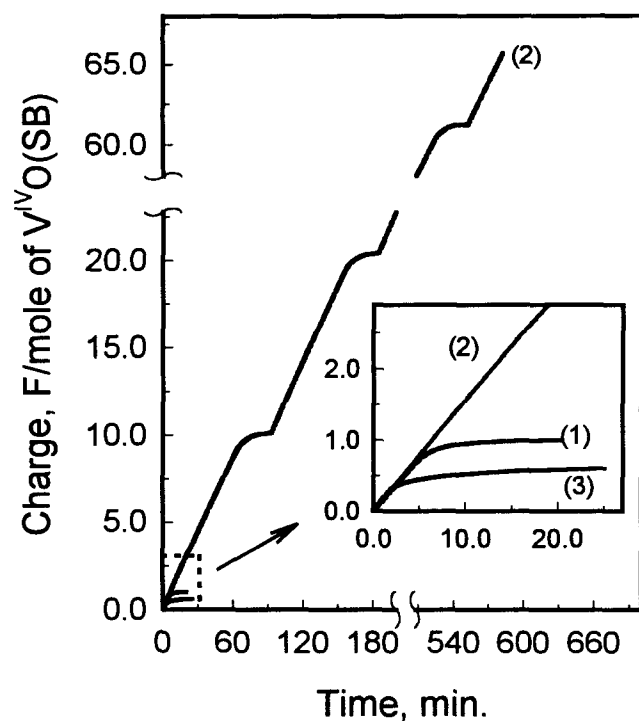
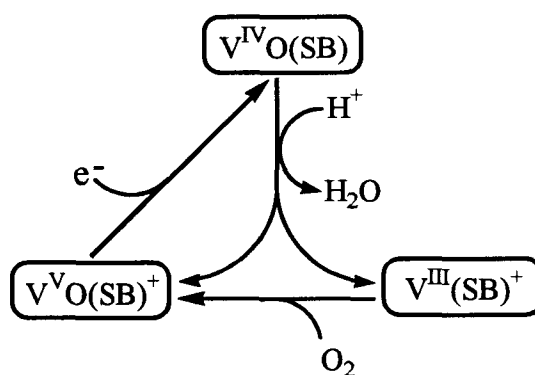


Figure 3.4. Cathodic charge flow during the electrolytic reductions at 0.55 V of stirred acetonitrile solutions prepared by adding 0.5 mmole per liter of $V^{IV}O(SB)$ ($SB =$ ligand 8 in Table 1) to 5.0 mM CF_3SO_3H . (1) Solution saturated with Ar. (2) Repeat of (1) with an O_2 -saturated solution. Additional aliquots of CF_3SO_3H were added to the solution to cause the charge flow to resume after the electrolysis had consumed all of the acid present. (3) Repeat of (2) using $V^{IV}O(salen)$ instead of $V^{IV}O(SB)$. The electrolysis potential was 0.45 V. Supporting electrolyte throughout: 0.1 M tetrabutylammonium perchlorate.

Figure 3.4). The flow of charge decreased to background levels (plateaus in curve 2) only after all of the acid present was consumed in the reduction of O_2 to H_2O by the combination of reactions 7-9, the inverse of half-reaction 2 and reaction 1, as shown in Scheme 1:

Scheme 1



The catalytic electroreduction resumed when additional acid was provided whereupon additional cathodic charge was consumed (curve 2 in Figure 3.4). More than 60 turn-overs of the vanadium-Schiff base catalyst occurred during the recording of curve 2 in Figure 3.4 without significant decomposition of the catalyst. By contrast, when the same experiment was performed using $V^{IV}O(\text{salen})$ (ligand No. 0 in Table 3.1) as the catalyst, the charge flow ceased even before one electron per vanadium had been consumed and well before all of the acid was consumed (curve 3 in the inset in Figure 3.4). We attribute this difference in behavior to a more rapid, acid-induced decomposition of $V^{III}(\text{salen})^+$ than of the other tested complexes. The complexes of ligands

2, 8 and 14 (Table 3.1) all exhibited stability in the presence of acid that was adequate to provide sustained catalytic electroreductions of O₂.

However, with none of the complexes was the rate of the overall reduction reaction high enough to be attractive for electrocatalytic applications.

CONCLUSIONS

The Schiff base ligands in Table 3.1 form oxovanadium(IV) complexes with similar properties that include reversible oxidation to oxovanadium(V) at potentials between 0.4 and 0.65 V and reversible disproportionation to V(III) and V(V) in the presence of acid in a reaction (reaction 1) that is governed by equilibrium constants of $\sim 10^5 - 10^8 \text{ M}^{-1}$. In the absence of acid, the deoxygenated vanadium(III) complexes react with O₂ to produce two moles of the oxovanadium(V) complexes. The kinetics of the reaction can be facilitated by bulky ligands. In the presence of acid, several of the complexes can act as catalysts for the electroreduction of O₂ to H₂O without significant decomposition of the catalyst. The mechanism of the catalysis is believed to involve an inner-sphere electron-transfer pathway coupled to the acid-induced disproportionation of the oxovanadium(IV) complex formed as an intermediate in the catalytic cycle.

APPENDIX III-A**Cyclic Voltammetry of $V^{IV}O(SB)$ in CH_2Cl_2**

Cyclic voltammograms (CV) of all the $V^{IV}O(SB)$ complexes recorded in CH_3CN exhibit a simple, reversible conversion to and from $V^{VO}(SB)^+$. However, voltammograms of such complexes in CH_2Cl_2 show more complicated features: They exhibit two closely spaced waves, as first reported by Choudhary et al.⁴ who also raised the question of the persistence of dinuclear species of these vanadium complexes in CH_2Cl_2 solution. We carried out more exploratory experiments with some of the complexes used in this study and observed that the presence or absence of the double waves depends on not only the solvent but also on several other factors, such as supporting electrolytes, concentration of the complex, and the particular ligand in a complex. The results, as summarized below, are supportive of the speculation of dimerization of the complexes.

Effect of supporting electrolytes. Four supporting electrolytes, $TBAPF_6$, $TBAClO_4$, $TBABF_4$ and $TBACF_3SO_3$, were used to record the CV of $VO(SB)$ for SB No. 2. As shown in Figure 3.5, only $TBAPF_6$ gave rise to the appearance of the double waves. This observation might be attributed to the relative basicity of the supporting electrolyte anions. In propylene carbonate, HPF_6 was reported to dissociate completely (Izutsu, K. *Acid-Base Dissociation Constants in Dipolar Aprotic Solvents*; Blackwell

Scientific Publications: Oxford, U.K. 1990), whereas HClO_4 and $\text{CF}_3\text{SO}_3\text{H}$ have pK_a values of 1.3-2.9 and 1.3-2.3, respectively. We also found that HBF_4 in CH_3CN is a weaker acid than HClO_4 and $\text{CF}_3\text{SO}_3\text{H}$.¹ There has been no report about the dissociation constants of these acids in CH_2Cl_2 . If the PF_6^- anion is the weakest base among the four supporting electrolyte anions in CH_2Cl_2 , its ion pairing with $\text{VO}(\text{SB})^+$, the oxidation product of $\text{VO}(\text{SB})$, would also be the poorest. Because CH_2Cl_2 is also a poor coordinating solvent, $\text{VO}(\text{SB})^+$ would probably be forced to associate with $\text{VO}(\text{SB})$ under such an environment. The observed electrochemistry would be accounted for with this speculation.

Effect of ligands. Shown in Figure 3.6 are CV's of $\text{VO}(\text{SB})$ with SB Nos. 1 and 2. The absence of the double waves of the latter can probably be attribute to the four bulky *tert*-butyl groups on the ligand which retard the dimerization process.

Concentration dependence. It was also found that the appearance of the double waves strongly depends upon the concentration of the complexes, as shown in Figure 3.7. For $\text{VO}(\text{SB})$ with SB No. 2, the double waves become observable when its concentration is higher than 1 mM in $\text{CH}_2\text{Cl}_2/0.1 \text{ M TBAPF}_6$. But for complexes with bulky ligands such as SB No. 1, the double waves are absent even at concentration as high as 10 mM in the same solution. Interestingly, when TBABF_4 was

used as supporting electrolyte, the double waves were observed for the complex with SB No. 2 when its concentration was higher than 2 mM.

Other experiments. Electrooxidation of several complexes were carried out in $\text{CH}_2\text{Cl}_2/0.1 \text{ M TBAPF}_6$. The electrolysis usually could not proceed to completion for complexes (ca. 2 mM) with less bulky ligands because of the formation of a precipitate on the electrode surface.

(Addition of CH_3CN dissolved the precipitate and allowed the electrolysis to resume.) The low solubility of the charged electrolysis product might also contribute to the appearance of the double waves observed in the CV of these complexes. For $\text{VO}(\text{salen})$ (3 mM), no precipitate was formed during the electrolysis which consumed 1 electron per vanadium. The CV of the product, presumably $\text{VO}(\text{salen})^+$, however, did not exhibit the double waves. Additional experiments are needed to explain these observations.

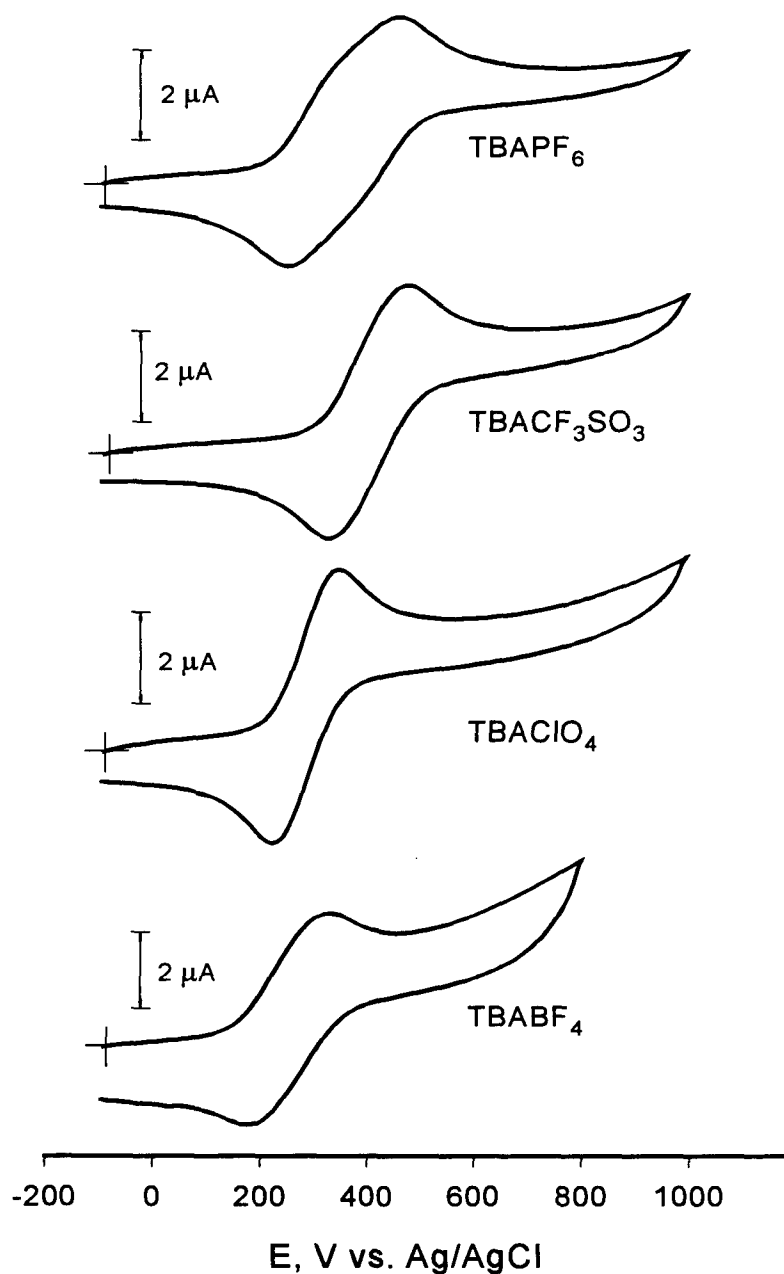


Figure 3.5. Cyclic voltammograms of 1 mM VO(SB) (SB No. 2 in Table 3.1) in CH₂Cl₂ containing 0.1 M different supporting electrolytes as labeled. Electrode: 0.5 mm glassy carbon; Scan rate: 50 mV s⁻¹.

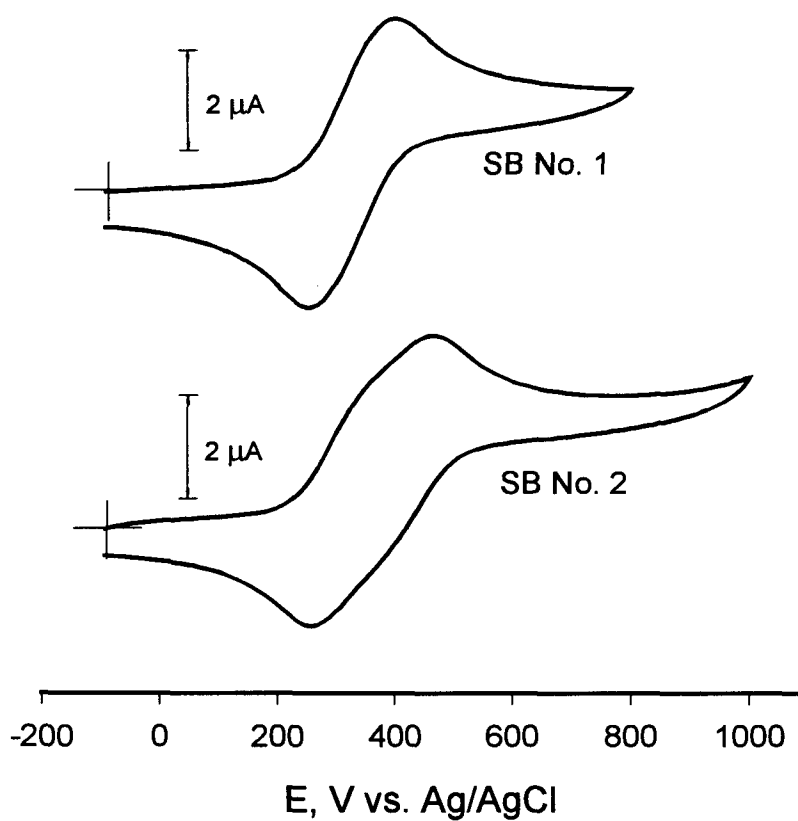


Figure 3.6. Cyclic voltammograms of 1 mM VO(SB) for SB Nos. 1 (top) and 2 (bottom) in Table 3.1 in CH_2Cl_2 containing 0.1 M TBAPF₆. Other conditions as in Figure 3.5.

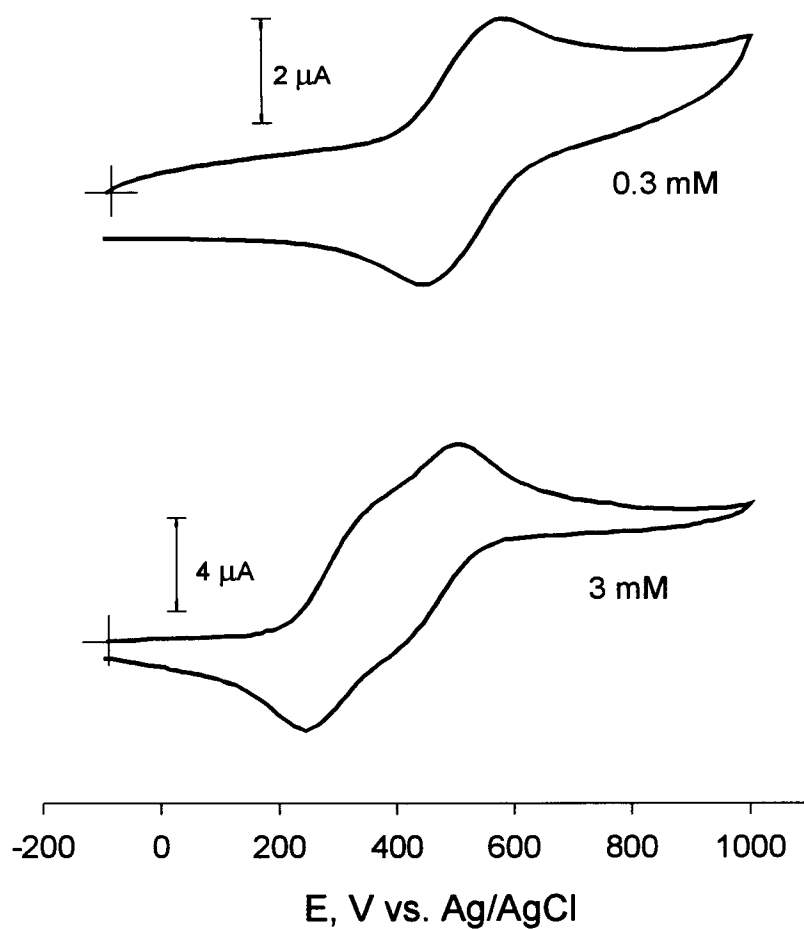


Figure 3.7. Cyclic voltammograms of 0.3 (top) and 3 (bottom) mM VO(SB) (SB No. 2 in Table 3.1) in CH_2Cl_2 containing 0.1 M TBAPF₆. Other conditions as in Figure 3.5.

REFERENCES

- (1) Liu, Z.; Anson, F. C. *Inorg. Chem.* **2000**, 39, 274, 1048.
- (2) (a) Oyaizu, K.; Yamamoto, K.; Yoneda, K.; Tsuchida, E. *Inorg. Chem.* **1996**, 35, 6634. (b) Tsuchida, E.; Yamamoto, K.; Oyaizu, K. *J. Am. Chem. Soc.* **1996**, 118, 12665. (c) Tsuchida, E.; Oyaizu, K.; Dewi, E. L.; Imai, T.; Anson, F. C. *Inorg. Chem.* **1999**, 38, 3704.
- (3) Zamin, J. R.; Dockal, E. R.; Castellano, G.; Oliva, G. *Polyhedron* **1995**, 14, 2411.
- (4) Choudhary, N. F.; Connelly, N. G.; Hitchcock, P. B.; Leigh, G. J. *J. Chem. Soc. Dalton Trans.* **1999**, 4437.
- (5) Methew, M.; Carry, A. J.; Palenik, G. J. *J. Am. Chem. Soc.* **1970**, 92, 3197.
- (6) Diehl, H.; Hask, C. *Synth.* **1950**, 3, 196.
- (7) Pasini, A.; Gulloti, M. *J. Coord. Chem.* **1974**, 3, 319.
- (8) Tsuchimoto, M.; Kasahara, R.; Nakajima, K.; Kojima, M.; Ohba, S. *Polyhedron* **1999**, 18, 3035.
- (9) Mazzanati, M.; Gabarotta, S.; Floriani, C.; Chiesi-Villa, A.; Guastini, C. *Inorg. Chem.* **1986**, 25, 2308.
- (10) McNeese, T. J.; Mueller, T. E. *Inorg. Chem.* **1985**, 24, 2981.
- (11) Munay, K. S.; Simm, G. R.; West, B. O. *Aust. J. Chem.* **1973**, 26, 991.

CHAPTER IV

**Rate Enhancements in the Four-electron Reduction of O₂ by
Mixtures of Vanadium(III)-Schiff Base Complexes and
Decamethylferrocene in Acetonitrile**

ABSTRACT

The otherwise slow reaction between O_2 and decamethylferrocene (DMFc) or $V^{III}(SB)^+$ (SB = Schiff base ligands) is significantly accelerated if these three reactants are present. In the absence of acid, the reduction of O_2 proceeds stoichiometrically to yield the two oxo groups in $(SB)V^{IV}O$. In the presence of acid, the reaction becomes catalytic and the O_2 is reduced to H_2O . In the presence of excess O_2 , the catalytic reaction ceases only when the supply of DMFc or acid is depleted. Preliminary investigation of the kinetics of the O_2 reduction processes leads to a reaction scheme that accounts for the rate enhancement by DMFc but not all of the kinetic data.

INTRODUCTION

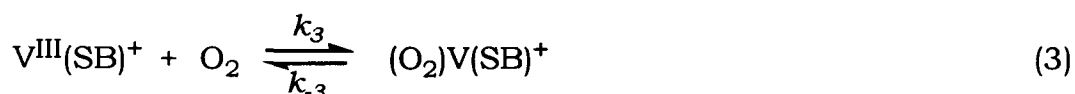
In a recent report¹ (see also Chapter III) the four-electron reduction of O₂ in acetonitrile by a set of Schiff base (SB) complexes of vanadium(III), V^{III}(SB)⁺, was described. The complexes involved various ligands analogous to the Schiff base salen (H₂salen = N, N'-ethylene-bis(salicylideneamine)). The reduction was shown to proceed according to the stoichiometry of the reaction 1:¹



The rate of the rather slow reduction was shown to follow the rate law given in equation 2:

$$\frac{-d[\text{V}^{\text{III}}(\text{SB})^+]}{dt} = 2k[\text{V}^{\text{III}}(\text{SB})^+][\text{O}_2] \quad (2)$$

with $k = 0.06$ to $0.5 \text{ M}^{-1} \text{ s}^{-1}$. The rate limiting step was believed to be the coordination of O₂ to the (SB)V^{III+} complex (reaction 3).



The rate of the reduction of O₂ is substantially enhanced if the auxiliary reducing agent decamethylferrocene (DMFc) is added to the reaction mixture. This was a surprising observation because DMFc does not react with V^{III}(SB)⁺ and its reaction with O₂ is much too slow to contribute to

the reactions observed. With the rate enhancement, the system can be utilized to carry out catalytic chemical reduction of O_2 to H_2O more efficiently than is the case in the electroreduction described in Chapter III. Exploration of the redox chemistry exhibited by the three-component $V^{III}(SB)^+-O_2-DMFc$ system in acetonitrile is the subject of this chapter.

EXPERIMENTAL

Materials

Distilled acetonitrile containing 0.001% water (EM Science) was stored over 3Å molecular sieves. Trifluoromethanesulfonic (triflic) acid (Sigma) was used as received. Sublimed decamethylferrocene (Alfa Aesar) was recrystallized from acetonitrile-dichloromethane. All supporting electrolytes were electrochemical grade (Fluka). They were placed under vacuum at 75 °C overnight before use. The diamines, aromatic hydroxaldehydes, and other reagents used in syntheses were obtained from commercial sources and used as received. The Schiff bases listed in Table 1 and their complexes with oxovanadium(IV) were prepared as described previously.¹ Schiff base complexes of vanadium(III) were prepared by reduction of the corresponding oxovanadium(IV) complexes with H_2 in the presence of a large area Pt gauze and 1 mol of triflic acid per mol of V(IV).^{1,2}

Apparatus and Procedures

Electrochemical measurements were carried out in conventional one- or two-compartment cells using a BAS model 100B/W electrochemical analyzer. Solutions were kept under an atmosphere of argon that was purified by passing through a gas scrubber (Oxiclear; Aldrich) and two columns filled with molecular sieves. The working electrode used in voltammetric experiments was a 10 μm diameter carbon microelectrode, which was polished with 0.3 μm and 0.05 μm alumina before use. A porous glassy-carbon working electrode was used for bulk electrolyses. Auxiliary electrodes were platinum wires or foils. The reference electrode was Ag/AgCl in acetonitrile saturated with NaCl. All potentials are quoted with respect to this electrode. Half-wave potentials of the ferrocinium/ferrocene couple measured from microelectrode voltammograms recorded in pure acetonitrile and in a 0.1 M tetrabutylammonium perchlorate solution in acetonitrile were 0.47 V and 0.44 V, respectively, vs. this reference electrode.

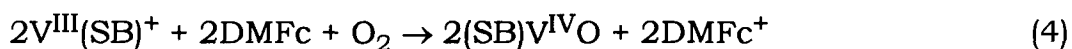
The kinetics of the three-component (SB)V^{III+}-O₂-DMFc system in acetonitrile were measured by monitoring the cathodic plateau current for the reduction of DMFc⁺ at the 10 μm carbon microelectrode. The solution temperature was maintained at 0 °C by sitting the cell in an ice-water bath. The solutions were kept saturated with pure O₂ or air during the measurements. EPR spectra were recorded on a Bruker EMX

spectrometer operating at X-band. A cylindrical quartz cell with a diameter of 2 mm was used as the sample tube.

RESULTS

Qualitative Observations

When $(\text{SB})\text{V}^{\text{III}+}$ is exposed to excess O_2 in acetonitrile, reaction 1 proceeds slowly but quantitatively. Addition of a stoichiometric quantity of DMFc to the resulting $(\text{SB})\text{V}^{\text{VO}+}$ complex (in the absence or presence of O_2) rapidly produces $(\text{SB})\text{V}^{\text{IVO}}$ and DMFc^+ as expected from the known formal potentials of the $(\text{SB})\text{VO}^{+/0}$ and $\text{DMFc}^{+/0}$ couples¹, 0.40 ~ 0.60 and - 0.05 V, respectively. (The possible reaction between O_2 and DMFc in acetonitrile was not observed under the experimental conditions employed.) These observations might lead one to expect that mixtures of all three components ($\text{V}^{\text{III}}(\text{SB})^+$, O_2 , DMFc) would react according to reaction 4:



with the overall reaction rate limited by the rate of reaction 1. In fact, mixtures of the three components do react according to the stoichiometry given in reaction 4, but the consumption of O_2 (and $\text{V}^{\text{III}}(\text{SB})^+$) proceeds much more rapidly than does reaction 1.

Quantitative Observations

To monitor the stoichiometry of the reaction, steady-state voltammetry with a carbon fiber microelectrode was employed as in our previous study.¹ Shown in Figure 4.1 are current-potential curves recorded with a solution initially containing equal concentrations of $V^{III}(SB)^+$ (SB = ligand 2 in Table 4.1) and DMFc (curve A). The two anodic plateau currents correspond to the oxidations of DMFc to $DMFc^+$ ($E_{1/2} = -0.05$ V) and of $V^{III}(SB)^+$ to $V^{III}(SB)^{2+}$ ($E_{1/2} = 0.75$ V). (The plateau current for the oxidation of DMFc is larger than that for the oxidation of $V^{III}(SB)^+$ because of the larger diffusion coefficient of DMFc.²) Curve B was recorded after 0.5 mol of O_2 per mol of $V^{III}(SB)^+$ was added to the solution used to record curve A. The cathodic wave with $E_{1/2} = -0.05$ V represents the reduction of the $DMFc^+$ produced in reaction 4. The new anodic wave with $E_{1/2} = 0.45$ V corresponds to the oxidation of $(SB)V^{IV}O$ (produced by the autoxidation of $V^{III}(SB)^+$) to $(SB)V^VO^+$. That $(SB)V^{IV}O$ was a product of the reaction with O_2 was confirmed by the room temperature ESR spectrum of the solution, which exhibited the characteristic eight-line spectrum of vanadium(IV).¹

Kinetics of Reaction 4

The rate of reaction 4 at room temperature is too high to be conveniently measured. However, at 0 °C, the reaction rate becomes low

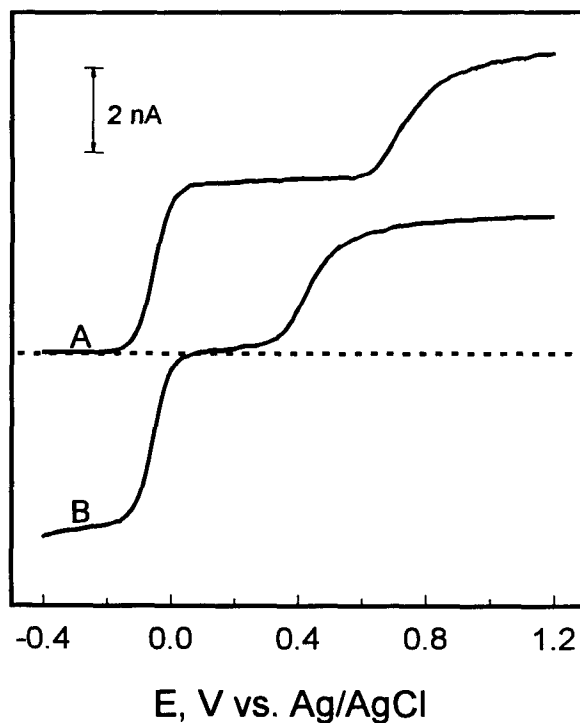


Figure 4.1. Steady-state voltammetry at a carbon microelectrode of a mixture of 1 mM $V^{III}(SB)^+$ (SB = ligand 2 in Table 4.1) and 1 mM DMFc in CH_3CN . (A) Solution saturated with argon. (B) After 0.5 mmol per liter of O_2 was injected into the solution. Supporting electrolyte: 10 mM tetrabutylammonium perchlorate. Scan rate: 10 mV s^{-1} . Ambient laboratory temperature. For this and subsequent figures the position of zero current is shown by the broken line.

enough to be monitored with the carbon fiber microelectrode. With the electrode potential maintained at -0.2 V, the cathodic current provides a direct measure of the concentration of DMFc^+ that is a product of the reaction (Figure 4.1, curve B). The course of the reaction could also be monitored with the electrode potential set at 0.2 V where the diminishing anodic current reflects the decreasing concentration of DMFc . The rate constants evaluated at either of these potentials were the same. If the electrode potential was set at ca. 0.5 V, the initial anodic current decreased only slightly as the reaction proceeded and the oxidizable DMFc was replaced stoichiometrically by the oxidizable $(\text{SB})\text{V}^{\text{IV}}\text{O}$. The current decrease at this potential reflects only the smaller diffusion coefficient of $(\text{SB})\text{V}^{\text{IV}}\text{O}$ compared with DMFc . However, this result confirmed that the rate of conversion of DMFc to DMFc^+ is a reliable measure of the rate of conversion of $\text{V}^{\text{III}}(\text{SB})^+$ to $(\text{SB})\text{V}^{\text{IV}}\text{O}$ as reaction 4 proceeds.

Shown in Figure 4.2A is a typical current-time curve obtained with the microelectrode potential set at -0.2 V during the autoxidation of $\text{V}^{\text{III}}(\text{salen})^+$ in the presence of excesses of O_2 and DMFc . A typical pseudo first order plot of such current-time data is shown in Figure 4.2B. The slope of the linear plot corresponds to a pseudo first-order rate constant of 0.018 s^{-1} . In the absence of DMFc , the same $\text{V}(\text{III})$ complex reduces O_2 at a rate (pseudo first order rate constant at 22°C : $5.0 \times 10^{-4} \text{ s}^{-1}$)² that is two to three orders of magnitude lower than this value.

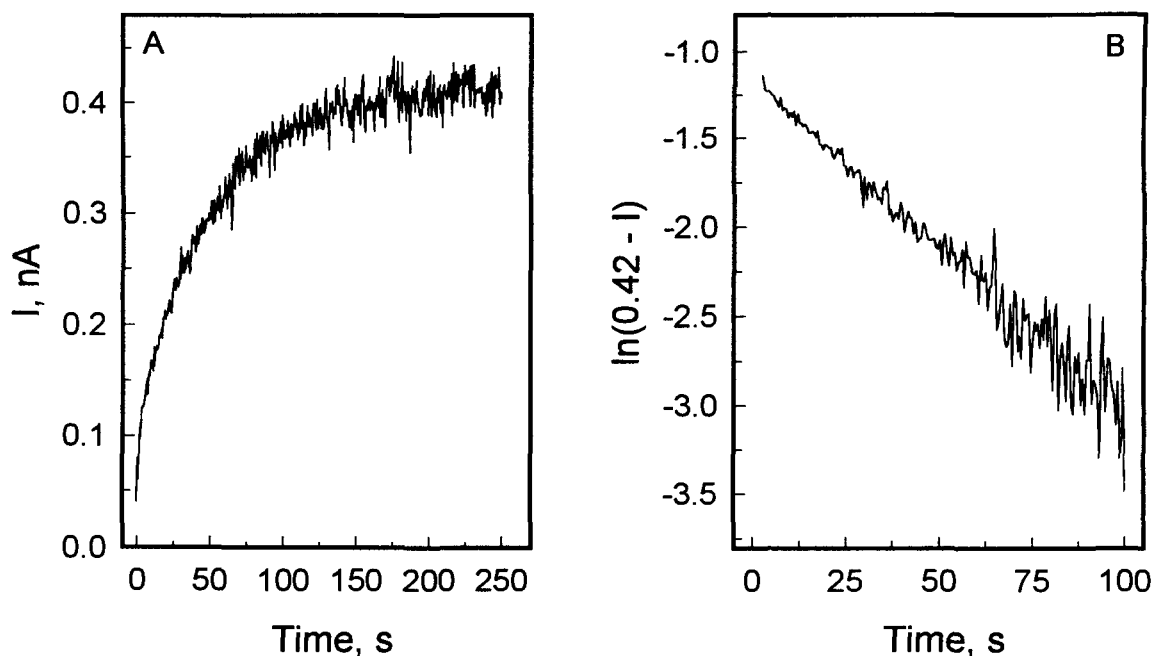


Figure 4.2. (A) Current-time transient recorded at 0 °C with a carbon microelectrode held at - 0.2 V in O₂-saturated CH₃CN initially containing 0.1 mM V^{III}(salen)⁺ (salen = ligand No. 1 in Table 4.1), 1.0 mM DMFc and 10 mM tetrabutylammonium perchlorate. (B) Pseudo-first-order kinetic plot of the data from (A). The number “0.42” in the logarithm term is the microelectrode current (in nA) after all the V^{III}(salen)⁺ is consumed (see the transient in A).

The rate constant did not change when the concentration of DMFc was varied between 0.5 and 2 mM. (The upper concentration is limited by the solubility of DMFc in CH₃CN at 0 °C.) When the concentration of O₂ was decreased five-fold (saturation with air instead of pure O₂), the reaction was found to be slightly slower: The pseudo first-order constant was 0.012 s⁻¹. Thus, with V^{III}(salen)⁺ as the limiting reactant, the reaction rate is zero order with respect to DMFc. The dependence of the reaction rate on O₂ concentration is less simple.

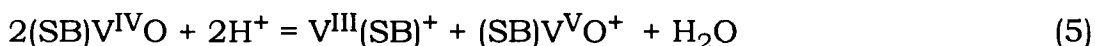
Similar results were obtained with V^{III}(SB)⁺ complexes with ligands 3, 5, 6, and 7 in Table 1. With ligands 2 and 4 the pseudo first-order rate was considerably higher; the rate constant was estimated to exceed 0.2 s⁻¹ in O₂-saturated CH₃CN.

Kinetic experiments conducted with DMFc instead of V^{III}(SB)⁺ as the limiting reactant exhibited more complex results: The reaction rate was lower than expected by extrapolation from Figure 2, the order of mixing of the three reactants affected the reaction rate, and an induction period appeared before the reaction began (see Appendix IV-A). Because of these complications, the kinetics of the reaction under these conditions were not pursued.

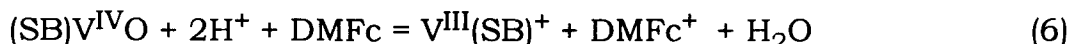
Catalysis by (SB)V^{IV}O of the Reduction of O₂ by DMFc

The results described so far were obtained in the absence of acid in

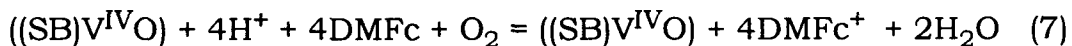
the acetonitrile solutions. In the presence of acid (HClO_4 or $\text{CF}_3\text{SO}_3\text{H}$), an additional reaction pathway becomes available in which the reduction of O_2 by DMFc is catalyzed by $(\text{SB})\text{V}^{\text{IV}}\text{O}$. It was demonstrated in our previous studies^{1,2} that $(\text{SB})\text{V}^{\text{IV}}\text{O}$ disproportionates rapidly in the presence of acid according to reaction 5:



If excess DMFc is also present, it reduces $(\text{SB})\text{V}^{\text{VO}^+}$ to $(\text{SB})\text{V}^{\text{IV}}\text{O}$, which can re-enter reaction 5 so that the net reaction becomes



If O_2 is also present in the solution the $\text{V}^{\text{III}}(\text{SB})^+$ produced in reaction 6 can undergo reaction 4 and a net four-electron reduction of O_2 to H_2O results in which DMFc is the reductant and $(\text{SB})\text{V}^{\text{IV}}\text{O}$ acts as a catalyst, as shown in reaction 7:



Shown in Figure 4.3 are microelectrode current-potential responses that demonstrate the chemistry just described. Curve A was recorded in a solution prepared by adding 2 mmoles per liter of DMFc, and 1 mmole per liter of $(\text{salen})\text{V}^{\text{IV}}\text{O}$ to anhydrous acetonitrile. The two anodic waves

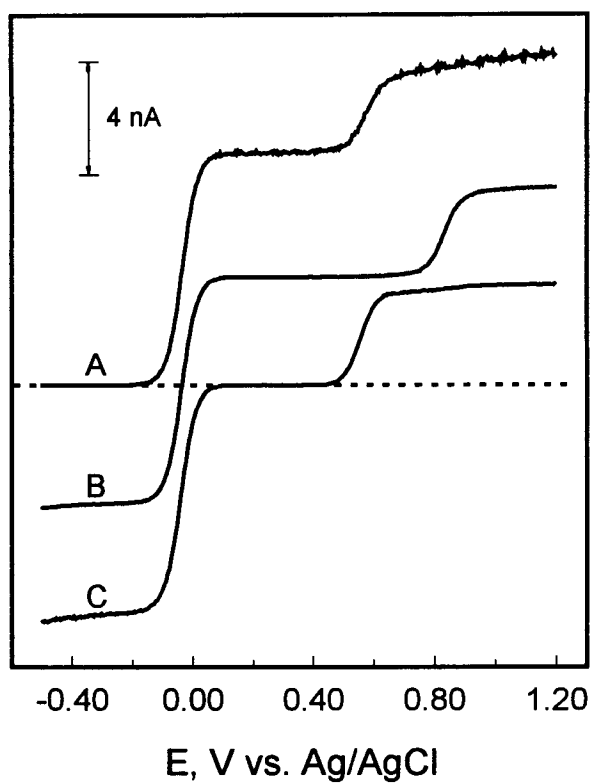


Figure 4.3. Steady-state voltammograms recorded with a carbon microelectrode in anhydrous CH_3CN . (A) Solution contained 2 mM DMFc and 1 mM $(\text{salen})\text{V}^{\text{IV}}\text{O}$ (salen = ligand 1 in Table 4.1); (B) After 2 mmol per liter of $\text{CF}_3\text{SO}_3\text{H}$ were added to the solution used in (A); (C) After 0.5 mol of O_2 per mole of vanadium was added to the solution used in (B). Other conditions as in Figure 4.1.

at -0.05 V and 0.6 V correspond to the $\text{DMFc}^{+/0}$ and $(\text{salen})\text{VO}^{+/0}$ couples, respectively. Curve B was obtained after 2 mmol per liter of $\text{CF}_3\text{SO}_3\text{H}$ were added to the solution used to record curve A. The three reactants present undergo reaction 6 to produce a solution that contains 1 mM each of DMFc and DMFc^+ , which are responsible for the composite cathodic-anodic wave at -0.05 V, as well as 1 mM $\text{V}^{\text{III}}(\text{salen})^+$, which gives rise to the anodic wave with $E_{1/2} = 0.8$ V. Curve C resulted after 0.5 mole of O_2 per mole of vanadium was added to the solution used to record Curve B: All of the DMFc was oxidized to DMFc^+ and all of the $\text{V}^{\text{III}}(\text{salen})^+$ was oxidized to $(\text{salen})\text{V}^{\text{IV}}\text{O}$ (which is electro-oxidized to $(\text{salen})\text{V}^{\text{VO}^+}$ at 0.6 V). If all three ingredients were added to acetonitrile at the same time, the response shown in Curve C was obtained immediately after mixing as a result of reaction 6 proceeding until all of the DMFc was consumed.

The catalytic role of $(\text{SB})\text{V}^{\text{IV}}\text{O}$ in the autoxidation of DMFc is confirmed by the results shown in Figure 4.4. As aliquots of a solution containing equimolar quantities of DMFc and $\text{CF}_3\text{SO}_3\text{H}$ were added to a dioxygen-saturated solution of $(\text{SB})\text{V}^{\text{IV}}\text{O}$ (with SB = ligand 4 in Table 4.1), the cathodic plateau current arising from reduction of DMFc^+ increased proportionately while the anodic plateau current, due to the oxidation of $(\text{SB})\text{V}^{\text{IV}}\text{O}$, was unaffected, as expected if it participates in reaction 7 only as a catalyst. The persistence of the $(\text{SB})\text{V}^{\text{IV}}\text{O}$ in all the solutions in

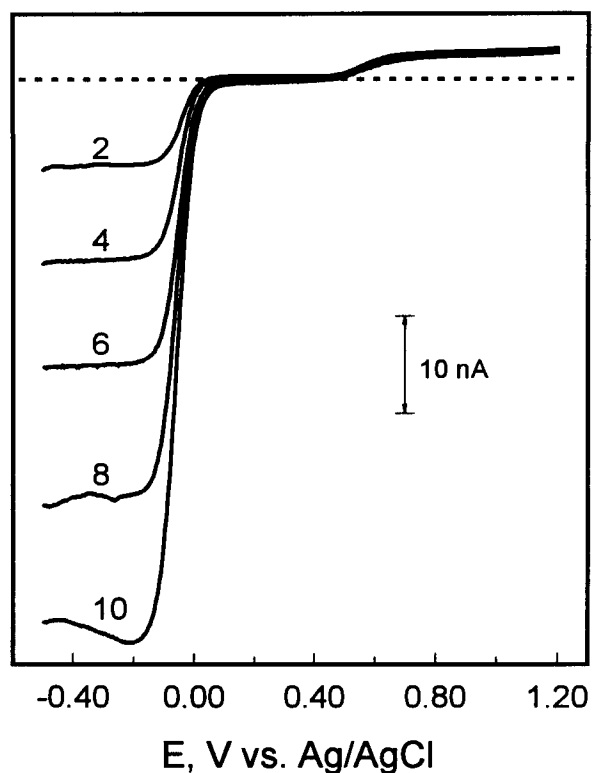


Figure 4.4. Steady-state voltammograms recorded with a carbon microelectrode in anhydrous CH_3CN saturated with O_2 and initially containing 1 mM $(\text{SB})\text{V}^{\text{IV}}\text{O}$ (SB = ligand 4 in Table 4.1). The numbers by each cathodic plateau give the total quantities (mmol per liter) of DMFc and $\text{CF}_3\text{SO}_3\text{H}$ that had been added in equimolar amounts to the solution before each curve was recorded. Other conditions as in Figure 4.1.

Figure 4.4 showed that the $\text{CF}_3\text{SO}_3\text{H}$ in each aliquot of the DMFc- $\text{CF}_3\text{SO}_3\text{H}$ mixture was fully consumed in reaction 6. If it were not, the acid-promoted disproportionation of $(\text{SB})\text{V}^{\text{IV}}\text{O}$ would have occurred.¹

The formation of water was detected by ^1H -NMR with CD_3CN (dried with 3Å molecular sieves before use) as the solvent to carry out an experiment similar to that

shown in Figure 4.4. By using the residual CHCD_2CN in the solvent as a convenient internal standard ($\delta = 1.96$ ppm, quintet), the water peak ($\delta = 2.15$ ppm) was found to increase significantly after addition of 20 mM DMFc and 20 mM $\text{CF}_3\text{SO}_3\text{H}$ to a 2 mM solution of the $(\text{SB})\text{V}^{\text{IV}}\text{O}$ (SB = ligand 4 in Table 4.1) under oxygen, which was dried through several columns filled with Drierite and molecular sieves before introduction into the solution.

The rate of oxidation of DMFc in acidified dioxygen-saturated acetonitrile was also monitored. The reaction was much too slow to have contributed significantly to the production of DMFc^+ during the experiments of Figure 4.4 (see Figure 4.5 in next section).

Kinetics of the Catalytic Reaction

The kinetics of the reduction of O_2 by DMFc as catalyzed by $(\text{SB})\text{V}^{\text{IV}}\text{O}$ in the presence of acid were monitored voltammetrically at 0 °C using a carbon microelectrode. The electrode was maintained at - 0.2 V where

the only electrode reaction that occurred was the reduction of DMFc^+ to DMFc (Figure 4.3). Shown in Figure 4.5 are current-time transients that resulted when small quantities of $(\text{SB})\text{V}^{\text{IV}}\text{O}$ (SB = ligand 7 in Table 4.1) were added to an acetonitrile solution saturated with O_2 and containing 1 mM DMFc and 2 mM $\text{CF}_3\text{SO}_3\text{H}$ (curves 1 and 2). Curve 3 in the figure shows the much lower rate of the reduction of O_2 by DMFc in the absence of the catalyst, $(\text{SB})\text{V}^{\text{IV}}\text{O}$. Subtraction (point by point) of curve 3 from curves 1 and 2 produced the transients shown in the insert in Figure 4.5. Only the initial portions of the current-time data were utilized to avoid both the kinetic complexities that are encountered with low concentrations of DMFc (*vide supra*) and the slow, acid-promoted decomposition of the $(\text{SB})\text{V}^{\text{IV}}\text{O}$ complexes.

The linearity of the two plots in the insert in Figure 4.5 is expected if reaction 7 were proceeding with the concentrations of all the reactants essentially constant. The slopes of the two plots differ by a factor of about 2, which matches the ratio of the $(\text{SB})\text{V}^{\text{IV}}\text{O}$ catalyst concentrations in the two experiments. Thus, the catalytic rate law is apparently first order in the concentrations of catalyst, as would be expected if the presence of acid serves only to replenish the supply of $\text{V}^{\text{III}}(\text{SB})^+$ (via rapid reactions 5 and 6) as it is consumed by reaction with O_2 . Assuming that the reaction rate is independent of the concentration of DMFc , just as it is in the absence of acid (*vide supra*), the pseudo first-order rate

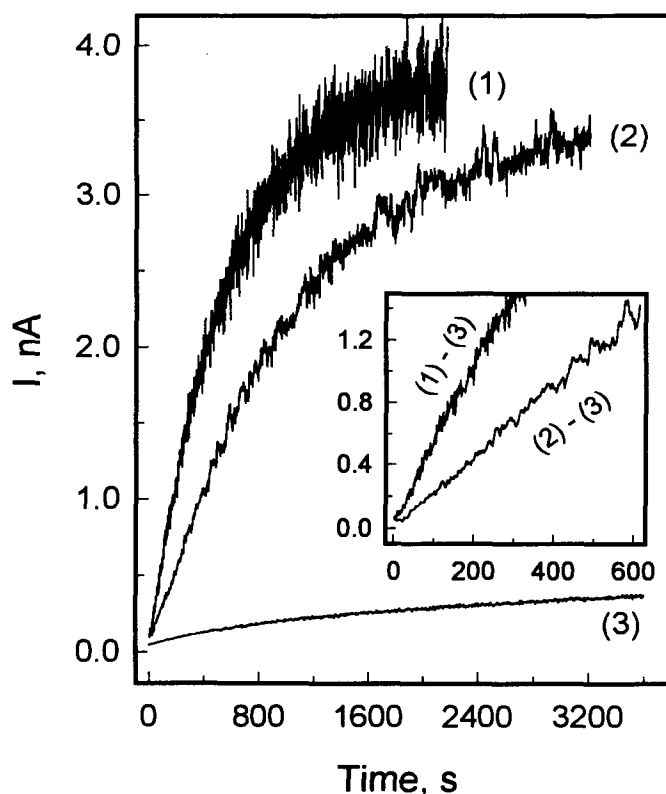


Figure 4.5. Current-time curves recorded at 0 °C with a carbon microelectrode held at -0.2 V in O₂-saturated CH₃CN containing 1 mM DMFc, 2 mM CF₃SO₃H and 10 mM TBAClO₄. The reaction was initiated by the addition of (1) 100, (2) 50, (3) 0 micromoles per liter of (SB)^{VI}VO (SB = ligand 7 in Table 4.1) to the solution. Other conditions as in Figure 4.2. Insert: Plots of the initial portions of curves 2 and 3 after point-by-point subtraction of curve 1 in each case.

constants with respect to the catalyst calculated from the slopes of the curves 1 and 2 in the insert in Figure 4.5 are 0.016 s^{-1} and 0.014 s^{-1} , respectively. These values are in reasonable agreement with the rate constant evaluated in the absence of acid, 0.018 s^{-1} , which supports the assumption that the addition of acid affects the kinetics only by means of reactions 5 and 6, both of which are much faster than reaction 7.

DISCUSSION

Comparison with Previous Studies

Our previous studies^{1, 2} have shown that dioxygen can be reduced to two oxo groups by vanadium(III)- Schiff base complexes. In dioxygen-saturated acetonitrile, the pseudo first-order rate constants of the reaction range from $5.0 \times 10^{-4} \text{ s}^{-1}$ to $4.0 \times 10^{-3} \text{ s}^{-1}$ (at ambient laboratory temperature), depending upon the Schiff base ligands in the vanadium complexes. The results from this study indicate that the presence of DMFc greatly enhances the rate of the reduction of dioxygen. Under similar conditions, the pseudo first-order rate constants (0.018 s^{-1} to 0.2 s^{-1} at $0 \text{ }^\circ\text{C}$) for the reduction (reaction 4) are two to three orders of magnitude higher than those obtained in the absence of DMFc.

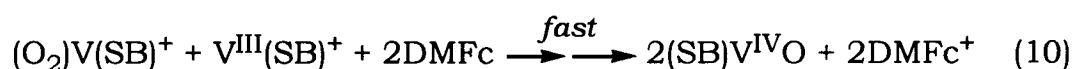
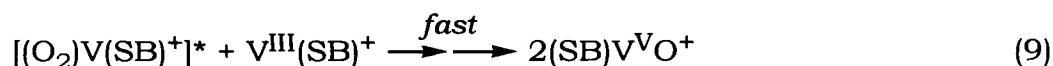
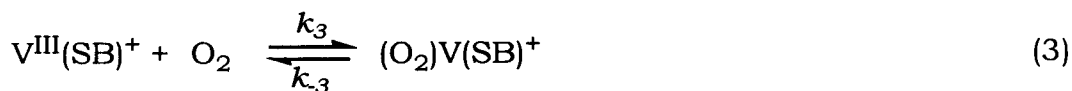
The problem of acid-induced decomposition of $\text{V}^{\text{III}}(\text{SB})^+$ encountered in our previous studies can also be alleviated when catalytic reduction of dioxygen is carried out with DMFc as the reducing agent, because the

more rapid oxidation of $V^{III}(SB)^+$ would result in shorter exposure time of the complex to acid. In our previous study,¹ only the V(III) complexes of ligands 3, 4, and 7 in Table 4.1 were stable enough to provide sustained catalytic electroreduction of O_2 in the presence of acid. In the present study, however, the complexes with all the ligands in Table 4.1 exhibited good catalytic activity for the reduction of oxygen by DMFc in acidified acetonitrile at room temperature. The turn-over numbers were estimated by using $50 \mu M (SB)V^{IV}O$ as the catalyst in O_2 -saturated acetonitrile. For complexes of ligands 1, 2, 5, and 6, which showed no catalytic activity in the electroreduction of oxygen due to the instability of the corresponding V(III) complexes,¹ more than 60 turn-overs were obtained. More than 180 turn-overs were reached with complexes of ligands 3, 4, and 7.

Mechanism of Reaction 4

The results shown in Figures 4.1 and 4.3 clearly established the stoichiometry of reaction 4. Experiments like those in Figure 4.2 demonstrated that the autoxidation of $(SB)V^{III+}$ is much more rapid when DMFc is present. The complex behavior obtained in kinetic experiments involving all three reactants thwarted attempts to establish a generally applicable rate law. However, the results obtained were sufficiently reproducible and clear-cut to support some speculations about the reaction chemistry believed to be involved. The three reactants involved

in reaction 4 consist of two reductants and one oxidant. Pairwise combination of the oxidant (O_2) with either reductant results only in very slow reaction rates; all three reactants are required to produce enhanced reaction rates. This behavior indicates that an intermediate formed by reaction between two of the reactants reacts rapidly with the third reactant to produce the rate enhancement. The association of DMFc with either O_2 or $V^{III}(SB)^+$ is unlikely. The presence of DMFc does not affect the electrochemistry of either O_2 or $V^{III}(SB)^+$. The only possibility left is that the intermediate is $(O_2)V(SB)^+$ (formed in reaction 3), which can be more rapidly reduced by DMFc than by $V^{III}(SB)^+$. Although this reaction pathway can explain the rate enhancing effect of DMFc on the autoxidation of $V^{III}(SB)^+$, it is not compatible with the mechanistic interpretation offered previously,^{1, 2} (in which the forward direction of reaction 3 was assigned as the rate-limiting step) because DMFc can not reduce $(O_2)V(SB)^+$ any faster than it is formed. A modification to the previous interpretation is outlined in Scheme I. In this scheme, the sum of reactions 3, 8, and 9 gives reaction 1, which describes the autoxidation of $V^{III}(SB)^+$ in the absence of DMFc. The key point in Scheme I is the introduction of reaction 8, according to which the O_2 -vanadium adduct formed in reaction 3 undergoes an intramolecular transformation, e.g., intramolecular electron-transfer, to produce the oxidant that reacts with a second $V^{III}(SB)^+$ molecule rapidly to form

Scheme I

two molecules of $(\text{SB})\text{V}^{\text{VO}}^+$ in reaction 9. As long as reaction 8 is slower than reaction 3, i.e., reaction 3 reaches equilibrium readily, reaction 1 is first order in both O_2 and $\text{V}^{\text{III}}(\text{SB})^+$. In this case, the second-order rate constant measured previously in the absence of DMFc would be the product of K_3 (the equilibrium constant of reaction 3) and k_8 , rather than k_3 , the constant governing the forward direction of reaction 3. In the presence of DMFc, the autoxidation of $\text{V}^{\text{III}}(\text{SB})^+$ (reaction 4) is realized by combining reactions 3 and 10. The acceleration of the overall reaction rate is regarded as the result of reaction 10 in which $(\text{O}_2)\text{V}(\text{SB})^+$ is reduced rapidly by DMFc (in the presence of $\text{V}^{\text{III}}(\text{SB})^+$) without having to undergo the slower intramolecular transformation depicted in reaction 8. Scheme 1 is thus compatible with the rate law of equation 2 in the absence of DMFc as well as the observed independence of the rate of the DMFc-

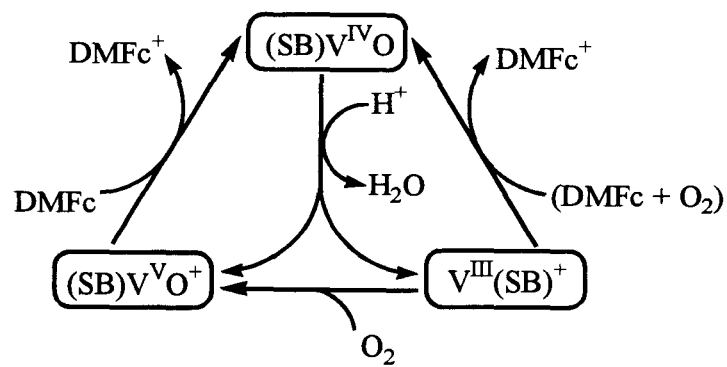
enhanced reaction on the concentration of DMFc (present in stoichiometric excess).

Several questions remain in Scheme I. First, the magnitude of the equilibrium constant, K_3 , is unknown, but it cannot be very large because no evidence of saturation kinetics was obtained (in the absence of DMFc) when $[O_2]$ was increased from 1.6 to 8 mM at room temperature. In the presence of DMFc, reaction 3 may or may not reach equilibrium, depending upon the overall rate of reaction 10. Second, the precise nature of reaction 8 and the reason (other than an increase in driving force) that DMFc is able to reduce $(O_2)V(SB)^+$ readily while $V^{III}(SB)^+$ is not are not clear. Third, the complicated kinetic behavior of reaction 4, including the dependence of its rate on the order of mixing of the three reactants, its less-than-first order dependence on O_2 , and the appearance of an induction period when DMFc is the limiting reactant, cannot be rationalized with Scheme I. An additional complication in the reaction kinetics was encountered when they were measured in the presence of stoichiometric excesses of both $(SB)V^{III+}$ and DMFc with O_2 as the limiting reactant. Under these conditions the overall reaction rate became so much lower that it could be monitored at room temperature. The source of this anomaly was not identified, but the behavior could possibly reflect the formation of a dioxo-bridged dimeric vanadium complex with considerably diminished reactivity toward DMFc. More

detailed kinetic studies are needed in order to offer a complete and satisfactory mechanism to be compatible with all these observations.

CONCLUSIONS

Although Scheme I cannot account for all the observed kinetic behavior, it provides a reasonable basis for understanding the pattern of reactivity of the $V^{III}(SB)^+/O_2/DMFc$ system. In particular, the chemistry by which $V^{III}(SB)^+$ reduces O_2 stoichiometrically to the oxo ligands (in $(SB)V^VO^+$ or $(SB)V^{IV}O$) is accounted for as is the ability of DMFc to enhance the rate of this reaction. The combination of Scheme I with previously demonstrated acid-induced disproportionation of $(SB)V^{IV}O$ (reaction 5) followed by the rapid reduction of $(SB)V^VO^+$ by DMFc (reaction 6) provides a chemical pathway to reduce dioxygen by four electrons to water, with the vanadium-Schiff base complexes as the catalyst, as shown in Scheme II. In this scheme, DMFc not only provides the electrons for the reduction, but also enhances the rate of the reduction of dioxygen by $(SB)V^{III+}$ (reaction 4).

Scheme II

APPENDIX IV-A**Kinetics of Reaction 4****When DMFc Is the Limiting Reactant**

As shown in Figure 4.6, kinetic experiments conducted with DMFc instead of $V^{III}(SB)^+$ as the limiting reactant exhibited more complex results: The reaction rate was lower than expected by extrapolation from Figure 4.2, the order of mixing of the three reactants affected the reaction rate, and an induction period appeared before the reaction began if $V^{III}(SB)^+$ and O_2 were mixed first.

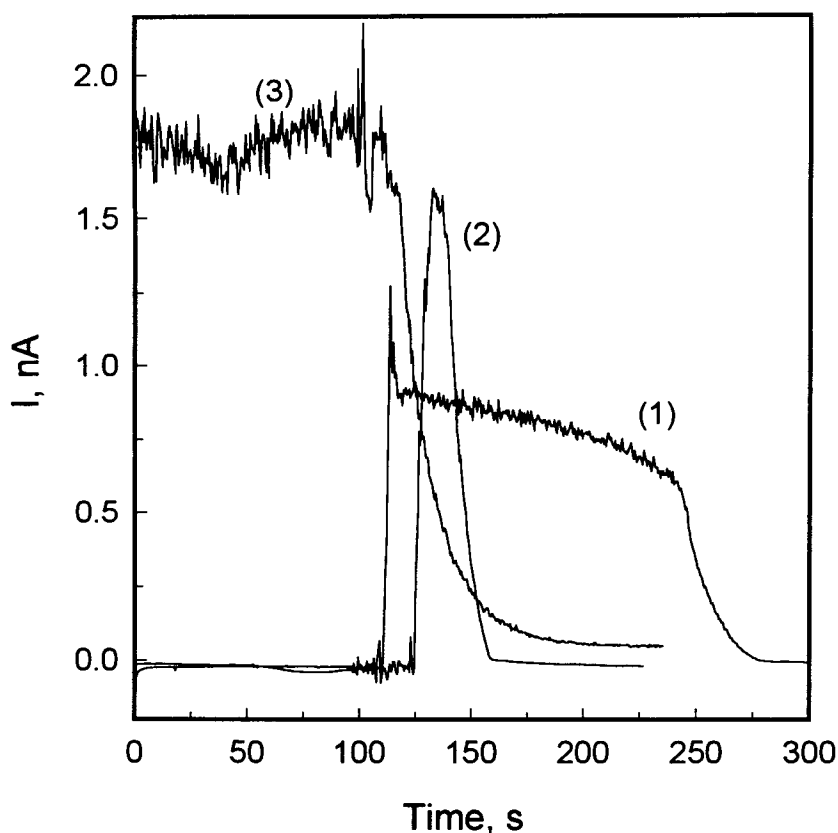


Figure 4.6. Current-time transients recorded with a carbon microelectrode in acetonitrile at 0 °C. The electrode was held at 0.2 V to monitor the DMFc oxidation current. (1) $V^{III}(\text{salen})^+$ (2.0 mmol per liter) was first added ($t = 0$ s) to O_2 -saturated acetonitrile, followed by the addition ($t \sim 110$ s) of DMFc (0.2 mmol per liter). (2) $V^{III}(\text{salen})^+$ (2.0 mmol per liter) and DMFc (0.4 mmol per liter) was first added to Ar-saturated acetonitrile, followed by bubbling O_2 into the solution ($t \sim 120$ s) and the solution was kept saturated with O_2 . (3) DMFc (0.4 mmol per liter) was first added ($t = 0$ s) to O_2 -saturated acetonitrile, followed by the addition ($t \sim 100$ s) of $V^{III}(\text{salen})^+$ (2.0 mmol per liter). Other conditions as in Figure 4.2.

REFERENCES

- (1) Liu, Z.; Anson, F. C. *Inorg. Chem.* **2001**, *40*, 1329-33.
- (2) Liu, Z.; Anson, F. C. *Inorg. Chem.* **2000**, *39*, 274-280, 1048.

CHAPTER V

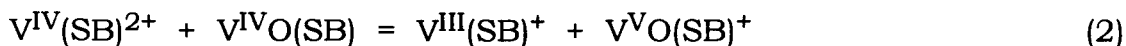
**Electrochemistry of Vanadium-N, N'-1, 2-phenylenebis-
(2-hydroxy-1-naphthylideneimine) Complexes
in Acetonitrile Containing Excess Acetic Anhydride**

ABSTRACT

Electrochemical study of vanadium-naphophen (naphophen = N, N'-1, 2-phenylenebis-(2-hydroxy-1-naphthylideneimine)) complexes in acetonitrile containing excess acetic anhydride was conducted. $V^{IV}O(\text{naphophen})$ was found to undergo deoxygenation by two equivalents of acid to give $V^{IV}(\text{naphophen})^{2+}$, which had not persisted in previous studies. The availability of this deoxygenated species made it possible to demonstrate directly several reactions proposed previously to describe the chemistry of vanadium-Schiff base complexes in acidified acetonitrile.

INTRODUCTION

In recent reports¹ (see also Chapters II and III), we described the acid-induced disproportionation of oxovanadium(IV)-Schiff base (SB) complexes, VO(SB), in anhydrous acetonitrile. The disproportionation (reaction 3) was proposed to proceed through a “deoxygenation” step (reaction 1) followed by a simple outsphere redox reaction (reaction 2), as shown below:





Reactions 1 and 2 could not be observed directly because they proceeded at rates close to the diffusion-limited value,² but the equilibrium constants for the two reactions could be calculated from the equilibrium constant of reaction 3 (measured by titration of VO(SB) with acid in the presence of excess water¹) and the formal potentials of the couples VO(SB)^{+ / 0} and V(SB)^{2+ / +}. For SB = salen (salen = N, N'-1, 2-ethylenebis-(salicylideneimine)), K₁ and K₂ are 42 M⁻¹ and 3.8 x 10⁴, respectively.^{1a}

We also attempted^{1a} to obtain V^{IV}(SB)²⁺ by electrooxidation of V^{III}(SB)⁺ but the resulting product was always V^{VO}(SB)⁺. The

observation that $V^{IV}(SB)^{2+}$ could not persist was explained on the basis of the following proposed reaction:



Reaction 4 shows that $V^{IV}(SB)^{2+}$ would disproportionate in the presence of water, which could be produced during the preparation of $V^{III}(SB)^+$ (by reaction of $V^{IV}O(SB)$ with H_2 and acid¹), or might be present in the incompletely dried solvent. Reaction 4 probably proceeds first by the reverse of reaction 1, followed by reaction 2. Its equilibrium constant can thus be calculated as $K_4 = K_2/K_1 = 9.0 \times 10^2$ M for the ligand salen. With such an equilibrium constant, it is understandable that $V^{IV}(SB)^{2+}$ could not persist in the presence of water in weakly acidified acetonitrile.

If water could be removed more effectively or if the acid concentration were sufficiently high, reaction 4 might be shifted to the left side. The latter is impractical because high acid concentration also causes other side reactions such as the decomposition of the Schiff base ligands. In this study, we examined the reaction of the oxovanadium complex with Schiff base N, N'-1, 2-phenylenebis-(2-hydroxy-1-naphthylidene-iminate) (naphophen, see SB No. 14 in Table 3.1 for its structure) with acid in the presence of excess acetic anhydride, which can remove the water in acetonitrile and the resulting acetic acid is weak enough not to react with the oxovanadium complex. $V^{IV}(\text{naphophen})^{2+}$ was found to

persist in such an environment and can be prepared in several ways, which makes it possible to demonstrate reactions 1, 2 and 4 directly. The results provide more supportive evidence for the chemistry proposed in our previous studies,¹ and help to clarify the nature of the reaction between oxovanadium-Schiff base complexes and acid in acetonitrile.^{3, 4}

EXPERIMENTAL

Materials

Distilled acetonitrile containing 0.001% water (EM Science) was stored over 3 Å molecular sieves. Trifluoromethanesulfonic (triflic) acid (Sigma) was used as received and was maintained O₂-free by saturation with Ar. Acetic anhydride (99%+, Aldrich) was used as received. All supporting electrolytes were electrochemical grade (Fluka). They were placed under vacuum at 75 °C overnight before use. The Schiff base ligand, H₂naphophen, was prepared by condensing 1-hydroxy-2-naphthaldehyde (Aldrich) with 1, 2-phenylenediamine (Aldrich) in ethanol. The resulting insoluble ligand, without further purification, was refluxed with VOSO₄ in ethanol to prepare V^{IV}O(naphophen), as described previously.^{1b, 5}

V^{III}(naphophen)⁺ was prepared as previously described¹ by reduction of V^{IV}O(naphophen) with H₂ in the presence of a large area Pt gauze and one mole of triflic acid per mole of V(IV) and was used in situ.

Apparatus and Procedures

Electrochemical measurements were carried out in conventional one- or two-compartment cells using a BAS Model 100B/W Electrochemical Analyzer. Solutions were kept under an atmosphere of argon which was purified by passage through a gas scrubber (Oxiclear, Aldrich) and two columns filled with molecular sieves. The working electrode in voltammetric experiments was a 10 μm carbon microelectrode or a 5mm glassy carbon disk, which were polished with 0.3 μm and 0.05 μm alumina paste before use. A porous glassy-carbon working electrode was used for bulk electrolyses. Auxiliary electrodes were platinum wires or foils. The reference electrode was Ag/AgCl in CH_3CN saturated with NaCl. All potentials are quoted with respect to this electrode. The half-wave potentials of the ferrocinium/ferrocene couple measured from microelectrode voltammograms recorded in pure acetonitrile and in a 0.1 M tetrabutylammonium perchlorate solution in acetonitrile were 0.47 V and 0.44 V, respectively, versus this reference electrode.

Solution IR spectra were obtained using a Perkin Elmer 1600 FT-IR spectrophotometer and a cell with CaF_2 windows separated by 1 mm. Baselines were obtained using pure acetonitrile. EPR spectra were recorded on a Bruker EMX spectrometer operating at X-band. A cylindrical quartz cell with a diameter of 2 mm was used as the sample tube.

RESULTS

Deoxygenation of $V^{IV}O(\text{naphophen})$

Acetic anhydride was found to be an effective reagent to remove water from acetonitrile. More importantly, the resulting acetic acid is such a weak acid that it does not induce the disproportionation of $V^{IV}O(\text{naphophen})$. A carbon microelectrode was used to monitor the reaction of $V^{IV}O(\text{naphophen})$ with triflic acid in the presence of excess acetic anhydride. Shown in Figure 5.1A are the results. The small oxidation wave in curve 1 was obtained in a suspension of 1 mmol per liter $V^{IV}O(\text{naphophen})$ (the solubility of this compound in acetonitrile is about 0.15 mM^{1b}) in pure acetonitrile containing 50 mM acetic anhydride. The addition of 2 mmol per liter of triflic acid to the suspension resulted in a clear solution that exhibited a voltammogram as shown in curve 2. The reduction wave seems to consist of two closely spaced waves (More electrochemical experiments are presented later regarding this observation.) but the total height corresponds to a one-electron per vanadium process. (Electrolysis of this solution confirmed the one-electron process, *vide infra*.) The EPR spectrum of this solution exhibited a set of eight-lines (curve 2 in Figure 5.1B: $A = 85 \text{ G}$, $g_0 = 1.993$) different from that of the starting $V^{IV}O(\text{naphophen})$ (curve 2 in Figure 5.1B: $A = 99 \text{ G}$, $g_0 = 1.987$), indicating that the solution contained a new V(IV) species. IR spectrum of the solution showed no V=O double

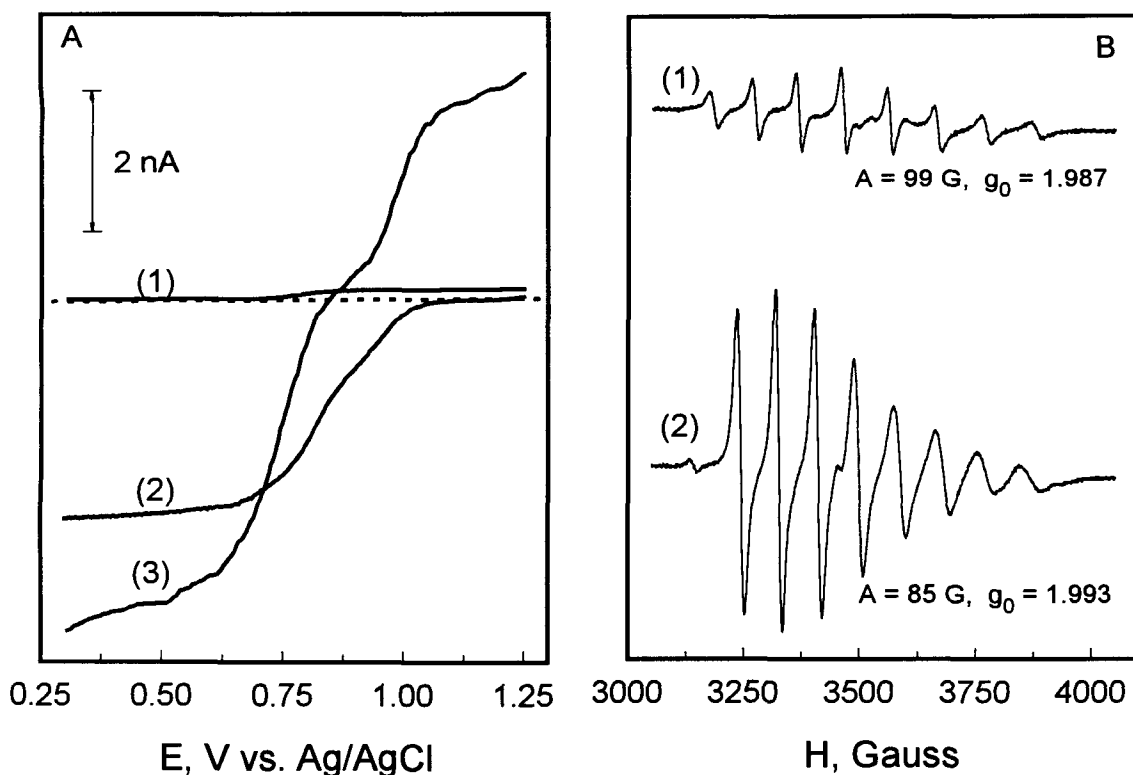


Figure 5.1. (A) Steady-state current potential curves recorded with a 10 μm carbon microelectrode in acetonitrile containing 50 mM acetic anhydride. (1) A 1 mmol per liter of $\text{V}^{\text{IV}}\text{O}(\text{naphophen})$ suspension; (2) After addition of 2 mmol per liter of $\text{CF}_3\text{SO}_3\text{H}$ to the suspension; (3) After 1 mmol per liter of $\text{V}^{\text{IV}}\text{O}(\text{naphophen})$ was added to the solution used to record curve 2. Scan rate: 10 mV s^{-1} ; Temperature: $22 \pm 2 \text{ }^\circ\text{C}$. The dotted line marks the position of zero current. (B) The EPR spectra of (1) a $\text{V}^{\text{IV}}\text{O}(\text{naphophen})$ -saturated solution in CH_2Cl_2 ; and (2) the solution used to record curve 2 in (A).

bond stretching peak. It was also found that exposure of this solution to air caused no change in the observed electrochemistry, as well as in the EPR and IR spectra. Based on these observations, this new species is assigned to be $V^{IV}(\text{naphophen})^{2+}$, which was produced by deoxygenation of $V^{IV}O(\text{naphophen})$ with two equivalents of acid in the presence of anhydride, as described by reaction 1.

If the new V(IV) species is $V^{IV}(\text{naphophen})^{2+}$, addition of more $V^{IV}O(\text{naphophen})$ to this solution should cause reaction 2 to proceed. Curve 3 in Figure 1A shows the expected result: Addition of equimolar $V^{IV}O(\text{naphophen})$ to the solution used to record curve 2 led to the disappearance of the reduction wave(s). Instead, two separated anodic and cathodic waves, corresponding to the oxidation of 1 mM $V^{III}(\text{naphophen})^+$ and the reduction of 1 mM $V^{V}O(\text{naphophen})^+$ respectively,^{1b} were produced. (The different heights of the two waves are probably due to a difference in the diffusion coefficients of the two species.) The EPR spectrum of the resulting solution also showed no V(IV) species were present. The net result of the process from curve 1 to curve 3 is just the acid-induced disproportionation of 2 mmol per liter of $V^{IV}O(\text{naphophen})$, as described by reaction 3. The presence of anhydride allowed the direct observation of the disproportionation in two steps, the deoxygenation and the redox reaction, described by reactions 1 and 2.

Demonstration of Reaction 4

The chemistry described by the two directions of reaction 4, i.e., the acid-induced comproportionation of $V^VO(\text{naphophen})^+$ and $V^{III}(\text{naphophen})^+$, and the water-induced disproportionation of $V^{IV}(\text{naphophen})^{2+}$, is demonstrated by results shown in Figure 5.2. Curve 1 shows the electrochemistry of an equimolar mixture of $V^VO(\text{naphophen})^+$ and $V^{III}(\text{naphophen})^+$, prepared by mixing equimolar amount of $VO(\text{naphophen})$ and acid in acetonitrile containing excess acetic anhydride (Curve 1 could also be obtained in the absence of acetic anhydride because it was the result of the acid-induced disproportionation of the oxovanadium(IV) complex, as demonstrated in our previous studies.¹). According to reaction 4, additional acid would shift this equilibrium to the left side, i.e., $V^VO(\text{naphophen})^+$ and $V^{III}(\text{naphophen})^+$ would comproportionate to give $V^{IV}(\text{naphophen})^{2+}$ because water is essentially removed by the excess anhydride. As shown in curve 2, the resulting voltammogram after the addition of stoichiometric amount of acid is identical to that shown in curve 2 of Figure 1A, which has been assigned to be the reduction of $V^{IV}(\text{naphophen})^{2+}$. If the anhydride is removed by adding an equimolar amount of water, the $V^{IV}(\text{naphophen})^{2+}$ would be expected to react with the original residual water in the solvent plus the water formed from the disproportionation of $V^{IV}O(\text{naphophen})$ to give back $V^VO(\text{naphophen})^+$

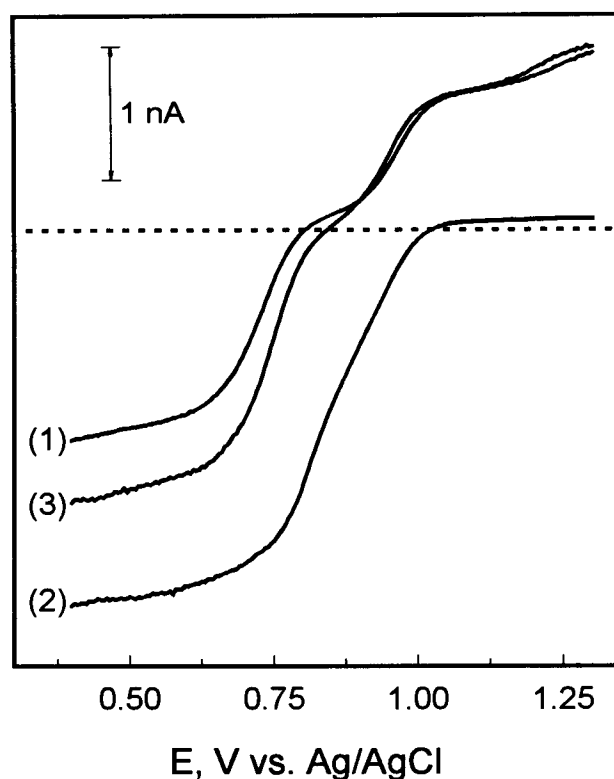


Figure 5.2. Microelectrode steady-state current potential curves recorded in anhydrous acetonitrile containing 50 mM acetic anhydride. (1) After 1 mmol per liter of VO(naphophen) and 1 mmol per liter of $\text{CF}_3\text{SO}_3\text{H}$ were mixed in the solution; (2) After an additional 1 mmol per liter of $\text{CF}_3\text{SO}_3\text{H}$ was introduced to the solution used to record curve 1; (3) After 50 mmol per liter of water was added to the solution used to record curve 2. Other conditions as Figure 5.1A.

and $V^{III}(\text{naphophen})^+$. Curve 3 shows exactly the expected result. Compared with curve 1, the reduction current of $V^VO(\text{naphophen})^+$ becomes higher. This increase can be attributed to the release of the added acid (1 mM) before recording curve 2, as a result of the disproportionation of $V^{IV}(\text{naphophen})^{2+}$ according to the forward direction of reaction 4. As described in our previous reports,^{1a} the enhancement of the $V^VO(\text{SB})^+$ reduction current in the presence of acid is caused by the regeneration of $V^VO(\text{SB})^+$ from the disproportionation of $V^{IV}(\text{SB})$, which is the electrochemical reduction product of $V^VO(\text{SB})^+$.

Electrooxidation of $V^{III}(\text{naphophen})^+$

Electrolysis of $V^{III}(\text{naphophen})^+$ at 1.1 V (on the plateau of its oxidation curve) in the absence of acetic anhydride was found to consume two moles of electrons per mole of vanadium and the final product was $V^VO(\text{naphophen})^+$. This observation is the same as those obtained previously with V(III) complexes of other Schiff base ligands.¹ The result can be explained on the basis of reaction 4: The product of the electrooxidation of $V^{III}(\text{naphophen})^+$, $V^{IV}(\text{naphophen})^{2+}$, disproportionates in the presence of water to produce $V^VO(\text{naphophen})^+$ and $V^{III}(\text{naphophen})^+$. The $V^{III}(\text{naphophen})^+$ thus formed is electrooxidized and reaction 4 occurs again. The process continues until all the V(III) is converted to V(V).

In the presence of excess anhydride, however, electrolysis of $V^{III}(\text{naphophen})^+$ at the same potential (with tetrabutylammonium triflate, $TBACF_3SO_3$, as the supporting electrolyte, *vide infra*) became a one-electron process. After the electrolysis, the product exhibited the same electrochemistry and EPR spectrum as the $V^{IV}(\text{naphophen})^{2+}$ obtained by direct deoxygenation of $V^{IV}O(\text{naphophen})$ with two equivalents of acid, as described earlier (Figure 5.1). This result is expected: The presence of anhydride effectively stops reaction 4 because of the lack of water. The electrooxidation of $V^{III}(\text{naphophen})^+$ described here thus provides another way to prepare $V^{IV}(\text{naphophen})^{2+}$.

Electrochemistry of $V^{III}(\text{naphophen})^+$ and $V^{IV}(\text{naphophen})^{2+}$

From the microelectrode voltammograms shown in Figures 5.1 and 5.2, it can be seen that the reduction wave of $V^{IV}(\text{naphophen})^{2+}$ consists of two closely spaced waves. In order to identify the origin of this observation, more electrochemical experiments were conducted. Shown in curve 1 of Figure 5.3 is the cyclic voltammogram of $V^{III}(\text{naphophen})^+$ at a 5 mm glassy carbon electrode with $TBACF_3SO_3$ as the supporting electrolyte. The cathodic peak, i.e., the reduction of $V^{IV}(\text{naphophen})^{2+}$, was broadened compared with the anodic peak. The solution used to record curve 1 was then subject to electrolysis at 1.1 V. Just like the electrolysis described in the last section, this one also consumed one

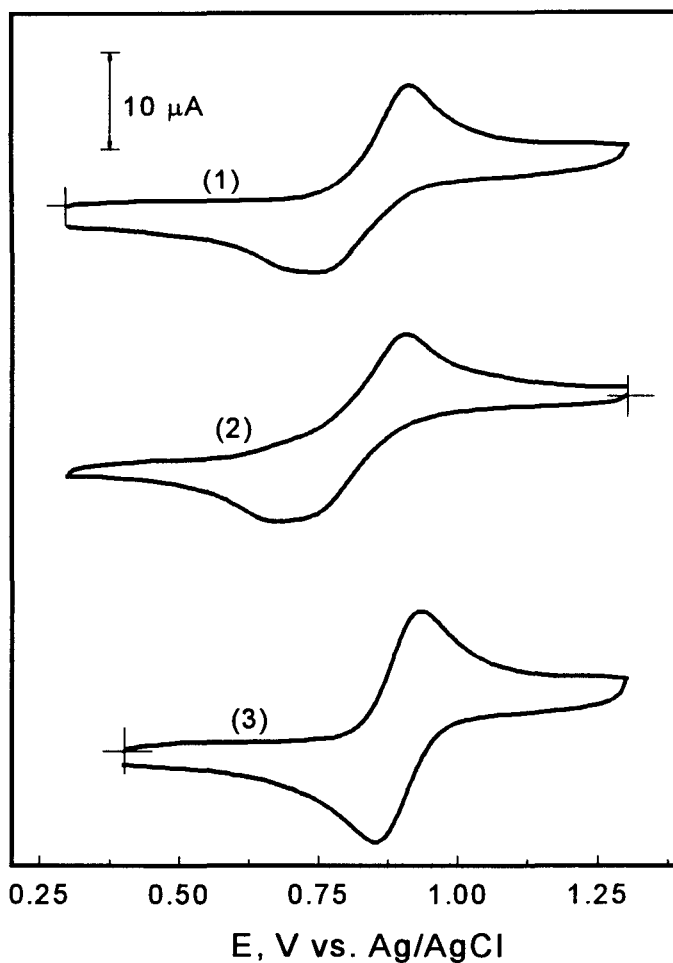


Figure 5.3. Cyclic voltammograms recorded at 50 mV s^{-1} with a 5 mm glassy carbon electrode in acetonitrile containing 50 mM acetic anhydride. (1) A solution containing 1 mM $\text{V}^{\text{III}}(\text{naphophen})^+$ and 50 mM $\text{TBACF}_3\text{SO}_3$; (2) After the solution used to record curve 1 was electrolyzed at 1.1 V; (3) A solution containing 1 mM $\text{V}^{\text{III}}(\text{naphophen})^+$ and 50 mM TBAClO_4 .

mole of electrons per mole of vanadium. The cyclic voltammogram of the resulting product, presumably $V^{IV}(\text{naphophen})^{2+}$, is shown in curve 2, which also exhibits a broadened cathodic peak similar to that in curve 1. The steady-state microelectrode voltammogram of the solution exhibited a similar shape to those shown in Figures 5.1 and 5.2 where the voltammograms were recorded in the absence of supporting electrolyte.

When $TBAClO_4$ was used as the supporting electrolyte, a symmetrical cyclic voltammogram of $V^{III}(\text{naphophen})^+$ was obtained, as shown in curve 3 of Figure 5.3. Subsequent electrolysis of the solution at 1.1 V, however, quickly resulted in the formation of precipitates, which prevented the study of the electrochemistry of the product. Further experiments with this supporting electrolyte were thus not pursued.

Reductive electrolysis of $V^{IV}(\text{naphophen})^{2+}$ was also performed. A solution of $V^{IV}(\text{naphophen})^{2+}$ was first made by the deoxygenation of $V^{IV}O(\text{naphophen})$ with acid in acetonitrile containing excess acetic anhydride. The steady-state voltammogram (Figure 5.4, curve 1) exhibited a two-step reduction, the same as observed earlier. The solution was then subject to electrolysis at $E_1 = 0.78$ V, a potential at which the second reduction does not proceed rapidly (well below the mass-transfer-controlled rate). The progress of the electrolysis was monitored by microelectrode voltammetry, as shown in Figure 4, curves 2~5. The n values on these curves correspond to the number of

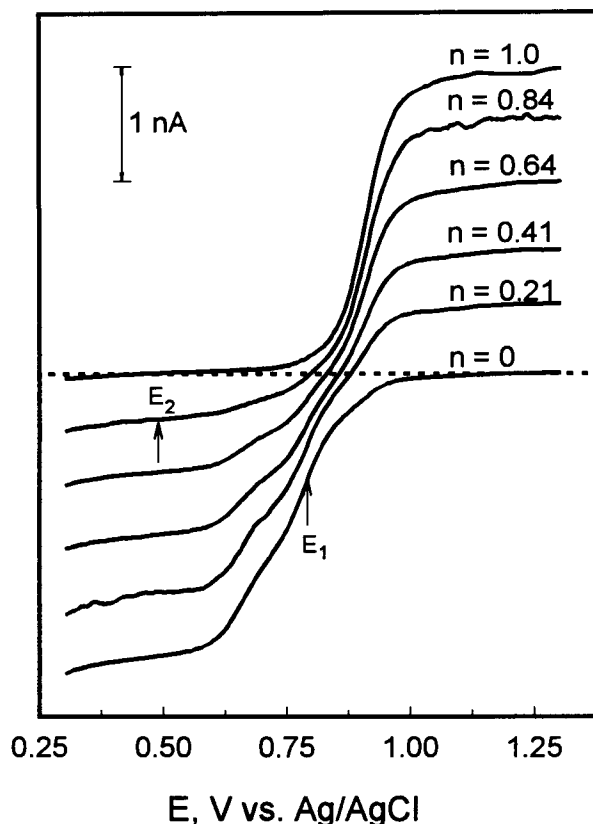


Figure 4. Microelectrode steady-state voltammograms recorded during the electrolysis of 1 mM $V^{IV}(\text{naphophen})^{2+}$ in anhydrous acetonitrile containing 50 mM acetic anhydride and 50 mM $TBACF_3SO_3$. The electrolysis was first carried out by holding the working electrode potential at $E_1 = 0.78$ V. The n values shown on each curve correspond to the number of electrons per vanadium calculated from the charge consumed by the electrolysis. The electrolysis was stopped at $n = 0.84$ because the current reached the background value. The electrode potential was then changed to $E_2 = 0.5$ V and the electrolysis was completed at this potential until $n = 1.0$.

electrons consumed per starting V(IV) calculated from the charge consumed. It can be seen from these voltammograms that the second reduction wave also became smaller along with the first one. The electrolysis proceeded until $n = 0.84$. The voltammogram (curve 5) at this stage indicates that there were still some reducible species remaining. The electrolysis was then resumed by changing the working electrode potential to $E_2 = 0.5$ V. It was completed after one electron per V(IV) was consumed. The final product shows only one oxidation wave corresponding to that of $V^{III}(\text{naphophen})^+$.

A $V^{IV}(\text{naphophen})^{2+}$ solution was also electrolyzed at 0.5 V from the beginning. Steady-state voltammograms similar to those in Figure 5.4 were observed during the electrolysis, which consumed one electron per vanadium and produced the same final product, $V^{III}(\text{naphophen})^+$. It was also found that $V^{III}(\text{naphophen})^+$ and $V^{IV}(\text{naphophen})^{2+}$ could be interconverted by electrolysis many times without decomposition as long as excess anhydride was present.

DISCUSSION

The purpose of this work was to further demonstrate the chemistry of vanadium-Schiff base complexes in acidified acetonitrile proposed in our previous studies.¹ The ligand naphophen was chosen because the V(III) complex of this ligand exhibits remarkable stability towards acid.^{1b}

Deoxygenation of V^{IV}O(naphophen)

The chemistry of vanadium(IV) is dominated by the stable oxovanadium (or vanadyl) cation, VO²⁺, which remains intact during many reactions.⁶ Deoxygenation of this stable diatomic cation coordinated with chelating or macrocyclic ligands has been realized by using halide-containing reagents, such as SOCl₂⁷ and Ph₃PBr₂.⁸ These methods inevitably produced dihalovanadium(IV) complexes. VO(salen) was also found to react with HCl to form VCl₂(salen).^{3b} Tsuchida et al.⁴ proposed the deoxygenation of VO(salen) by other strong acids but the actual chemistry was disproportionation, as identified in our recent reports.¹ In the current study, we carried out the deoxygenation of V^{IV}O(naphophen) with acid. To our knowledge, this work represents the first example of deoxygenating vanadyl with non-halide-containing reagents. The success is attributed to the presence of excess acetic anhydride, which prevents the water-induced disproportionation of the deoxygenated complex (reaction 4). Since there are no extraneous ligands used in the deoxygenation reaction, the product could serve as a precursor to prepare V(IV)-Schiff base complexes containing other desired axial ligands.

Electrochemistry of V^{IV}(naphophen)²⁺

The broadened electrochemical reduction wave or peak of

$V^{IV}(\text{naphophen})^{2+}$ observed in all voltammograms suggests that there are probably some interactions between $V^{IV}(\text{naphophen})^{2+}$ and another species in the solution, possibly $CF_3SO_3^-$ (Even in the case where no $TBACF_3SO_3$ was added, triflate was always the counter ion of $V^{IV}(\text{naphophen})^{2+}$). The interaction might be the weak coordination of the triflate anions to the axial sites in the complex:



where x could be 1 or 2. Such complexes might have higher solubility than those obtained with ClO_4^- as the counter ion. The excess acetic anhydride might also be involved in reaction 5. These different species may have slightly different redox potentials. The peak broadening observed could result if the rates of the interconversion among these species are slow on the time scale of voltammetrical experiments. More experiments are needed to confirm these speculations.

CONCLUSIONS

The previously proposed chemistry (reactions 1, 2 and 4) concerning the nature of the reaction between oxovanadium(IV)-Schiff base complexes and strong acids in acetonitrile is directly demonstrated. In the presence of excess acetic anhydride, $V^{IV}O(\text{naphophen})$ can undergo either deoxygenation (reaction 1) with two equivalents of acid, or disproportionation (reaction 3) with one equivalent acid. In the absence of anhydride, only disproportionation is possible, no matter how much acid is used. In either case, the disproportionation is just the final net result of the deoxygenation and a subsequent redox reaction between the starting oxovanadium(IV) complex and its deoxygenated form.

REFERENCES AND NOTES

- (1) (a) Liu, Z.; Anson, F. C. *Inorg. Chem.* **2000**, 39, 274, 1048. (b) Liu, Z.; Anson, F. C., *Inorg. Chem.*, **2001**, 40, 1329. (c) Liu, Z. *Electrochem. Soc. Interface*, **2001**, 10, 58.
- (2) Obtained by digital simulation of the system, see page II-45 in Chapter II.
- (3) (a) Bonadies, J. A.; Pecoraro, V. L.; Carrano, C. J. *J. Chem. Soc., Chem. Commun.* **1986**, 1218. (b) Bonadies, J. A.; Butler, W. M.; Pecoraro, V. L.; Carrano, C. J. *Inorg. Chem.* **1987**, 26, 1218.
- (4) Tsuchida, E.; Yamamoto, K.; Oyaizu, K.; Iwasaki, N.; Anson, F. C. *Inorg. Chem.* **1994**, 33, 1056.
- (5) El-Baradie, K. Y.; Gaber, M.; Issa, R. M.; El-Wafa, S. M. A. *Egypt. J. Chem.* **1996**, 39, 509.
- (6) Cotton, F. A.; Wilkinson, G. *Advanced Inorganic Chemistry*, 4th ed.; Interscience: New York, 1987.
- (7) Pasquali, M.; Marchetti, F.; Floriani, C. *Inorg. Chem.* **1979**, 18, 2401.
- (8) Callahan, K. P.; Durand, P. J. *Inorg. Chem.* **1980**, 19, 3211.

CHAPTER VI

**Electrochemistry of Oxoanadium-N, N'-1, 2-phenylenebis-
(2-hydroxy-1-naphthylideneimine) Complexes
Irreversibly Adsorbed on Edge Plane Graphite Electrodes**

ABSTRACT

Electrochemical study on vanadium-naphophen (naphophen = N, N'-1, 2-phenylenebis-(2-hydroxy-1-naphthylideneimine)) complexes in acetonitrile indicates that both $V^{IV}O(naphophen)$ and $V^{V}O(naphophen)^+$ spontaneously adsorb on EPG electrodes and exhibit remarkable stability towards acid after adsorption. Their surface electrochemical behavior was studied and characterized using cyclic voltammetry. The results are further supportive of the solution chemistries proposed in previous chapters.

INTRODUCTION

In previous chapters, the chemistry and electrochemistry of vanadium(III, IV, V)-Schiff base complexes in acetonitrile solutions have been described. Based on the solution chemistry of these complexes, dioxygen was reduced by four electrons to water both electrochemically and chemically in acidified acetonitrile. In attempts to achieve this process electrocatalytically, we found that several of the oxovanadium complexes with Schiff base ligands containing the phenylenediamine linker (ligand Nos. 2, 8 and 14 in Table 3.1, see page III-8) could be confined to the surface of edge plane graphite (EPG) electrodes via spontaneous adsorption. But the solution chemistry encountered earlier, such as the acid-induced disproportionation of oxovanadium(IV) complexes, could not be realized on the electrode surface. Such surface-confined complexes exhibited remarkable stability towards acid and dioxygen. As a result, electrocatalytic reduction of dioxygen could not be carried out. Nonetheless, the results of the surface electrochemistry of these complexes serve to support their solution chemistry proposed and described in previous chapters. Described in this chapter is the electrochemical behavior of oxovanadium(IV, V)-naphophen (N, N'-1, 2-phenylenebis-(2-hydroxy-1-naphthylideneimine)) complexes strongly adsorbed on EPG electrodes.

EXPERIMENTAL**Materials**

Distilled acetonitrile containing 0.001% water (EM Science) was stored over 3 Å molecular sieves. Trifluoromethanesulfonic (triflic) acid (Sigma) was used as received and was maintained O₂-free by saturation with Ar. All supporting electrolytes were electrochemical grade (Fluka). They were placed under vacuum at 75 °C overnight before use. The Schiff base ligand, H₂naphophen, was prepared by condensing 1-hydroxy-2-naphthaldehyde (Aldrich) with 1, 2-phenylenediamine (Aldrich) in ethanol.. The resulting insoluble ligand, without further purification, was refluxed with VOSO₄ in ethanol to prepare V^{IV}O(naphophen), as described previously.^{1b, 2}

A 0.75 mM V^{VO}(naphophen)CF₃SO₃ solution was prepared by bubbling O₂ for 30 minutes into an equimolar mixture of V^{IV}O(naphophen) and triflic acid (0.75 mmol per liter each) in acetonitrile. The resulting solution was stable for months under air and was used as a stock solution in this study. V^{III}(naphophen)⁺ was prepared as previously described¹ by reduction of V^{IV}O(naphophen) with H₂ in the presence of a large area Pt gauze and one mole of triflic acid per mole of V(IV) and was used in situ.

Apparatus and Procedures

Electrochemical measurements were carried out in conventional one- or two-compartment cells using a BAS Model 100B/W Electrochemical Analyzer. Solutions were kept under an atmosphere of argon which was purified by passage through a gas scrubber (Oxiclear, Aldrich) and two columns filled with molecular sieves. The working electrodes in voltammetric experiments were 6 mm edge plane pyrolytic graphite rods (Union Carbide Co.) mounted on stainless steel shafts using heat-shrinkable tubing. They were polished before use with No. 600 SiC paper (3M Co.) to produce a smooth but not reflective surface. Auxiliary electrodes were platinum wires. The reference electrode was Ag/AgCl in CH₃CN saturated with NaCl. All potentials are quoted with respect to this electrode. The formal potential of the ferrocinium/ferrocene couple measured with the EPG electrodes in a 0.1 M tetrabutylammonium perchlorate solution in acetonitrile were 0.44 V versus this reference electrode.

RESULTS AND DISCUSSION

Adsorption of OV(IV, V)-naphophen on EPG

The electrochemistry of the VO(naphophen)^{+ / 0} couple at either a platinum or a mirror-polished glassy carbon electrode is the same as the VO(salen)^{+ / 0} couple and other oxovanadium-Schiff base complexes as

described in our previous reports.¹ The cyclic voltammogram shows one set of reversible peaks corresponding to the interconversion of the V(IV) and V(V) complexes, as shown in Figure 6.1 curve A. Quite different behavior results when an EPG electrode is employed to record the voltammograms. Two sets of voltammetric peaks are present as labeled I and II in curves B and C of Figure 6.1. The formal potential for peak set I is close to that in curve A. Peak set II at ca. 0.9 V has a symmetrical shape with minimal peak separation. Increasing scan rate causes more significant peak current increase in set II than in set I (curve C). These observations suggest that peak set I is assignable to the dissolved complex in solution while peak set II arises from the adsorbed complex(es) on the electrode surface.³ That peak set II appears at a more positive potential (as a prepeak) than the diffusion peak (set I) indicates the reduced form, $V^{IV}O(\text{naphophen})$, adsorbs more strongly than the oxidized form, $V^{VO}(\text{naphophen})^+$.

The features of the adsorption peak can be studied in more detail when the concentration of the complex is decreased to lower than 10 μM because the diffusion peak becomes negligible. Figure 6.2 shows the cyclic voltammogram of a 7.5 μM $V^{VO}(\text{naphophen})^+$ solution recorded at an EPG electrode. The increase of the peak current indicates the accumulation of $V^{VO}(\text{naphophen})^+$ on the electrode surface. After about 12 minutes (6 scans between 1.2 V and 0.6 V at 10 mV s^{-1}), the

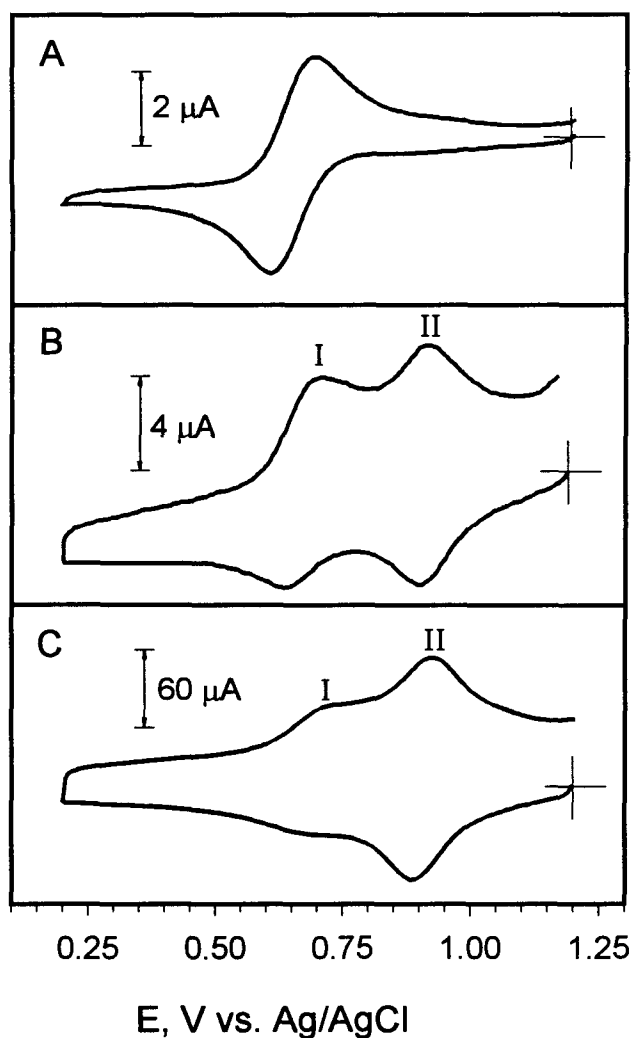


Figure 6.1. Cyclic voltammograms of a 0.1 mM $VVO(\text{naphophen})CF_3SO_3$ solution in CH_3CN at (A) a 5 mm glassy carbon electrode; (B) and (C) a 6 mm EPG electrode. Supporting electrolyte: 0.1 M tetrabutylammonium perchlorate ($TBAClO_4$); Scan rate: (A) and (B) 10, (C) 200 $mV s^{-1}$.

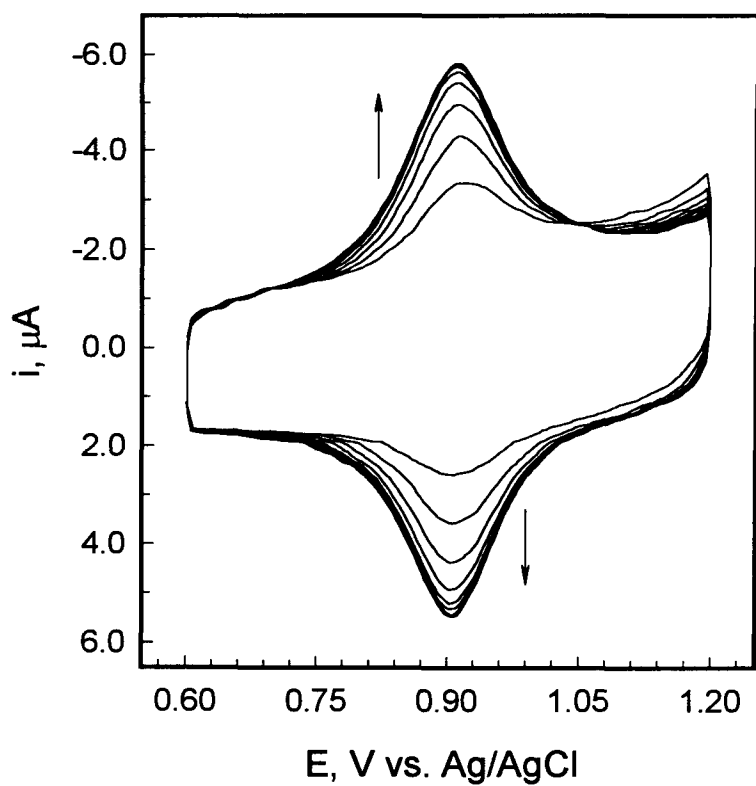


Figure 6.2. Cyclic voltammogram of a $7.5 \mu\text{M V}^{\text{VO}}(\text{naphophen})\text{CF}_3\text{SO}_3$ solution in CH_3CN at a 6 mm EPG electrode which was continuously scanned between 0.6 and 1.2 V at 10 mV s^{-1} . Supporting electrolyte: 0.1 M TBAClO_4 .

adsorption reached saturation. The electrode used to record Figure 6.2 was then removed from the solution, washed with CH_3CN and placed in a supporting electrolyte free of $\text{V}^{\text{V}}\text{O}(\text{naphophen})^+$. The adsorption peak can still be observed. The area of the peak (either the anodic or the cathodic one) corresponds to ca. 1.3×10^{-9} mol/cm² (based on the geometric area of the 6 mm EPG electrode) of the complex adsorbed on the electrode surface. The magnitude of the peak current decreases slowly over a period of many hours (about 50% loss in 10 hours). Polishing the electrode immediately removes the adsorbed complex as indicated by the elimination of the adsorption peak. All these observations can also be obtained with a solution of the reduced form of the complex, i.e., $\text{V}^{\text{IV}}\text{O}(\text{naphophen})$. This neutral complex leaves the electrode surface in pure acetonitrile even slower than its charged counterpart. The direct observation of the electrochemical behavior of such strongly adsorbed surface species for extended periods in solutions free of the attached reactants has been reported in few instances.⁴

Cyclic voltammograms of the adsorption peak at different scan rates are shown in Figure 6.3A. A plot of peak current vs. scan rate indicates the expected linear relationship for an adsorption peak, as shown in Figure 6.3B. Parameters concerning the characteristics of the peak, such as ΔE_p (peak separation) and $\Delta E_{p,1/2}$ (half-peak width) measured from these voltammograms, are listed in Table 6.1. The values of ΔE_p

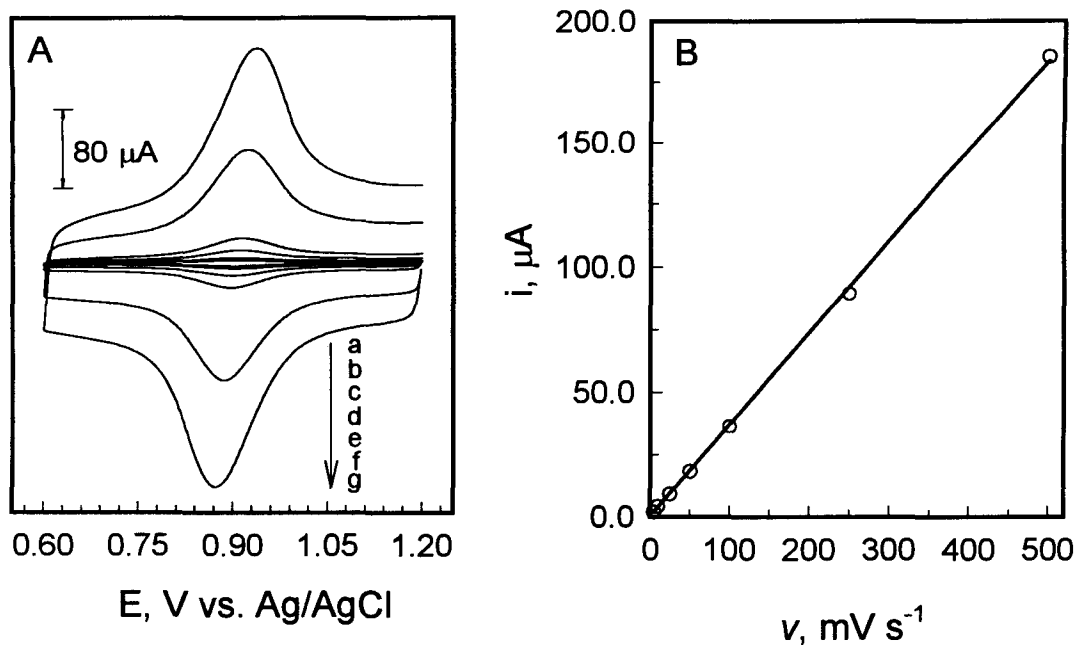


Figure 6.3. (A) Cyclic voltammogram of a $7.5 \mu\text{M V}^{\text{VO}}(\text{naphophen})\text{CF}_3\text{SO}_3$ solution in CH_3CN at a 6 mm EPG electrode. Scan rates: (a) 5, (b) 10, (c) 25, (d) 50, (e) 100, (f) 250, (g) 500 mV s^{-1} . Supporting electrolyte: 0.1 M TBAClO_4 . (B) Plot of peak current vs. scan rate.

and $\Delta E_{p,1/2}$ increase slightly with scan rate, indicating that the surface electron transfer is not completely nernstian (A completely nernstian system would give 0 and 90.6 mV for ΔE_p and $\Delta E_{p,1/2}$ respectively.³). The rate constant for the electron transfer can be estimated by using the following equation:⁵

$$m = (RT/nF)(k/\nu) \quad (1)$$

where k is the rate constant for the electron transfer; n is number of electrons involved, and equals one here; ν is the scan rate; R , T , and F are molar gas constant, temperature and Faraday's constant respectively; m is a parameter related to ΔE_p and can be determined using a table in reference 5, which applies when ΔE_p is less than 220 mV and the transfer coefficient is 0.5. The k values calculated in such a way are also listed in Table 6.1. The relatively high rate constant value indicates that the system is close to nernstian.

Table 6.1. Parameters Obtained From Figure 6.3A and Electron-Transfer Rate Constants Calculated From Equation 1

ν (mV s ⁻¹)	ΔE_p (mV)	$\Delta E_{p,1/2}$ (mV)	k (s ⁻¹)
5	3	95	-
10	5	96	-
25	9	98	-
50	17	100	-
100	21	106	6.5
250	36	112	9.7
500	64	118	9.7

A plot of the surface concentration Γ (calculated by integration of the adsorption peak areas in cyclic voltammograms such as those in Figure 6.3A) as a function of the concentration of $V^{VO}(\text{naphophen})^+$ in solution is shown in Figure 6.4. The extent of adsorption becomes independent of the solution concentration of $V^{VO}(\text{naphophen})^+$ at ca. 2.0×10^{-7} M and reaches ca. 1.3×10^{-9} mol cm^{-2} , which corresponds to one monolayer of the complex. The adsorption decreases to 10% of a monolayer at ca. 10^{-8} M.

Stability of the Adsorbed Complexes towards Acids

In previous chapters (and reports¹), it has been shown that oxovanadium (IV) Schiff base complexes, including $V^{IV}O(\text{naphophen})$, undergo disproportionation in acidified acetonitrile solution. The adsorbed $V^{IV}O(\text{naphophen})$, however, exhibited remarkable stability towards acid. The cyclic voltammogram of the adsorbed complex (as shown earlier in Figures 6.1 and 6.2) on EPG electrodes did not change even in the presence of 0.1 M triflic acid in acetonitrile. The dramatic difference between the solution chemistry and the surface behavior is understandable in several ways based on the mechanism of the disproportionation reaction as demonstrated in Chapter V. First, the adsorption shifts the redox potential of the $VO(\text{naphophen})^{+/0}$ couple on

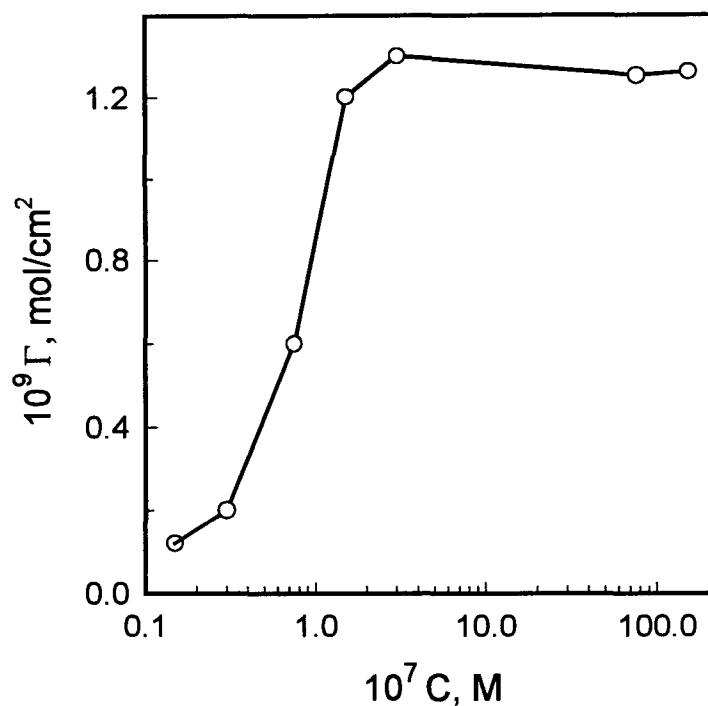


Figure 6.4. Surface concentration Γ of $\text{V}^{\text{V}}\text{O}(\text{naphophen})^+$ on a 6 mm EPG electrode vs. its solution concentration (in log scale) in acetonitrile. Γ values were calculated from the adsorption peak areas of cyclic voltammograms recorded with the electrode after the adsorption reached equilibrium.

the surface to ca. 0.9 V, at which $V^{IV}O(\text{naphophen})$ has much less reducing power than the free species in solution ($E^f = 0.65$ V). The redox reaction between $V^{IV}O(\text{naphophen})$ and $V^{IV}(\text{naphophen})^{2+}$ required by the disproportionation (see equation 2 on page V-3) thus becomes much less thermodynamically favorable (the formal potential for the $V^{IV}(\text{naphophen})^{2+}/+$ couple is also 0.9 V^{1b}). Second, the reactivity of the complexes confined to electrode surface is probably different from those in solution. The kinetics of the disproportionation reaction can thus be retarded. Third, the oxo groups play some important (but unknown) role in the adsorption of the vanadium complexes (Complexes of the same ligand but without the oxo group do not adsorb on EPG electrode, *vide infra*). The oxo groups of the adsorbed complexes may become less reactive towards protons due to adsorption.

The adsorption layer of the complex was also stable in aqueous acid. Figure 6.5 shows the adsorption peak in 50 mM perchloric acid in water. The peak potential shifts to more negative potential (The diffusion peak potential is not available because the complex is not soluble in water.). The stability of the adsorption layer is demonstrated by holding the electrode potential at the negative end to generate $V^{IV}O(\text{naphophen})$. After five minutes, the scan was resumed and an anodic peak with the same shape and height as the cathodic peak was observed.

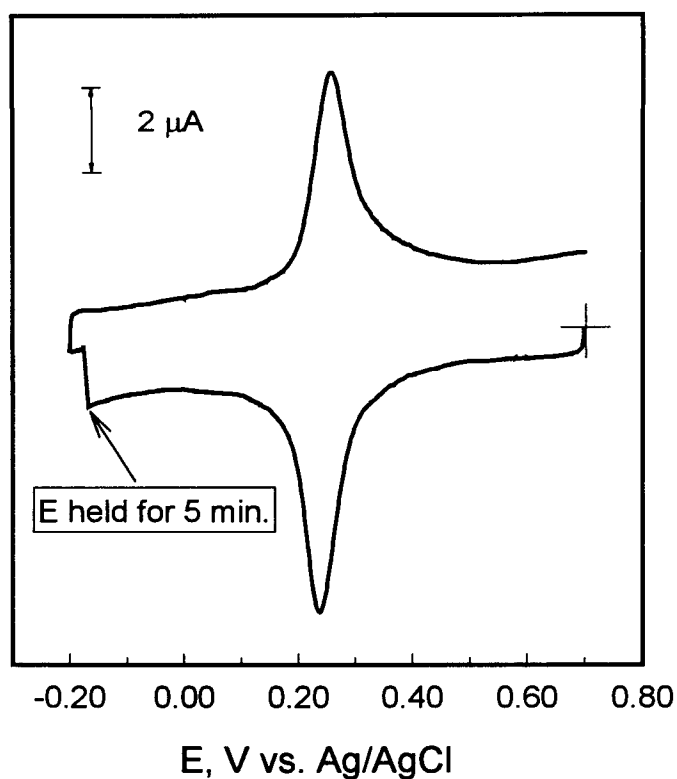


Figure 6.5. Cyclic voltammogram of adsorbed $V^VO(\text{naphophen})^+$ on a 6 mm EPG electrode in 50 mM HClO_4 . Scan rate: 50 mV s^{-1} . The electrode was prepared by first placing in a 0.3 mM $V^VO(\text{naphophen})\text{CF}_3\text{SO}_3$ in CH_3CN for 10 minutes, followed by washing with pure CH_3CN and transferring to the aqueous acid solution.

Electrochemical Desorption

In addition to mechanical polishing, the adsorbed vanadium complexes can be stripped electrochemically by reduction of either the adsorbed complexes or oxygen in solution. As shown in Figure 6.6A, the adsorbed $V^{IV}O(\text{naphophen})$ can be reduced electrochemically at ca. -1.25 V as a irreversible peak. The same peak also appeared at a glassy carbon electrode from the complex dissolved in solution. The nature about the reduction is not known. It caused the gradual loss of the adsorption layer, as indicated by the decrease of the magnitude of the adsorption peak. If the electrode is cycled between +1.2 and -1.0 V, the adsorption peak can remain stable. Figure 6.6B shows the desorption of the adsorption layer by O_2^- produced by electrochemical reduction of O_2 in acetonitrile at ca. -0.9 V.

Behavior of $V^{III}(\text{naphophen})^+$

As proposed in our previous reports¹ and demonstrated in Chapter V (see equation 4 on page V-4), the product of the electrooxidation of $V^{III}(\text{naphophen})^+$, i.e., $V^{IV}(\text{naphophen})^{2+}$, reacts with water to produce $V^VO(\text{naphophen})^+$, which should be observable with an EPG electrode because of its strong adsorption. Figure 6.7 shows the expected results. Shown in Figure 6.7A is the cyclic voltammogram of a $V^{III}(\text{naphophen})^+$ solution containing excess water recorded with an EPG electrode. The peak at ca. 0.75 V corresponds to the oxidation of the V(III) complex.

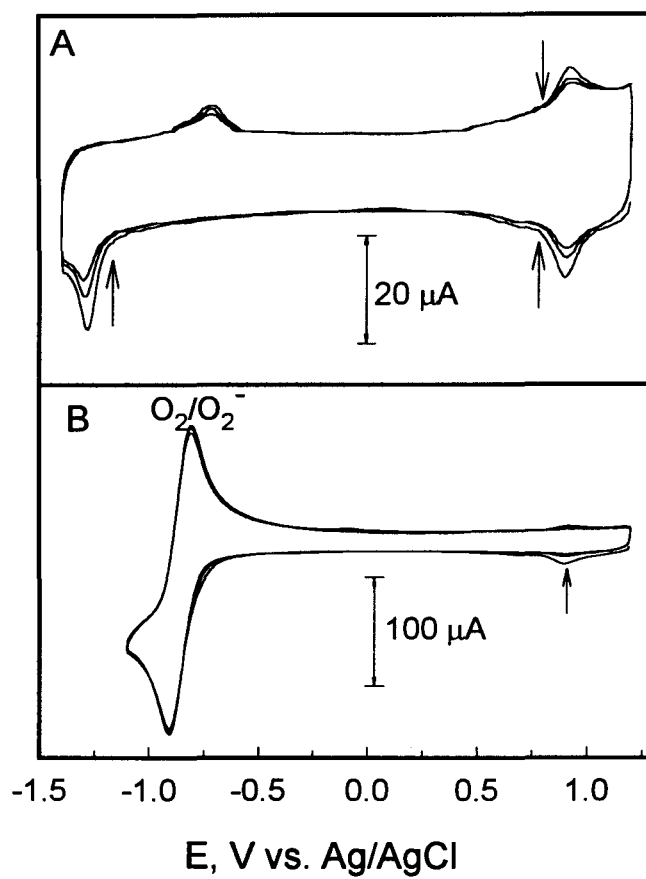


Figure 6.6. Cyclic voltammograms of adsorbed $\text{V}^{\text{V}}\text{O}(\text{naphophen})^+$ on EPG electrodes in pure supporting electrolyte (0.1 M TBAClO_4) solutions saturated with (A) argon; (B) air. The electrode with adsorbed layer was prepared as described in Figure 6.5.

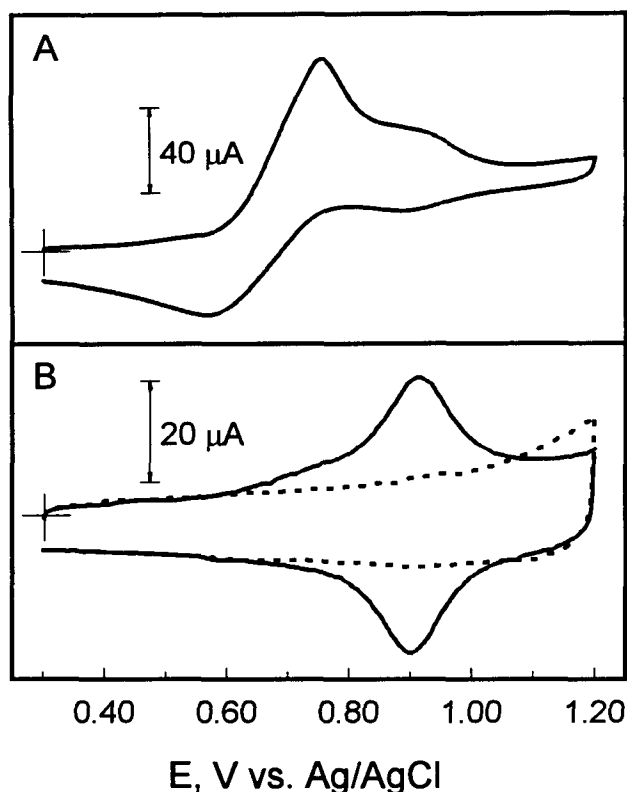


Figure 6.7. (A) Cyclic voltammogram of a 1 mM solution of $V^{III}(\text{naphophen})^+$ in Ar-saturated acetonitrile containing 40 mM of water (added deliberately) recorded with a 6 mm EPG electrode. (B) Solid line: cyclic voltammogram obtained in Ar-saturated acetonitrile containing only 0.1 M TBAClO₄ with the electrode used in (A), which had been washed with Ar-saturated acetonitrile after recording (A) and transferred over under an Ar atmosphere; Dotted line: repeat of the solid line except that the electrode was placed in the solution used to record (A) but not scanned. Scan rates: (A) 20, (B) 50 mV s⁻¹.

The symmetrical peak at ca. 0.9 V arises from the adsorption of the expected oxovanadium(IV) complex formed as just described. The electrode used to record curve A was then washed with Ar-saturated CH_3CN and transferred into a pure supporting electrolyte solution to record another cyclic voltammogram, which exhibited only the characteristic peak of the adsorbed oxovanadium complex, as shown with the solid line in Figure 6.7B. The whole process was performed under an atmosphere of argon and all solutions used were saturated with argon to avoid the oxidation of $\text{V}^{\text{III}}(\text{naphophen})^+$ by oxygen from air to form the strongly adsorbing $\text{V}^{\text{VO}}(\text{naphophen})^+$. In order to rule out the possibility that trace amounts of oxovanadium complexes might exist in the original $\text{V}^{\text{III}}(\text{naphophen})^+$ solution, and to ensure that the adsorption peak in curve B is not from the oxidation of $\text{V}^{\text{III}}(\text{naphophen})^+$ by air, another freshly polished EPG electrode was placed in the solution used to record curve A for 10 minutes, and then was transferred to a pure supporting electrolyte solution following the same procedure to record another voltammogram, as shown in the dotted line in Figure 6.7B. Only background current was detected. This observation confirms that the oxovanadium complex detected in the solid line of Figure 6.7B was from the electrooxidation of $\text{V}^{\text{III}}(\text{naphophen})^+$. At the same time, it also indicates that $\text{V}^{\text{III}}(\text{naphophen})^+$ does not adsorb on EPG electrodes. The reason for the different adsorption behavior of the oxo and non-oxo

complexes remains to be elucidated. The oxo group must play a critical role in this difference.

CONCLUSIONS

Electrochemical study of vanadium-naphophen complexes revealed that only the oxo-containing complexes adsorb strongly on EPG electrodes. The adsorption dramatically changes the chemistry that these complexes exhibit in solution. The changes can be understood on the basis of the surface electrochemistry and the solution chemistry mechanisms described in previous chapters.

REFERENCES

- (1) (a) Liu, Z.; Anson, F. C. *Inorg. Chem.* **2000**, 39, 274, 1048. (b) Liu, Z.; Anson, F. C. *Inorg. Chem.* **2001**, 40, 1329. (c) Liu, Z. *Electrochem. Soc. Interface*, **2001**, 10, 58.
- (2) El-Baradie, K. Y.; Gaber, M.; Issa, R. M.; El-Wafa, S. M. A. *Egypt. J. Chem.* **1996**, 39, 509.
- (3) Bard, A. J.; Faulkner, L. R. *Electrochemical Methods: Fundamentals and Applications*; Wiley: New York, **2001**; Chapter 14.
- (4) (a) Brown, A. P.; Koval, C.; Anson, F. C. *Electroanal. Chem.* **1976**, 72, 379. (b) Watkins, B. F.; Behling, J. R.; Kariv, E.; Miller, L. L. *J. Am. Chem. Soc.* **1975**, 97, 3549.
- (5) Laviron, E. *J. Electroanal. Chem.* **1979**, 101, 19.